

# The Effects of I/Q Imbalance and Improper Gaussian Noise on Different Wireless Communication Systems

by

MALEK ALSMADI

Graduate Program

in

Department of Electrical and Computer Engineering

A thesis submitted in partial fulfillment of the requirements  
for the degree of Doctor of Philosophy (Ph.D.)

The Faculty of Graduate Studies

Lakehead University

Thunderbay, Ontario, Canada

July 2020

© Malek Alsmadi 2020

## Examining Committee Membership

The following served on the Examining Committee for this thesis. The decision of the Examining Committee is by majority vote.

External Examiner:            Georges Kaddoum  
   Professor, Dept. of Electrical Engineering,  
   École de Technologie Supérieure, Canada

Internal Members:            Zubair Fadlullah  
   Associate Professor, Dept. of Software Engineering,  
   Lakehead University, Canada

   Abdulsalam Yassine  
   Assistant Professor, Dept. of Computer Science,  
   Lakehead University, Canada

Supervisor:                    Salama Ikki  
   Associate Professor, Dept. of Electrical Engineering,  
   Lakehead University, Canada

I hereby declare that I am the sole author of this thesis. This is a true copy of the thesis, including any required final revisions, as accepted by my examiners.

I understand that my thesis may be made electronically available to the public.

## Acknowledgements

First and foremost, all praise and thanks are due to Allah for helping me to complete this work. I could never have finished this thesis without his help and guidance.

I would like to express my sincere gratitude to my supervisor, Dr. Salama Ikki, for his patience, motivation, and immense knowledge. Over the last four years, he has been more than a teacher and a supervisor, he has been more like a big brother and mentor. I would never achieve what I have achieved today without his unlimited and unconditional help and support. I also would like to express my gratitude and thanks to prof. Abdelhamid Tayebi for his valuable guidance and all the support he provided me. His support and insightful advice were crucial to my academic success and my development as a researcher.

I am also thankful to Prof. Georges Kaddoum, Dr. Zubair Fadlullah, and Dr. Abdulsalam Yassine for serving on my thesis committee and for providing constructive comments which have improved my thesis. I am also thankful to Dr. Hosam El-Ocla and Dr. Abdulsalam Yassine for serving on my seminar and comprehensive exam committees and for providing constructive comments that guided me to finish this thesis. I am also grateful to all my colleagues in the Electrical and Computer Engineering department in Lakehead University for making my PhD study such a great experience. Special thank to my fiends, Ahmad cheema, Mohannad Al-Mousa, and Ibrahim Al-Hurani for their help and valuable discussions.

Finally, I would like to express my gratitude and appreciation to my family. My sincere appreciation to my dear deceased father for his great role in my life and his numerous sacrifices for me and for our family. Thanks to my mother whose endless love and sincere prayers have always been with me. Special thanks to my wife who have been great sources of encouragement. Shafiq, this work would never have been completed without your tremendous love and sacrifice. Thanks to my brothers and sisters for the love and pray. Thanks also to my father-in-law and mother-in-law for their continuous support. Thanks for my cousin Abdelhameed Alsumadi and his family for their help and support. Last but not least, thanks to our lovely kids, Mohammad, Anas, Marya and Zahraa being so cute and filling our life with love and hope.

## Abstract

The next-generation of wireless networks is required to support a myriad of new demands, including higher data rate, lower latency, greater system capacity, massive connectivity, as well as increased power efficiency. Among various technologies, spatial modulation (SM) and non-orthogonal multiple access (NOMA) have been proposed as promising technologies that can achieve high spectral and energy efficiency. Furthermore, utilizing cognitive radio (CR) systems and millimeter-wave (mmWave) bandwidth have been offered as novel solutions to the spectrum scarcity problem. Interestingly, SM, NOMA, CR, and mmWave can be integrated together to fulfill some of the upcoming generation's wireless network requirements. Being able to design of reliable transceivers that can meet these requirements is of great interest in the electronics and communications communities. Direct-conversion transceivers are built with the objective of directly up-converting the baseband signal to radio frequency (RF) at the transmitter and directly down-converting the received signal at the receiver. This characteristic makes it a promising transceiver architecture due to its small size, low cost, and more efficient energy consumption. While these advantages are very favourable, the direct-conversion transceivers are susceptible to some hardware impairments (HWIs) which limits the communication system performance. In-phase/quadrature-phase (I/Q) imbalance represents one of the most critical direct-conversion transceivers HWIs.

This thesis studies the effects of I/Q imbalance and improper Gaussian noise (IGN) on the performance of modern communication system techniques. Different receiver designs are proposed to optimize the system bit error rate (BER) when the transmitter and receiver operate under the effects of the I/Q imbalance in the presence of IGN at the receiver. More specifically, underlay CR secondary, quadrature spatial modulation (QSM), space shift keying (SSK), and two user NOMA receivers are studied and analyzed. Closed forms of average pairwise error probability (APEP) and upper bound of the average BER formulas are derived for all receivers. These formulas are derived considering the Beckmann fading channel model, where most of the well-known fading channel models can be considered as special cases. The proposed designs show solid performance against I/Q imbalance effects. In fact, these effects can be totally mitigated if they exist at the receiver and can be

significantly reduced if they are at the transmitter. All analytical results are verified by computer simulations.

This thesis affords important results for the building of future wireless receivers. In particular, it can be used for developing digital signal processing (DSP) chips to mitigate the I/Q effects and properly treat the IGN at the receiver. Conclusively, this thesis and the related publications can be extended to design receivers that can mitigate the effects of HWIs on new promising technology. For example, the impact of HWIs on cell-free massive multiple-input multiple-output (MIMO) and intelligent reflecting surface (IRS) is still an active issue.

# Table of Contents

List of Tables	xi
List of Figures	xii
Abbreviations	xvi
List of Symbols	xxi
<b>1 Introduction</b>	<b>1</b>
1.1 Background and Motivation . . . . .	1
1.2 Thesis Contributions . . . . .	4
1.3 Thesis Outline . . . . .	5
1.4 List of Publications . . . . .	6
<b>2 Background and Preliminaries</b>	<b>8</b>
2.1 Communications System Architectures . . . . .	8
2.2 Complex Random Vectors . . . . .	11
2.3 MGF of Quadratic Form of Noncentral Chi-Squared Distribution . . . . .	14
2.4 Beckmann Channels . . . . .	15
2.5 Imperfect CSI Model . . . . .	17
2.6 I/Q Imbalance Model . . . . .	18
2.7 IGN Model . . . . .	22

2.8	Multiple Access Techniques . . . . .	24
2.9	Space Modulation Techniques (SMTs) . . . . .	25
<b>3</b>	<b>Cognitive Networks in the Presence of I/Q Imbalance, IGN and Imperfect CSI</b>	<b>27</b>
3.1	Introduction and Related Works . . . . .	27
3.2	System and Channel Models . . . . .	30
3.2.1	Underlay CR Systems . . . . .	30
3.2.2	Transceiver I/Q imbalance Model . . . . .	31
3.2.3	Imperfect CSI Model . . . . .	32
3.2.4	IGN at the SRx . . . . .	33
3.3	Receiver Designs and Performance Analysis . . . . .	34
3.3.1	Optimal ML Receiver Design . . . . .	35
3.3.2	WLE Receiver Design . . . . .	38
3.3.3	Traditional (Blind) ML Receiver . . . . .	39
3.4	CRLB Derivation . . . . .	41
3.5	Complexity Analysis . . . . .	43
3.6	Numerical Analysis and Results . . . . .	44
3.7	Conclusion . . . . .	55
<b>4</b>	<b>QSM Under the Effects of I/Q Imbalance, IGN and Imperfect CSI</b>	<b>56</b>
4.1	Introduction and Related Works . . . . .	56
4.2	System and Channel Models . . . . .	60
4.2.1	Imperfect CSI Model . . . . .	61
4.2.2	Transceiver I/Q Imbalance Model . . . . .	62
4.3	Accumulative Noise at the Receiver . . . . .	63
4.4	Optimal ML Receiver Design . . . . .	65
4.5	Error Performance Analysis . . . . .	66

4.5.1	Average Pairwise Error Probability . . . . .	66
4.5.2	Asymptotic Analysis . . . . .	70
4.6	Imperfect CSI and IGN Effects on SSK . . . . .	71
4.6.1	System and Channel Models . . . . .	71
4.6.2	Optimal ML Receiver . . . . .	72
4.6.3	CRLB Derivation . . . . .	74
4.6.4	Traditional (Blind) ML Receiver . . . . .	74
4.7	Numerical Analysis and Results . . . . .	75
4.8	Conclusion . . . . .	86
<b>5</b>	<b>Down-link NOMA Networks in the Presence of I/Q imbalance, IGN and Imperfect SIC</b>	<b>87</b>
5.1	Introduction and Related Works . . . . .	87
5.2	System and Channel Models . . . . .	89
5.2.1	Power-domain NOMA System . . . . .	89
5.2.2	Imperfect SIC . . . . .	90
5.2.3	Transceiver I/Q Imbalance Model . . . . .	91
5.3	Receiver Design and Performance Analysis . . . . .	93
5.3.1	Optimal Down-link NOMA Receiver Designs . . . . .	93
5.3.2	Traditional (Blind) NOMA Receivers . . . . .	97
5.3.3	BER Calculations . . . . .	99
5.4	Numerical Analysis and Results . . . . .	100
5.5	Conclusion . . . . .	108
<b>6</b>	<b>Conclusions and Future Work</b>	<b>109</b>
6.1	Conclusions . . . . .	109
6.2	Future Work . . . . .	110

<b>APPENDICES</b>	<b>110</b>
<b>A Proofs of CRN Chapter</b>	<b>125</b>
A.1 Proof of the result in 3.30 . . . . .	125
A.2 Proof of the result in 3.42 . . . . .	128
A.3 Proof of the result in 3.46 . . . . .	129
<b>B Proofs of QSM Chapter</b>	<b>131</b>
B.1 Proof of the result in 4.5 . . . . .	131
B.2 Proof of the result in 4.50 . . . . .	132

# List of Tables

2.1	The relation between Beckmann fading model and other fading models in the literature. The Beckmann fading parameters are in bold. . . . .	16
3.1	Number of multiplications and summations required for each frame. . . . .	43

# List of Figures

2.1	Block diagram of a typical communication system. . . . .	9
2.2	Heterodyne up-conversion RF transmitter's block diagram. . . . .	10
2.3	Direct up-conversion RF transmitter's block diagram. . . . .	11
2.4	Direct down-conversion RF transmitter's block diagram. . . . .	11
2.5	IRR values versus the amplitude mismatch and the phase imbalance. This figure assumes the transmitter and receiver have the same level of I/Q impairments. . . . .	21
2.6	The result of phase imbalance when $\beta_{t,r} = 10^\circ$ , $\xi_{t,r} = 1$ , and SNR=23 dB. . . . .	21
2.7	The result of amplitude imbalance when $\beta_{t,r} = 0^\circ$ , $\xi_{t,r} = 1.5$ , and SNR=23 dB. . . . .	22
2.8	The result of transmitter and receiver I/Q imbalances applied to the 4-QAM and 64-QAM signal constellation diagrams when $\beta_{t,r} = 5^\circ$ , $\xi_{t,r} = 1.2$ , and SNR=23 dB. . . . .	23
2.9	The scattering diagrams of zero mean additive white Gaussian noise. $x$ is the real part and $y$ is the imaginary part. . . . .	24
3.1	Underlay cognitive radio system under the effect of I/Q imbalance. . . . .	31
3.2	APEP at 3 dB amplitude mismatch and $5^\circ$ phase imbalance at both STx/SRx and assuming PGN and perfect CSI at SRx. . . . .	45
3.3	ABER performance at different values of $\sigma_{nI}^2$ , $\sigma_{nQ}^2$ and $\rho_n$ assuming perfect I/Q matching and perfect CSI. . . . .	46

3.4	Effect of amplitude mismatching at STx side and assuming perfect CSI ( $\beta_t = 10^\circ$ ). . . . .	47
3.5	Effect of phase imbalance at STx side and assuming perfect CSI ( $\xi_t = 3$ dB). . . . .	48
3.6	Effect of amplitude mismatching at SRx side and assuming perfect CSI ( $\beta_r = 10^\circ$ ). . . . .	49
3.7	Effect of phase imbalance at SRx side and assuming perfect CSI ( $\xi_r = 3$ dB). . . . .	49
3.8	SRx in the presence of low, average and high levels of I/Q imbalance at STx/SRx with perfect CSI and PGN at the SRx (4-QAM). . . . .	50
3.9	SRx in the presence of low, average and high levels of I/Q imbalance at STx/SRx with perfect CSI and PGN at the SRx (16-QAM). . . . .	50
3.10	SRx in the presence of low, average and high levels of I/Q imbalance at STx/SRx with perfect CSI and PGN at the SRx (256-QAM). . . . .	51
3.11	ABER at 4 dB amplitude mismatch and $10^\circ$ phase imbalance at STx or SRx alone with perfect CSI or channel estimation errors that has CRLB variance. . . . .	52
3.12	The effect of number of pilots on the channel estimation error at Perfect I/Q matching condition assuming $\sigma_e^2 = \text{CRLB}$ and PGN at the SRx. . . . .	53
3.13	The effect of number of pilots on the channel estimation error with imperfect I/Q matching ( $\beta_{t,r} = 10^\circ$ , $\xi_{t,r} = 4$ dB), PGN, and assuming $\sigma_e^2 = \text{CRLB}$ . . . . .	53
3.14	The effect of channel parameters assuming $\sigma_e^2 = \text{CRLB}$ , PGN, and I/Q impaired transmitter and receiver where $\xi_{t,r}=2$ dB and $\beta_{t,r} = 5^\circ$ . . . . .	54
3.15	Number of multiplications of the proposed receivers assuming that the frame size is 1000 symbols. . . . .	54
3.16	Number of summations of the proposed receivers assuming that the frame size is 1000 symbols. . . . .	55
4.1	The scheme of QSM wireless communication system employing a homodyne architecture transceiver. . . . .	60
4.2	APEP of QSM system over Beckmann channels conditions with perfect CSI, PGN, and I/Q impaired transmitter and receiver. . . . .	77

4.3	2×2 QSM MIMO system with 4-QAM modulation in the presence of different levels of amplitude imbalance at the transmitter side with fixed $\beta_t = 5^\circ$ . . .	78
4.4	2×2 QSM MIMO system with 4-QAM modulation in the presence of different levels of angle mismatches at the transmitter side with fixed $\xi_t=0.3$ dB. . .	79
4.5	2×2 QSM MIMO system with 4-QAM modulation in the presence of different levels of amplitude imbalance at the receiver side with fixed $\beta_r = 5^\circ$ . . . . .	79
4.6	2×2 QSM MIMO system with 4-QAM modulation in the presence of different levels of angle mismatches at the receiver side with fixed $\xi_r=0.3$ dB. . . . .	80
4.7	2 × 2 QSM MIMO system with 16-QAM modulation in the presence of different levels of I/Q imbalance. . . . .	80
4.8	4×2 QSM MIMO system with 4-QAM modulation in the presence of different levels of I/Q imbalance. . . . .	81
4.9	4 × 1, 4 × 2, and 4 × 4 QSM MIMO systems with 4-QAM modulation in the presence of I/Q imbalance where $\xi_{t,r}=0.3$ dB and $\beta_{t,r} = 5^\circ$ . . . . .	82
4.10	ABER performance of 2 × 2 QSM system over Beckmann channels when the transmitter and receiver under the effect of I/Q imbalance ( $\xi_{t,r}=0.3$ dB and $\beta_{t,r} = 5^\circ$ ). . . . .	83
4.11	ABER performance of 2 × 2 QSM with different levels of improper channel estimation errors when $\xi_{t,r}=0.3$ dB and $\beta_{t,r} = 5^\circ$ . . . . .	83
4.12	ABER performance of 2 × 2 QSM with different levels of IGN assuming that $\sigma_I^2 + \sigma_Q^2=1$ . . . . .	84
4.13	ABER performance of the SSK-MIMO system in the presence of imperfect CSI and IGN: red, blue, green and black curves represent the cases of $\sigma_I^2 = 0.5, \rho = 0$ ; $\sigma_I^2 = 0.2, \rho = 0$ ; $\sigma_I^2 = 0.5, \rho = 0.7$ and $\sigma_I^2 = 0.2, \rho = 0.7$ , respectively.	85
4.14	ABER performance of the optimal 2 × 2 SSK MIMO system under the effect of IGN using CRLB at different number of pilots ( $N_p$ ) where $\sigma_I^2 = 0.2, \rho = 0.7$ , respectively. . . . .	85

5.1	Two users power-domain down-link NOMA systems under the effect of I/Q imbalance. . . . .	90
5.2	APEP of $U_1$ at 1 dB amplitude mismatch and $5^\circ$ phase imbalance when $\mu_{h_1^I} = 0.1$ , $\mu_{h_1^Q} = 0.2$ , $\sigma_{h_1^I}^2 = 0.6$ , $\sigma_{h_1^Q}^2 = 1.4$ , $\rho_{h_1} = 0.3$ , and $\sigma_e^2 = 0.002$ . . . . .	101
5.3	APEP of $U_2$ at 1 dB amplitude mismatch and $5^\circ$ phase imbalance when $\mu_{h_2^I} = 0.1$ , $\mu_{h_2^Q} = 0.05$ , $\sigma_{h_2^I}^2 = 0.2$ , $\sigma_{h_2^Q}^2 = 0.3$ , and $\rho_{h_2} = 0.3$ . . . . .	102
5.4	ABER performance of $U_1$ when the transmitter under the effects of different levels of I/Q imbalances and $\alpha = 0.8$ . . . . .	103
5.5	ABER performance of $U_1$ when the receiver under the effects of different levels of I/Q imbalances and $\alpha = 0.8$ . . . . .	103
5.6	ABER performance of $U_2$ when the transmitter under the effects of different levels of I/Q imbalances and $\alpha = 0.8$ . . . . .	104
5.7	ABER performance of $U_2$ when the receiver under the effects of different levels of I/Q imbalances and $\alpha = 0.8$ . . . . .	105
5.8	ABER performance of $U_1$ when using different power allocation factors. . . . .	106
5.9	ABER performance of $U_2$ when using different power allocation factors. . . . .	106
5.10	ABER performance of $U_1$ under the effects of different imperfect SIC levels when $\xi_{t,r} = 1$ dB and $\beta_{t,r} = 5^\circ$ . . . . .	107
5.11	$U_1$ 's optimal receiver performance over Beckmann fading channels with imperfect SIC ( $\sigma_e^2 = .001$ ) and I/Q impaired transmitter and receiver ( $\xi_{t,r}=1.5$ dB, $\beta_{t,r}=5^\circ$ ). . . . .	107
5.12	$U_2$ 's optimal receiver performance over Beckmann fading channels with I/Q impaired transmitter and receiver ( $\xi_{t,r}=1.5$ dB, $\beta_{t,r}=5^\circ$ ). . . . .	108

# Abbreviations

**3GPP** 3rd generation partnership project 3

**5G** fifth generation 3, 56

**ABER** average bit error rate 5, 38, 45–48, 51, 52, 58, 59, 76, 78, 81, 84, 100, 104, 105, 109

**ADC** analog to digital converter 8, 10, 61

**AF** amplify-and-forward 28, 29

**APEP** average pairwise error probability 5, 36, 44, 46, 55, 67, 70, 71, 73, 75, 76, 86, 94, 109

**APM** amplitude/phase modulation 25, 26, 57

**AWGN** additive white Gaussian noise 22, 23, 30, 33, 34, 42, 59, 64, 67, 90, 109, 127

**BER** bit error rate 88, 99, 109

**BPSK** binary phase shift keying 25

**CCI** co-channel interference 57, 58

**CDMA** code division multiple access 24, 25

**CR** cognitive radio 1, 4–6, 27–30, 35, 39, 40, 44, 55, 58, 109, 110

**CRLB** Cramer-Rao lower bound 5, 29, 30, 41, 42, 51, 55, 71, 74, 84–86, 109, 132, 133

**CSI** channel state information 4, 6, 17, 18, 27–29, 32, 35, 36, 38, 44–48, 51, 55, 57–59, 71, 73–76, 82, 84, 86, 94

**DAC** digital to analog converter 8, 9

**dB** decibel 58

**DDC** direct down-conversion 60

**DF** decode-and-forward 28, 29

**DSP** digital signal processing 8

**EE** energy efficiency 56, 57

**FDMA** frequency division multiple access 24

**FIM** Fisher information matrix 55, 109, 132, 133

**GQSM** quadrature spatial modulation 26

**GQSSK** quadrature space shift keying 26

**GSM** generalized spatial modulation 25

**GSSK** generalized space shift keying 25

**HWIs** Hardware impairments 2–4, 10, 18, 23, 28, 29, 57, 88, 109, 110

**I** in-phase 9, 10, 18, 22, 52, 60, 81

**I/Q** in-phase/quadrature-phase 2–6, 8, 10, 18–20, 22, 23, 27–35, 38, 39, 41, 42, 44–48, 51, 55, 58, 59, 62–65, 67, 71, 75–78, 82, 86–89, 91–94, 97, 100–102, 104, 108–110, 125

**ICI** inter-channel interference 1, 26, 56, 57

**IF** intermediate frequency 9, 10

**IGN** improper Gaussian noise 4–6, 18, 23, 24, 27, 29, 32–34, 44, 55, 57–59, 64, 71, 72, 74–76, 82, 85, 86, 97, 109, 110

**IoT** Internet of things 1, 3

**IRR** image rejection ratio 3, 20

**LNA** low-noise amplifier 61

**LO** local oscillators 9, 10, 18, 19, 61, 91

**LoS** line of sight 16, 37, 52, 70, 81, 105

**LPF** low pass filter 19, 61

**LTE** long-term evolution 3, 56

**MGF** moment generating function 14, 37, 70, 73, 95

**MIMO** multiple-input multiple-output 2, 6, 56–59, 61, 71, 77, 78, 81, 82, 84, 110

**ML** maximum likelihood 4, 5, 17, 32, 35, 38–40, 45, 55, 57–59, 64–66, 71, 74, 75, 86, 93, 94, 97

**mmWave** millimeter-wave 1–3, 58, 59

**MVPA** mean-value power allocation 36, 37, 44

**NOMA** non-orthogonal multiple access 1, 2, 4, 6, 24, 25, 87–89, 93, 94, 96, 97, 100, 104, 108–110

**OFDMA** orthogonal frequency-division multiple access 28, 110

**OMA** orthogonal multiple access 24, 87

**PAs** power amplifiers 60

**PDF** probability density function 15–17, 29, 35, 37, 39, 40, 65, 67, 69, 72, 75, 93–97

**PEP** pairwise error probability 5, 44, 55, 58, 59, 66, 67, 71, 73, 75, 89, 100

**PGN** proper Gaussian noise 18, 22, 23, 33, 34, 41, 42, 55, 58, 64, 73, 74, 76, 100, 109, 127

**PRx** primary receiver 30, 36, 44

**PTx** primary transmitter 30

**Q** quadrature-phase 9, 10, 18, 52, 60, 81

**QSM** quadrature SM 4, 6, 26, 57–62, 65, 73, 75–78, 81, 82, 86, 109, 110

**QSSK** quadrature space shift keying 26

**RF** radio frequency 2, 8–10, 56, 57, 60, 87

**RV** random variable 3, 11–15, 18, 22, 23, 30, 33, 34, 36–40, 42, 63, 66, 69, 72, 92, 94, 95

**SE** spectral efficiency 25, 57, 58

**SIC** successive interference cancellation 2, 4, 6, 18, 88–93, 97, 100, 101, 104, 105, 108, 109

**SIMO** single-input multiple-output 58

**SIR** signal-to-interference ratio 20

**SISO** single-input single-output 44, 100

**SM** spatial modulation 1, 2, 4, 25, 26, 56–58, 71

**SNR** signal-to-noise ratio 28, 39, 40, 44, 46–48, 76–78, 82, 88, 97, 99, 100, 104, 105, 108

**SRx** secondary receiver 29–33, 35, 38–42, 44–48, 55, 109

**SSK** pace shift keying 4, 6, 25, 26, 57, 59, 71, 73–75, 84, 86, 132

**STx** secondary transmitter 29–32, 35, 36, 38–42, 44–48

**TA** transmitter antenna 25, 26, 57, 60, 62, 66

**TDMA** time division multiple access 24

**WiMAX** worldwide interoperability for microwave access 56

**WLE** widely linear equalization 4–6, 35, 38, 39, 43–48, 52

# List of Symbols

$\mathbf{x}$	vector $\mathbf{x}$
$\mathbf{X}$	matrix $\mathbf{X}$
$\mathcal{N}(\mu, \sigma^2)$	real Gaussian random variable with $\mu$ mean and $\sigma^2$ variance
$\mathcal{CN}(\boldsymbol{\mu}, \boldsymbol{\Gamma})$	complex random Gaussian variable where $\boldsymbol{\mu}$ is the mean vector and $\boldsymbol{\Gamma}$ is the covariance matrix of the real and imaginary parts
$(\cdot)^I$ or $(\cdot)_I$	in-phase component of the complex number/variable
$(\cdot)^Q$ or $(\cdot)_Q$	quadrature component of the complex number/variable
$(\cdot)^{-1}$	matrix inverse
$ \cdot $	matrix determinant
$[\cdot]^T$	vector or matrix transpose
$ \cdot $	magnitude of the complex number or variable
$\ \cdot\ $	the Euclidean norm of the vector
$a_j$	the $j^{th}$ element of any column or row vector $\mathbf{a}$
$(\cdot)^*$	complex conjugate
$\mu_z$	the mean of the random variable $z$
$\sigma_z^2$ or $\text{var}(z)$	variance of the random variable $z$

$\sigma_z$	standard deviation the random variable $z$
$\text{cov}(x, y)$	the covariance between the random variables $x$ and $y$
$\mathbb{E}\{\cdot\}$	the expectation operator
$\rho_i$	the correlation between the real and imaginary parts of a complex random variable $i$
$\Re\{\cdot\}$	the real part of a complex number or variable
$P(\cdot)$	is the probability of the event
$Q(u)$	$\frac{1}{\sqrt{2\pi}} \int_x^\infty \exp\left(\frac{-u^2}{2}\right) du$

# Chapter 1

## Introduction

### 1.1 Background and Motivation

Due to the rapid increase of mobile devices and the ever-growing range of applications in the Internet of things (IoT), the next-generation wireless technologies must support higher data rate, lower latency, greater system capacity, massive connectivity, as well as increased power-consumption efficiency. In fact, a huge increase in the data traffic is expected to be seen in the next years, which might overcrowd the limited available spectrum and substantially increase power consumption [1–3]. In order to meet these requirements, more advanced communication technologies need to be developed and integrated to maximize the achievable throughput and reduce the deployment cost.

Among various technologies, spatial modulation (SM) and non-orthogonal multiple access (NOMA) have been proposed as prospective technologies to achieve high spectral and energy efficiency. On the other hand, exploiting the millimeter-wave (mmWave) bandwidth and using the cognitive radio (CR) networks have been introduced as strategies to confront the spectrum scarcity problem. Interestingly, SM, NOMA, mmWave and CR can be integrated together to further increase the data rate, support the massive connectivity, achieve lower latency communication and obtain the maximum benefit of the available spectrum.

The advantages of SM include giving higher energy efficiency, requiring lower receiver complexity, having free inter-channel interference (ICI). Furthermore, it does not need

inter-antenna synchronization and it also compatible with multiple-input multiple-output (MIMO) techniques. On the other hand, most SM research assumes a two users scenario while current multi-user SM receivers suffer from inter-user interference [4]. In this context, NOMA can be used to serve a large number of users at different power levels simultaneously using the same channel resources [5, 6]. These resources can be multiplexed in the power domain via superposition coding at the transmitter. At the receiver, one of the multi-user detection techniques, such as successive interference cancellation (SIC), can be exploited to cancel the inter-user interference.

mmWave has a widely available spectrum bandwidth in the range 30-300 GHz. Proper use for this bandwidth can support a substantial increase in the data traffic in a cost-efficient manner compared with the expensive and exhausted radio resources in traditional frequency bands (below 6 GHz) [7, 8]. However, communications in short wavelength bands experience high propagation loss. To overcome this stumbling block, directional beamforming using a large number of antennas can be used to compensate for this loss. Fortunately, the significant reduction in the wavelength of mmWave band can easily support the massive MIMO technology, which is considered as a basic technology for the next-generation wireless communication systems. While the conventional mmWave MIMO system has some practical limitations, using the mmWave SM MIMO can overcome them [9]. Different works in the literature have considered the integration of mmWave in NOMA. mmWave NOMA not only increases the NOMA beam gain, but also covers multiple NOMA users [10, 11]. Moreover, the work in [12] studied the integration of mmWave NOMA with MIMO technique, further achieving better performance in terms of spectrum and energy efficiency.

Hardware impairments (HWIs), such as in-phase and in-phase/quadrature-phase (I/Q) imbalance in the radio frequency (RF) front-end, imperfect manufacturing of the high-power amplifier, and the non-linearity of the low noise amplifier can dramatically degrade the communication system's performance [13, 14]. Although all HWIs can degrade the system performance, I/Q imbalance represents one of the most significant sources of analog impairments in high-speed wireless communication systems [15]. Specifically, this degradation in performance is due to the insufficient rejection of the image frequency band [16, 17]. Moreover, taking into account the effects of I/Q imbalance is not only important in the de-

sign of the transceiver, but also in choosing coding techniques and in resource management of radio communication systems [18]. Furthermore, HWIs have a negative impact on the system secrecy [19]. It has also been reported that I/Q imbalance effects are more severe at higher carrier frequencies such as millimeter-wave bands [20], which is expected to play a major role in 5G and beyond communication systems. [2].

Three main reasons make the effects of I/Q imbalance critical for the next-generation communication systems. First, the I/Q imbalance effects become harsher with larger signal constellations since the probability of incorrect detection increases when the distances between the constellations becomes smaller. This is not very compatible with the next-generation requirements, where more dense constellations are required to obtain higher data rates. For example, IEEE 802.11ax pushes constellation density by adding 1024-QAM to support more efficient communications [21]. Second, fifth generation (5G) and IoT require a massive number of connected devices. This can be supported by manufacturing low-cost transceivers which are expected to come with poor quality [22,23]. Third, new technologies such as mmWave might not always able to meet the standard requirements for acceptable levels of I/Q imbalance.

3rd generation partnership project (3GPP) long-term evolution (LTE)/LTE-advanced constrains the minimum level of the image rejection ratio (IRR) to 25 dB [24]. It was reported in many works such as in [25,26] that the IRR values do not meet the requirements of the standards. For example, in [26], IRR operation was measured to be around 13 and 22.5 dB for the operational frequencies of 57.5 and 64 GHz respectively. These three points together produce a future where a massive number of connected devices can use higher order signal constellations and depend on the mmWave range, calling to attention the importance of designing receivers which can mitigate the effects of I/Q imbalance for the next-generation wireless communication systems. In the meanwhile, modeling the effects of HWIs, including the I/Q imbalance as a zero-mean circularly-symmetric complex Gaussian random variable (RV) fails to reflect its asymmetric characteristics. Therefore, it is necessary to consider the effects of HWIs as improper RV to capture their characteristics [27].

The severe impact of HWIs and the shortcomings in the existing literature motivated us to pursue the following objectives:

- Study the effects of I/Q imbalance and improper Gaussian noise (IGN) on modern wireless communication technologies (SM, CR and NOMA).
- Investigate the joint effects of I/Q imbalance and IGN with other practical conditions, such as imperfect channel state information (CSI) and SIC.
- Design appropriate receivers that can mitigate the effects of I/Q imbalance and properly treat the IGN. The obtained optimum receivers can be used as a benchmark for other sub-optimal receivers.

We tackled these objectives by:

- Developing analytical frameworks to accurately model the accumulative effects of the previously discussed impairments on the technologies investigated in this thesis.
- Utilizing the maximum likelihood (ML) and widely linear equalization (WLE) techniques to design the appropriate receivers.
- Formulating several Monte Carlo simulation scenarios to validate all analytical results.

## 1.2 Thesis Contributions

Compared to the existing literature and motivated by the importance of the thesis topic, the contributions of this work can be summarized as follows:

1. The performance of three timely wireless communication technologies (CR, quadrature SM (QSM), phase shift keying (SSK), and NOMA) is studied under the joint effects of I/Q imbalance at transmitter and receiver sides alongside the existence of IGN at the receiver side. In addition, we study the impact of other practical conditions including the imperfect CSI and SIC in the existence of the I/Q imbalance.

2. An optimal ML receiver designs that can diminish the effect of I/Q imbalance and properly treat the IGN are presented and examined. Specifically, a closed-form expressions for the average pairwise error probability (APEP) and a tight upper bounds of the average bit error rate (ABER) are derived. The simulated results prove that the presented designs outperform all other existing receivers.
3. Moreover, the WLE receiver, which achieves a performance close to the optimal receiver with less complexity, is proposed and analyzed for the underlay CR. The exact pairwise error probability (PEP) is derived and the APEP is calculated analytically. Interestingly, the obtained results show that this receiver outperforms the traditional ML receiver if there is I/Q imbalance at both transmitter and receiver sides. In addition, it has the same performance with the optimal receiver if the I/Q imbalance is only at receiver side. Moreover, the computational complexities of the proposed receivers are calculated and compared with the traditional blind receiver. Our calculations show that the WLE receiver has a computational complexity close to the blind one.
4. Moreover, an exact expression is derived for the Cramer-Rao lower bound (CRLB) of the channel estimation in the presence of the I/Q imbalance and IGN. This expression can be used as a benchmark to predict and evaluate the performance of the estimators.
5. We find the APEP assuming Beckmann fading channel model. In this model, no assumptions on the statistics of the amplitudes and phases of the fading channel are assumed. This leads to a more general fading channel model, where most of the well-known fading channel models can be considered as special cases of this general model.

### 1.3 Thesis Outline

The rest of the thesis is organized as follows:

In Chapter 2, we introduce some relevant background on the fundamentals of com-

munication systems architecture, complex random vectors, fading channel models. We also briefly introduce the various types of functional conditions of wireless communications such as imperfect CSI, imperfect I/Q balance, and IGN. Finally, multiple access and space modulation techniques are discussed at the end of the chapter.

In Chapter 3, the system and channel models of underlay CR are presented. Then, optimal and WLE are receiver designs are suggested to tackle the I/Q imbalance effects at the secondary system transceivers. After that, the complexity analysis of the suggested designs are presented. The results are then discussed.

In Chapter 4, the system and channel models of QSM MIMO are presented. An optimal receiver design to tackle the I/Q imbalance effects is discussed. Following that, SSK MIMO system is discussed. Different MIMO scenarios are studied in the numerical analysis and results section.

In Chapter 5, the system and channel models of two user NOMA are presented. Then, optimal receiver designs are derived to tackle the effects of I/Q imbalance at both users. Moreover, the impacts of imperfect SIC at the user with strong channel conditions are explored. Also, the effect of power allocation factor on the system performance is presented. Finally, the results are discussed.

In Chapter 6, we offer a summary of our investigation and some important conclusions. We also suggest some potential topics for future research.

Appendices A and B contain the detailed proofs of chapters 3 and 4.

## 1.4 List of Publications

- **Related to the thesis**

1. M. M. Alsmadi, N. Abu Ali, M. Hayajneh, and S. S. Ikki, "Down-link NOMA networks in the presence of IQI and imperfect SIC: Receiver design and performance analysis," *IEEE Transactions on Vehicular Technology*, pp. 1-1, 2020.

I am the main contributor of this work, and I played a leading role in the theoretical modeling and planning of the publication.

2. M. Alsmadi, A. E. Canbilen, N. A. Ali, S. S. Ikki and E. Basar, "Cognitive Networks in the Presence of I/Q Imbalance and Imperfect CSI: Receiver Design and Performance Analysis," in *IEEE Access*, vol. 7, pp. 49 76549 777, 2019..

I am the main contributor of this work, and I played a leading role in the theoretical modeling and planning of the publication.

3. A. E. Canbilen, M. M. Alsmadi, E. Basar, S. S. Ikki, S. S. Gultekin and I. Develi, "Spatial Modulation in the Presence of I/Q Imbalance: Optimal Detector and Performance Analysis," in *IEEE Communications Letters*, vol. 22, no. 8, pp. 1572-1575, Aug. 2018.

I helped in fromulating the research problem and performed the related simulations and the required revisions.

4. M. M. Alsmadi, and S. S. Ikki, "SSK in the presence of improper Gaussian noise: Optimal receiver design and error analysis," *2018 IEEE Wireless Communications and Networking Conference (WCNC), Barcelona, 2018*, pp. 1-6.

I am the main contributor of this work, and I played a leading role in the theoretical modeling and planning of the publication.

5. M. Alsmadi, A. E. Canbilen, S. S. Ikki, E. Basar, S. Gultekin, and I. Develi, "Imperfect CSI and improper Gaussian noise effects on SSK: optimal detection and error analysis," in *2018 IEEE Global Communications Conference: Signal Processing for Communications (Globecom2018 SPC), Abu Dhabi, United Arab Emirates, Dec. 2018*.

I am the main contributor of this work, and I played a leading role in the theoretical modeling and planning of the publication.

#### • Unrelated to the thesis

1. A. RazaCheema, M. Alsmadi and S. Ikki, "Survey of Identity-Based Attacks Detection Techniques in Wireless Networks Using Received Signal Strength," *2018 IEEE Canadian Conference on Electrical & Computer Engineering (CCECE), Quebec City, QC, 2018*, pp. 1-6.

I helped in the literature review and writtting the paper.

# Chapter 2

## Background and Preliminaries

### 2.1 Communications System Architectures

Modern digital communication systems require considerable digital signal processing (DSP) and advanced analog circuitry. On a high level, the communication system can be represented using some basic stages: starting from a bitstream at the transmitter to a physical channel and ending with a bitstream at the receiver. This can be illustrated in Fig. 2.1. In an I/Q-based RF transmitter, a digital signal is converted to an analog one using a digital to analog converter (DAC). The transmitted signal is then modulated (up-converted) to a higher RF in order to be transmitted. Consequently, there are two stages of signal processing, digital and analog. DSP chips can perform modulation and pulse-shape filtering in the digital stage. Because the signal processing is performed digitally, the error is minimal. On the other hand, in the analog stage, the signal is subject to many sources of analog impairments. At the receiver, analog to digital converter (ADC) is required to convert the signal from an analog signal to a digital one. In addition, the received signal is demodulated (down-converted) to retrieve the baseband transmitted signal. The two typical approaches to up-conversion and down-conversion are direct (homodyne) conversion, and heterodyne (intermediate frequency) conversion.

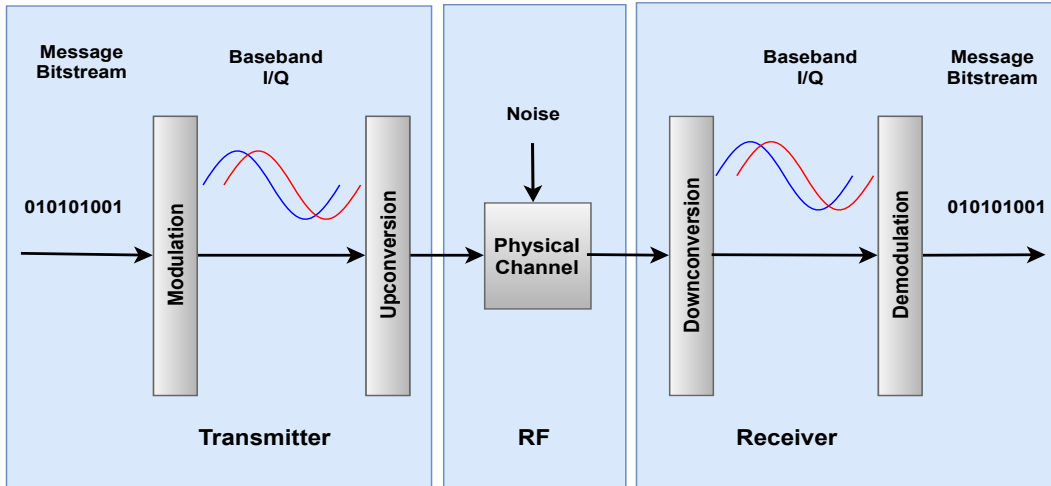


Figure 2.1: Block diagram of a typical communication system.

The heterodyne up-conversion method uses an intermediate frequency (IF). With this method, the baseband in-phase (I) and quadrature-phase (Q) signals first undergo direct up-conversion to the IF. After that, they are mixed with an additional local oscillators (LO) to reach the RF frequency. Fig. 2.2 expresses the heterodyne up-conversion approach.

As the figure shows, digital up-conversion to an IF occurs first. Then the IF digital signal is generated by a single DAC before being up-converted to a RF signal. Here, the maximum RF bandwidth depends on the IF frequency. For example, for an IF of 20 MHz, the maximum RF bandwidth is 40 MHz and requires a DAC with 40 MHz of bandwidth or greater. However, this typically requires wider bandwidth DACs, which are more susceptible to errors. In addition, existing filters after the multiple stages of LOs require more complicated circuitry. Therefore, most commercial circuits are implemented relying on direct up-conversion because of their low-cost and simplicity.

The direct-conversion transceiver is built upon the principle of directly up-converting the baseband signal to RF at the transmitter and directly down-converting the received signal at the receiver [28–30]. In the direct up-conversion, the digital I and Q are converted to analog I and Q signals first. Then, they are mixed with respective I and Q versions (90°degrees out of phase) of a LO. The LO frequency is the carrier frequency of the RF signal. Finally, the translated I and Q components are summed (or subtracted) to produce

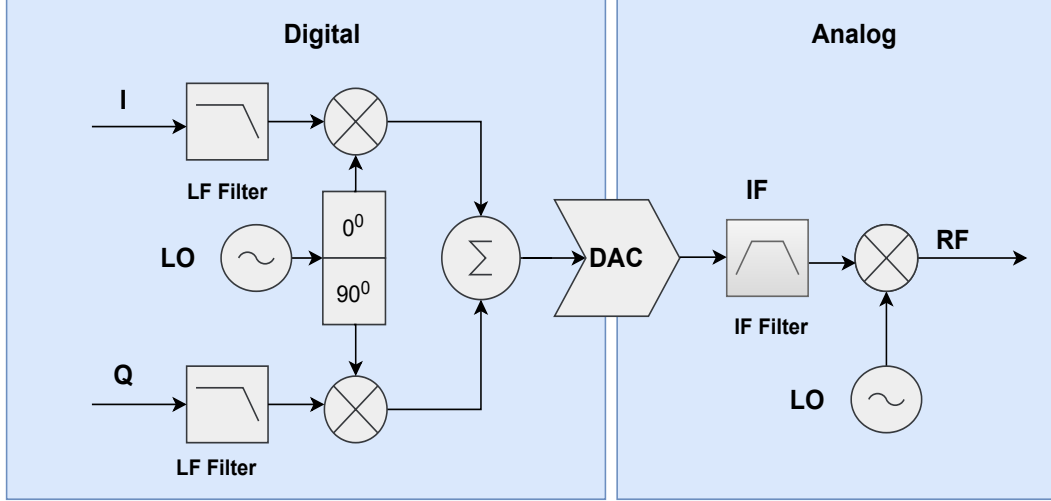


Figure 2.2: Heterodyne up-conversion RF transmitter's block diagram.

the final RF signal. Fig. 2.3 expresses the direct up-conversion approach.

In direct down-conversion, the received signal is amplified by a low-noise amplifier, and then passed through a LO quadrature mixer. After that, I and Q parts are filtered by LPFs before they go through an ADC. Fig. 2.4 expresses the direct down-conversion approach. As shown in Figs. 2.3 and 2.4, direct-conversion transceivers have a simple, low cost and flexible structure with less analog components and low power implementation [31]. Since direct-conversion transceivers convert the RF signal directly to the baseband instead of using an IF, it does not need either external IF or image rejection filters [31]. Beside these advantages, it is appropriate for higher levels of integration [13] because no need to use IF filters. As such, direct-conversion transceivers have attracted remarkable attention in next-generation wireless communication system studies, which require flexible and software reconfigurable transceivers that are capable to satisfy demands of desired quality of service [20]. This is directly attributable to the fact that direct-conversion transceivers require less analog components and low power implementation. However, HWIs, such as nonlinearities, phase noise and I/Q imbalance, limit the direct-conversion transceivers system performance in practical scenarios [20, 31, 32]. Specifically, they can limit the deployment of high frequency circuitry, and result in distinct phase/amplitude errors [33]. Hence, considering the effects of HWIs play a major role in the analysis of the system performance and the proposal of effective compensation techniques [13].

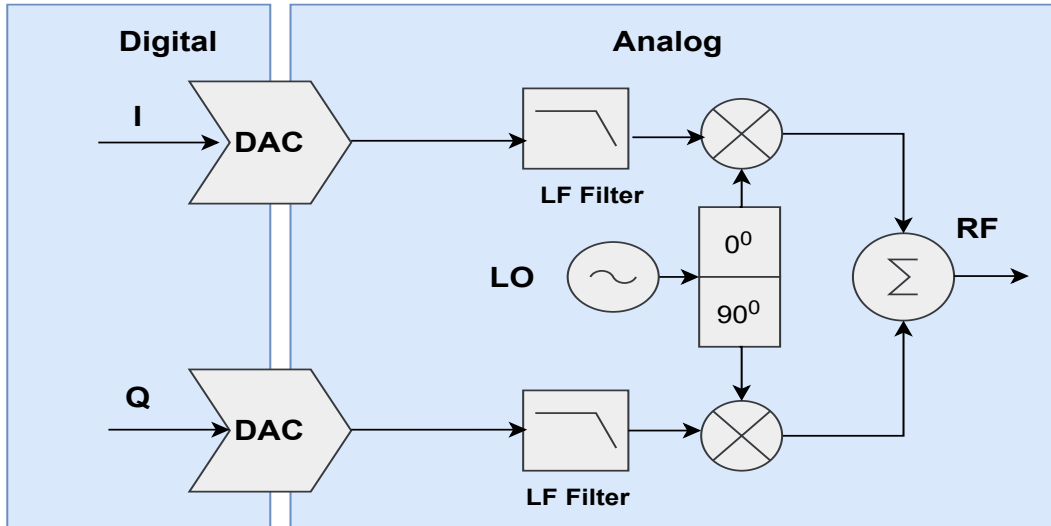


Figure 2.3: Direct up-conversion RF transmitter's block diagram.

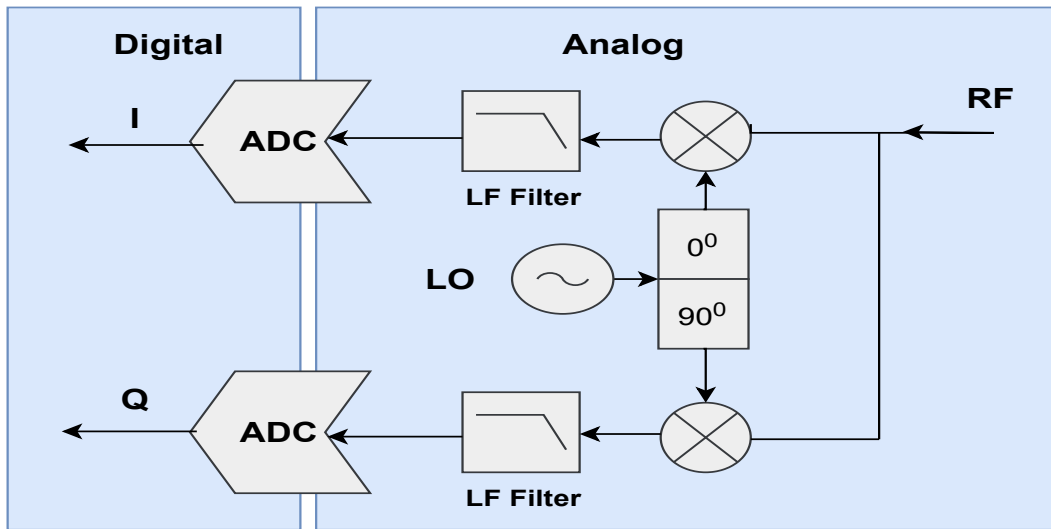


Figure 2.4: Direct down-conversion RF transmitter's block diagram.

## 2.2 Complex Random Vectors

Let  $\mathbf{x}$  be a vector of complex RVs where  $\mathbf{x} = \mathbf{u} + j\mathbf{v}$ , and  $\mathbf{u}$  and  $\mathbf{v}$  are two real valued vectors of RVs. Denoting  $\mathbf{z}$  to be the composite real random vector  $\mathbf{z} = [\mathbf{u}^T \ \mathbf{v}^T]^T$ . The

mean vector  $\boldsymbol{\mu}_z$  of  $\mathbf{z}$  is given by

$$\boldsymbol{\mu}_z = \mathbb{E}\{\mathbf{z}\} = \begin{bmatrix} \mathbb{E}\{\mathbf{u}\} \\ \mathbb{E}\{\mathbf{v}\} \end{bmatrix} = \begin{bmatrix} \boldsymbol{\mu}_u \\ \boldsymbol{\mu}_v \end{bmatrix}, \quad (2.1)$$

and its covariance matrix is given by

$$\mathbf{R}_{zz} = \mathbb{E}(\mathbf{z} - \boldsymbol{\mu}_z)(\mathbf{z} - \boldsymbol{\mu}_z)^T = \begin{bmatrix} \mathbf{R}_{uu} & \mathbf{R}_{uv} \\ \mathbf{R}_{uv}^T & \mathbf{R}_{vv} \end{bmatrix}. \quad (2.2)$$

Here,  $\mathbf{R}_{uu} = \mathbb{E}(\mathbf{u} - \boldsymbol{\mu}_u)(\mathbf{u} - \boldsymbol{\mu}_u)^T$ ,  $\mathbf{R}_{vv} = \mathbb{E}(\mathbf{v} - \boldsymbol{\mu}_v)(\mathbf{v} - \boldsymbol{\mu}_v)^T$ , and  $\mathbf{R}_{uv} = \mathbb{E}(\mathbf{u} - \boldsymbol{\mu}_u)(\mathbf{v} - \boldsymbol{\mu}_v)^T$ . It was shown in [34] that the complete second-order characterization of  $\mathbf{x}$  can be completely characterized by its augmented vector  $\hat{\mathbf{x}}$ , where the mean vector  $\boldsymbol{\mu}_{\hat{\mathbf{x}}}$  and the augmented covariance matrix  $\mathbf{R}_{\hat{\mathbf{x}}\hat{\mathbf{x}}}$  are given by

$$\boldsymbol{\mu}_{\hat{\mathbf{x}}} = \begin{bmatrix} \mathbb{E}\{\mathbf{x}\} \\ \mathbb{E}\{\mathbf{x}^*\} \end{bmatrix} = \begin{bmatrix} \boldsymbol{\mu}_u + j\boldsymbol{\mu}_v \\ \boldsymbol{\mu}_u - j\boldsymbol{\mu}_v \end{bmatrix}, \quad (2.3)$$

$$\mathbf{R}_{\hat{\mathbf{x}}\hat{\mathbf{x}}} = \mathbb{E}(\hat{\mathbf{x}} - \boldsymbol{\mu}_{\hat{\mathbf{x}}})(\hat{\mathbf{x}} - \boldsymbol{\mu}_{\hat{\mathbf{x}}})^H = \begin{bmatrix} \mathbf{R}_{xx} & \tilde{\mathbf{R}}_{xx} \\ \tilde{\mathbf{R}}_{xx}^* & \mathbf{R}_{xx}^* \end{bmatrix}, \quad (2.4)$$

where the normal (Hermitian) covariance matrix  $\mathbf{R}_{xx}$  is given by

$$\mathbf{R}_{xx} = \mathbb{E}(\mathbf{x} - \boldsymbol{\mu}_x)(\mathbf{x} - \boldsymbol{\mu}_x)^H = \mathbf{R}_{uu} + \mathbf{R}_{vv} + j(\mathbf{R}_{uv}^T - \mathbf{R}_{uv}) = \mathbf{R}_{xx}^H, \quad (2.5)$$

and the pseudo-covariance matrix  $\tilde{\mathbf{R}}_{xx}$  is given by

$$\tilde{\mathbf{R}}_{xx} = \mathbb{E}(\mathbf{x} - \boldsymbol{\mu}_x)(\mathbf{x} - \boldsymbol{\mu}_x)^T = \mathbf{R}_{uu} - \mathbf{R}_{vv} + j(\mathbf{R}_{uv}^T + \mathbf{R}_{uv}) = \tilde{\mathbf{R}}_{xx}^T. \quad (2.6)$$

The pseudo-covariance matrix which uses the transpose rather than the Hermitian is called conjugate covariance matrix or complementary covariance matrix. Both the Hermitian and the transpose covariance matrices are important to fully characterize the complex random vector. This can be explained by noting that if  $\mathbf{u}$  and  $\mathbf{v}$  are perpendicular and correlated then the diagonal of  $\mathbf{R}_{xx}$  does not contain any information about the correlation between each element of RVs in  $\mathbf{u}$  and the corresponding RVs in  $\mathbf{v}$ . This correlation is preserved in  $\tilde{\mathbf{R}}_{xx}$  which confirms the importance of both kinds of covariance matrices.

*Definition 1:* A zero mean complex RV is called a proper or circular RV if its pseudo-variance is equal to zero, otherwise it is called non-circular or improper RV [35–37]. From this definition, The pseudo-variance equals to zero if and only if the following two conditions are satisfied:

$$\mathbf{R}_{uu} = \mathbf{R}_{vv}. \quad (2.7)$$

$$\mathbf{R}_{uv} = -\mathbf{R}_{uv}^T. \quad (2.8)$$

If  $\mathbf{x}$  is proper RV, its pseudo-covariance matrix  $\tilde{\mathbf{R}}_{\mathbf{x}\mathbf{x}} = 0$  and its Hermitian covariance matrix is

$$\mathbf{R}_{\hat{\mathbf{x}}\hat{\mathbf{x}}} = 2\mathbf{R}_{uu} - j\mathbf{R}_{uv} = 2\mathbf{R}_{vv} + 2j\mathbf{R}_{uv}^T. \quad (2.9)$$

If  $x$  is a scalar RV, the (normal) Hermitian covariance of  $x$  is given by [35–37]

$$\sigma_x^2 = \sigma_u^2 + \sigma_v^2, \quad (2.10)$$

and the pseudo-covariance is given by

$$\tilde{\sigma}_x^2 = \sigma_u^2 - \sigma_v^2 + j2\sigma_{uv}. \quad (2.11)$$

However, if  $x$  is proper, then its pseudo-covariance is equal to zero. Consequently,  $\sigma_{uu} = \sigma_{vv}$ , and  $\sigma_{uv} = 0$ . There are two special cases for improper RVs. Case 1 is when the real and imaginary parts are correlated and have equal variances (identical correlated RV). Case 2 is when the real and imaginary parts are not correlated but have different variances (non-identical uncorrelated RV).

*Definition 2:* The impropriety degree of a complex RV  $x$  (with finite variance) is measured by the noncircularity coefficient  $\tau_x$  and defined as the quotient between the pseudo-variance and the variance [35–37].  $\tau_x$  can be written as

$$\tau_x = \left( \frac{\sigma_u^2 - \sigma_v^2}{\sigma_u^2 + \sigma_v^2} \right) + j \left( \frac{2\sigma_{uv}}{\sigma_u^2 + \sigma_v^2} \right). \quad (2.12)$$

As it can be seen from (2.12), the real part of  $\tau_x$  measures the power difference between  $u$  and  $v$  while the imaginary part measures the correlation between them. Those real and imaginary parts are normalized. Based on this,  $\tau_x$  is independent from the changes

in the power of  $x$  and only it hides information about its proneness. Again, if  $u$  and  $v$  are perpendicular and correlated then the covariance  $\sigma_x^2 = \sigma_u^2 + \sigma_v^2$  does not contain any information about the correlation between  $u$  and  $v$  while this information can be found in  $\tilde{\sigma}_x^2 = \sigma_u^2 - \sigma_v^2 + j2\sigma_{uv}$ . This demonstrates the importance of both, the covariance and pseud-variance to fully characterize the complex RV.

## 2.3 MGF of Quadratic Form of Noncentral Chi-Squared Distribution

Let  $\mathbf{A}$  denote an  $n \times n$  symmetric matrix with real entries and let  $\mathbf{x}$  denote an  $n \times 1$  column vector. The quadratic expression of a correlated Gaussian RVs vector  $\mathbf{x} \sim \mathcal{N}(\boldsymbol{\mu}, \boldsymbol{\Sigma})$  is given by

$$Q(\mathbf{x}) = \mathbf{x}^T \mathbf{A} \mathbf{x}, \quad (2.13)$$

where  $\boldsymbol{\mu}$  is the mean vector and  $\boldsymbol{\Sigma}$  is the positive definite covariance of  $\mathbf{x}$ , and matrix  $\mathbf{A}$  is the quadratic matrix. Assuming  $\mathbf{y} = \boldsymbol{\Sigma}^{-\frac{1}{2}} \mathbf{x}$ ,  $Q(\mathbf{x})$  can be rewritten as

$$Q(\mathbf{x}) = \mathbf{y}^T \boldsymbol{\Sigma}^{\frac{1}{2}} \mathbf{A} \boldsymbol{\Sigma}^{\frac{1}{2}} \mathbf{y}. \quad (2.14)$$

Denoting  $\mathbf{P}$  to be an orthonormal  $p \times p$  matrix which diagonalizes  $\boldsymbol{\Sigma}^{\frac{1}{2}} \mathbf{A} \boldsymbol{\Sigma}^{\frac{1}{2}}$ . This means that  $\mathbf{P}^T \boldsymbol{\Sigma}^{\frac{1}{2}} \mathbf{A} \boldsymbol{\Sigma}^{\frac{1}{2}} \mathbf{P} = \text{Diag}(\lambda_1, \dots, \lambda_p)$ . As shown in [38],  $Q(\mathbf{x})$  can be rewritten as

$$Q(\mathbf{x}) = \sum_{j=1}^p \lambda_j (U_j + b_j)^2, \quad (2.15)$$

where  $\lambda_1, \dots, \lambda_p$  represents the eigenvalues of  $\boldsymbol{\Sigma}^{\frac{1}{2}} \mathbf{A} \boldsymbol{\Sigma}^{\frac{1}{2}}$ ,  $b_1, \dots, b_p = (\mathbf{P}^T \boldsymbol{\Sigma}^{-\frac{1}{2}} \boldsymbol{\mu})^T$ , and  $U_j$  represents independently distributed standard normal RVs. Based on this,  $Q(\mathbf{x})$  is distributed as a linear combination of independent noncentral (central if  $b_i = 0$ ) chi-square variables.

The moment generating function (MGF) of the quadratic form in (2.15) can be given in terms of the eigenvalues of  $\boldsymbol{\Sigma}^{\frac{1}{2}} \mathbf{A} \boldsymbol{\Sigma}^{\frac{1}{2}}$  as in the following equation [38–41]

$$M_Q(t) = \prod_{j=1}^p \frac{1}{\sqrt{1 - 2t\lambda_j}} \exp \left\{ t \sum_{j=1}^p \frac{b_j^2 \lambda_j}{1 - 2t\lambda_j} \right\}. \quad (2.16)$$

If  $\boldsymbol{\mu} = \mathbf{0}$ , then  $Q(\mathbf{x})$  is distributed as a linear combination of independent central chi-square variables. In this case, (2.16) can be abbreviated to

$$M_Q(t) = \prod_{j=1}^p \frac{1}{\sqrt{1 - 2t\lambda_j}}. \quad (2.17)$$

## 2.4 Beckmann Channels

The complex fading coefficient  $h$  can be expressed in terms of its real and imaginary components as,

$$h = \sum_{i=0}^{L-1} (h_i^I + jh_i^Q) = h^I + jh^Q. \quad (2.18)$$

Thus,  $h^I$  and  $h^Q$ , which are the real and imaginary components of the fading coefficient are derived by assuming a sufficiently large number of random multipath components  $h_i^I$  and  $h_i^Q$ . This assumption is practical and valid, especially in a rich urban setting which may have a large number of scattering surfaces. Central Limit Theorem states that a normalized RV derived from the sum of a large number of independent identically distributed random components converges to a Gaussian RV. By assuming a sufficiently large number of paths and depending on the Central Limit Theorem [42], the fading channel can be modeled as a complex Gaussian RV.

This topic was originally addressed by Beckmann [43, 44] in its more general form by assuming an arbitrary mean and variance for the real and imaginary parts.  $h$  can be modeled as  $\mathcal{CN}(\boldsymbol{\mu}_h, \boldsymbol{\sigma}_h^2)$  where the mean vector and the covariance matrix of  $h$  are given by  $\boldsymbol{\mu}_h$  and  $\boldsymbol{\sigma}_h^2$  respectively

$$\boldsymbol{\mu}_h = \begin{bmatrix} \mu_{h^I} & \mu_{h^Q} \end{bmatrix}, \quad \boldsymbol{\sigma}_h^2 = \begin{bmatrix} \sigma_{h^I}^2 & \rho_h \sigma_h^Q \sigma_h^I \\ \rho_h \sigma_h^Q \sigma_h^I & \sigma_{h^Q}^2 \end{bmatrix}. \quad (2.19)$$

The joint probability density function (PDF) of the  $h^I$  and  $h^Q$  components is given by

$$f_{h^I h^Q}(x, y) = \frac{1}{2\pi \sigma_{h^I} \sigma_{h^Q} \sqrt{1 - \rho_h^2}} \times \exp \left\{ -\frac{1}{2(1 - \rho_h^2)} \left[ \left( \frac{x - \mu_{h^I}}{\sigma_{h^I}} \right)^2 + \left( \frac{y - \mu_{h^Q}}{\sigma_{h^Q}} \right)^2 - 2\rho_h \frac{(x - \mu_{h^I})(y - \mu_{h^Q})}{\sigma_{h^I} \sigma_{h^Q}} \right] \right\}. \quad (2.20)$$

Table 2.1: The relation between Beckmann fading model and other fading models in the literature. The Beckmann fading parameters are in bold.

Channels	Beckman Fading Parameters
One-sided Gaussian	$\mathbf{r} = 1, \quad \mathbf{q} = 0, \quad \mathbf{K} = 0, \quad \boldsymbol{\rho}_h = 0$
Rayleigh	$\mathbf{r} = 1, \quad \mathbf{q} = 1, \quad \mathbf{K} = 0, \quad \boldsymbol{\rho}_h = 0$
Hoyt (Nakagami-q)	$\mathbf{r} = 1, \quad \mathbf{q} = q, \quad \mathbf{K} = 0, \quad \boldsymbol{\rho}_h = 0$
Rician with parameter k	$\mathbf{r} = 1, \quad \mathbf{q} = 1, \quad \mathbf{K} = K, \quad \boldsymbol{\rho}_h = 0$
Another form Rician without LoS	$\mathbf{r} = 1, \quad \mathbf{q} = 1, \quad \mathbf{K} = 0, \quad \boldsymbol{\rho}_h = \rho_h$

Making no assumptions on the statistics of the amplitudes and phases of the fading channel (i.e., allowing  $h^I$  and  $h^Q$  to have different means and variances, or being correlated) leads to a more general fading channel model, where most of the well-known fading channel models can be considered as special cases of this general model. For example, when the quadrature components are Gaussian, uncorrelated, zero mean, and equal in variance, this results in the Rayleigh PDF. The Rician PDF is the result when the variances are equal and either one or both components have non-zero mean, whereas the Hoyt PDF assumes zero means and non-equal variances. A form of the Rician distributed envelope also results when the quadrature components are correlated but both of them have zero means [45]. Furthermore, Beckmann channel model can be described by the following parameters

$$q^2 = \frac{\sigma_{h^I}^2}{\sigma_{h^Q}^2}, \quad r^2 = \frac{\mu_{h^I}^2}{\mu_{h^Q}^2}, \quad k = \frac{\mu_{h^I}^2 + \mu_{h^Q}^2}{\sigma_{h^I}^2 + \sigma_{h^Q}^2}, \quad \Omega = \mu_{h^I}^2 + \mu_{h^Q}^2 + \sigma_{h^I}^2 + \sigma_{h^Q}^2. \quad (2.21)$$

As in Rician fading model, the parameter  $K$  indicates the ratio between the line of sight (LoS) and non-LoS power. Moreover, as in Hoyt (Nakagami-q) fading model  $q^2$  measures the power imbalance between the quadrature non-LoS components. The parameter  $r^2$  indicates the power imbalance between quadrature LoS components. Finally, the parameter  $\Omega$  indicates the average power of the fading channel. Table. 2.1 shows the relation between Beckmann fading model and other fading models in the literature.

To study the effect of fading channel  $h$  on the wireless communication system, the

envelope of the channel is needed.  $h$  in (2.18) can be given as

$$h = Re^{j\theta}, \quad (2.22)$$

where  $R = \sqrt{(h^I)^2 + (h^Q)^2}$  and  $\theta = \tan^{-1}(h^Q/h^I)$  are the envelope and phase of  $h$ , respectively. The envelope's PDF of  $R$  can be given as [46]

$$p_R(r) = \frac{r}{2\sigma_{h^I}\sigma_{h^Q}} \exp\left[-\frac{1}{2}\left(\frac{\mu_{h^I}^2}{\sigma_{h^I}^2} + \frac{\mu_{h^Q}^2}{\sigma_{h^Q}^2} + \frac{r^2}{2\sigma_{h^I}^2} + \frac{r^2}{2\sigma_{h^Q}^2}\right)\right] \sum_{n=0}^{\infty} \frac{\varepsilon_n I_n\left(\frac{r^2}{4\sigma_{h^I}^2} - \frac{r^2}{4\sigma_{h^Q}^2}\right)}{\left[\left(\frac{r\mu_{h^I}}{\sigma_{h^I}^2}\right)^2 + \left(\frac{r\mu_{h^Q}}{\sigma_{h^Q}^2}\right)^2\right]^n} \times \left\{ I_{2n}\left(\sqrt{\left(\frac{r\mu_{h^I}}{\sigma_{h^I}^2}\right)^2 + \left(\frac{r\mu_{h^Q}}{\sigma_{h^Q}^2}\right)^2}\right) \right\} \sum_{k=0}^n \delta_k C_k^n \left[\left(\frac{r\mu_{h^I}}{\sigma_{h^I}^2}\right)^2 - \left(\frac{r\mu_{h^Q}}{\sigma_{h^Q}^2}\right)^2\right]^{n-k} \left(2\frac{r^2\mu_{h^I}\mu_{h^Q}}{\sigma_{h^I}^2\sigma_{h^I}^2}\right)^k \Bigg\}, \quad (2.23)$$

where,  $C_k^n$  is the binomial coefficient,  $I_n(\cdot)$  is the  $n$ -th order modified Bessel function of the first kind where

$$\varepsilon_n = \begin{cases} 1, & \text{if } n = 0 \\ 2, & \text{if } n \neq 0 \end{cases}, \quad (2.24)$$

$$\delta_k = \begin{cases} 0 & \text{if } k \text{ is even} \\ 2(-1)^{k/2} & \text{if } k \text{ is odd} \end{cases}. \quad (2.25)$$

## 2.5 Imperfect CSI Model

In practical systems, the exact CSI is not available at the receiver and one of the channel estimators such as ML or mean square error estimators is used to get a channel estimate. In this case, the channel estimate in the presence of imperfect CSI can be modeled as [47–53]

$$h = \hat{h} + e, \quad (2.26)$$

where  $\hat{h}$  is the channel estimation and  $e$  is the channel estimation error. Here we assume that  $h$  and  $\hat{h}$  are jointly ergodic and stationary Gaussian processes. Further, assuming orthogonality between the channel estimate and the estimation error. Note that the variance of  $e$  includes the information of the channel estimation quality [47–53].

This thesis studies practical scenarios of different wireless communication systems. These practical scenarios including imperfect CSI, imperfect SIC, I/Q imbalance, and additive IGN at the receiver. It was shown in our works [54, 55] that the channel estimation error can be modeled as an improper RV if the receiver noise is IGN and as a proper RV if receiver noise is proper Gaussian noise (PGN). In addition, it was shown that the channel estimation error when using an optimal estimator that considers the I/Q parameters at the transmitter/receiver can be modeled as a proper RV even though the I/Q imbalance changes the receiver noise from PGN to IGN. Based on this, the channel estimation error in the presence of IGN can be modeled as  $\mathcal{CN}(\mathbf{0}, \boldsymbol{\sigma}_e^2)$  where the covariance matrix  $\boldsymbol{\sigma}_e^2$  is given by

$$\boldsymbol{\sigma}_e^2 = \begin{bmatrix} \sigma_{eI}^2 & \rho_e \sigma_e^Q \sigma_e^I \\ \rho_e \sigma_e^Q \sigma_e^I & \sigma_{eQ}^2 \end{bmatrix}.$$

Here, it is worth noting that  $\boldsymbol{\sigma}_e^2$  indicates the quality of the estimation and its value depends on the channel dynamics and the estimation method.

## 2.6 I/Q Imbalance Model

The direct-conversion architecture is widely used in low-cost, low-power transceivers in modern wireless systems. However, HWIs of practical systems occur at LO, phase shifter and I/Q mixer. Consequently, due to the imperfections: 1) the phase difference between the I and Q parts of the transmitter and/or receiver signals might not be exactly 90 degrees which is called phase imbalance, 2) small variations might be between the amplitude of the I and Q parts of the signal at the transmitter and/or receiver, which is called amplitude imbalance. Then, I/Q imbalance can dramatically affect the system's performance by changing the transmitted signal at the transmitter or corrupting the received signal at the receiver.

Let us explain how the amplitude and phase imbalances affect receiver performance. Denoting  $\xi_r$  and  $\beta_r$  to be the receivers' amplitude and phase imbalances respectively. The

carrier signal of an imbalanced LO with carrier frequency  $f_c$  can be represented by

$$x_{LO}(t) = \cos(2\pi f_c t) - j\xi_r \sin(2\pi f_c t + \beta_r). \quad (2.27)$$

considering the exponential representations of cosine and sine (2.27) can be written as

$$x_{LO}(t) = K_1 e^{-j\pi f_c t} + K_2 e^{j\pi f_c t}, \quad (2.28)$$

where  $K_1 = \frac{1}{2}(1 + \xi_r e^{-j\beta_r})$  and  $K_2 = \frac{1}{2}(1 - \xi_r e^{j\beta_r})$  are the I/Q imbalance parameters at the receiver. Considering the transmitted passband wireless signal  $\bar{s}(t)$ , which is sent across a wireless channel. Such a passband signal can be described analytically as  $\bar{s}(t) = 2\Re\{s(t)e^{2\pi f_c t}\}$ . Here,  $s(t)$  is the complex baseband representation of the transmitted signal. From [56], the received signal can be detected by using a low pass filter (LPF) for the signal  $\{\bar{s}(t).s_{LO}(t)\}$ . Based on this, the received impaired signal can be given by

$$y(t) = K_1 s(t) + K_2 s^*(t). \quad (2.29)$$

Therefore, in indirect-conversion receivers, the impact of I/Q mismatch can be seen as a self-image problem, where the complex conjugate of the baseband interferes with the baseband signal itself.

The effects of I/Q imbalance at the transmitter can be explained using the same logic as at the receiver. By denoting  $\xi_t$  and  $\beta_t$  to be the transmitters' amplitude and phase imbalances respectively, the carrier waveform of an imbalanced LO can be represented by

$$x_{LO}(t) = \cos(2\pi f_c t) + j\xi_t \sin(2\pi f_c t + \beta_t). \quad (2.30)$$

Therefore, the interpretation of self-image effects at the receiver is also applicable at the transmitter side, and the output of the transmitter under the effects of I/Q imbalance is

$$s(t) = G_1 x(t) + G_2 x^*(t), \quad (2.31)$$

where  $G_1 = \frac{1}{2}(1 + \xi_t e^{j\beta_t})$  and  $G_2 = \frac{1}{2}(1 - \xi_t e^{j\beta_t})$  are the I/Q imbalance parameters at the transmitter side.

Assuming a narrowband signal model, and assuming I/Q imbalance exists at both the transmitter and receiver sides, the transmitted baseband signal  $x$  is received as

$$\begin{aligned}
y &= K_1(\sqrt{E}hs + n) + K_2(\sqrt{E}hs + n)^* \\
&= K_1[\sqrt{E}h(G_1x + G_2x^*)] + K_2(\sqrt{E}h[G_1x + G_2x^*])^* + K_1n + K_2n^* \\
&= \sqrt{E}[(K_1G_1h + K_2G_2^*h^*)x + (K_1G_2h + K_2G_1^*h^*)x^*] + K_1n + K_2n^*, \tag{2.32}
\end{aligned}$$

where  $h$  is a flat-fading wireless channel,  $E$  is the transmitted energy, and  $n$  is the noise at the receiver. The term  $\sqrt{E}(K_1G_1h + K_2G_2^*h^*)x$  is the signal part, and the term  $\sqrt{E}(K_1G_2h + K_2G_1^*h^*)x^*$  is the image part. This image is treated as a self-interference signal. The IRR (which is known as signal-to-interference ratio (SIR)) can be calculated from (2.32) and given by

$$\text{IRR} = \frac{|K_1G_1h + K_2G_2^*h^*|^2|x|^2}{|K_1G_2h + K_2G_1^*h^*|^2|x^*|^2}. \tag{2.33}$$

If we disregard the effect of the channel (i.e., assume that  $h = 1$ ), then the above equation can be simplified to

$$\text{IRR} = \frac{|K_1|^2|G_1|^2 + |K_2|^2|G_2|^2}{|K_1|^2|G_2|^2 + |K_2|^2|G_1|^2}. \tag{2.34}$$

If the I/Q imbalance is at the transmitter side only, then  $K_1 = 1$  and  $K_2 = 0$  and IRR is given as

$$\text{IRR} = \frac{|G_1|^2}{|G_2|^2}. \tag{2.35}$$

If the I/Q imbalance is at the receiver side only, then  $G_1 = 1$  and  $G_2 = 0$  and IRR is given as

$$\text{IRR} = \frac{|K_1|^2}{|K_2|^2}. \tag{2.36}$$

If there are no I/Q imbalances at the transmitter or receiver, then IRR goes to  $\infty$ , this is the ideal case. Fig. 2.5 shows that small changes in I/Q parameters lead to significant changes in the IRR values. Equation (2.34) shows that the signaling constellation does not have any effect on the IRR value. At the same time, it is well-known that the I/Q imbalance

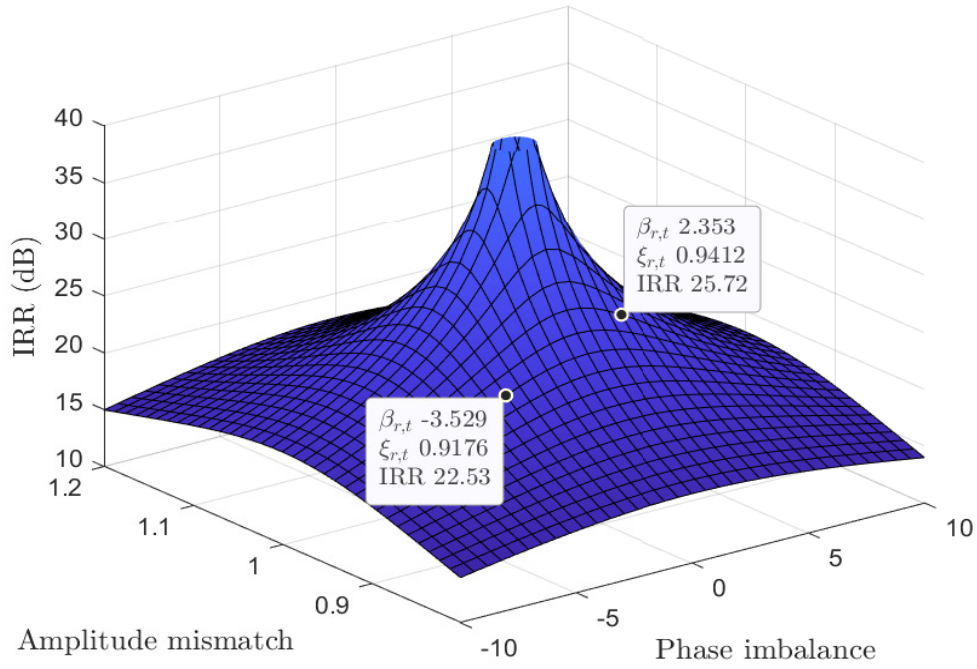


Figure 2.5: IRR values versus the amplitude mismatch and the phase imbalance. This figure assumes the transmitter and receiver have the same level of I/Q impairments.

effects become harsher with bigger signal constellations since the probability of incorrect detection increases when the distances between the constellations becomes smaller.

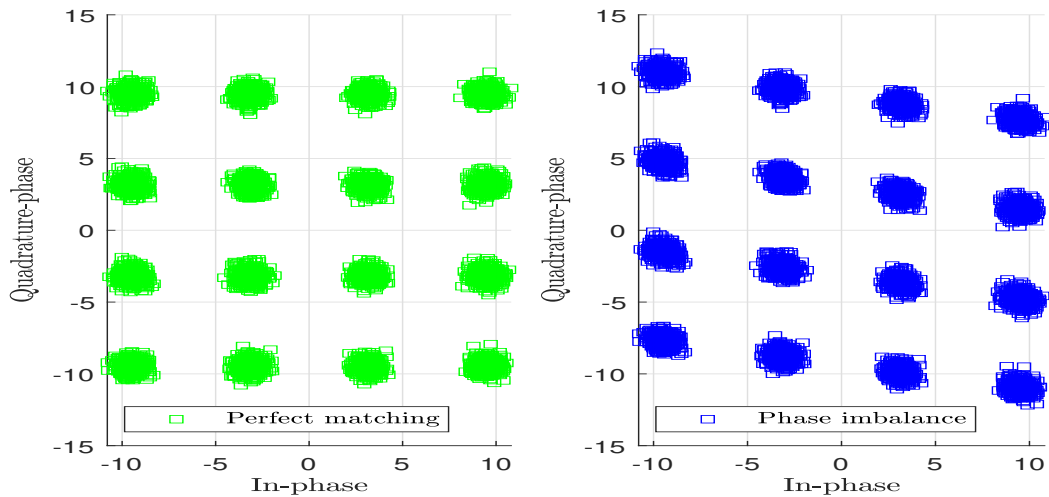


Figure 2.6: The result of phase imbalance when  $\beta_{t,r} = 10^\circ$ ,  $\xi_{t,r} = 1$ , and SNR=23 dB.

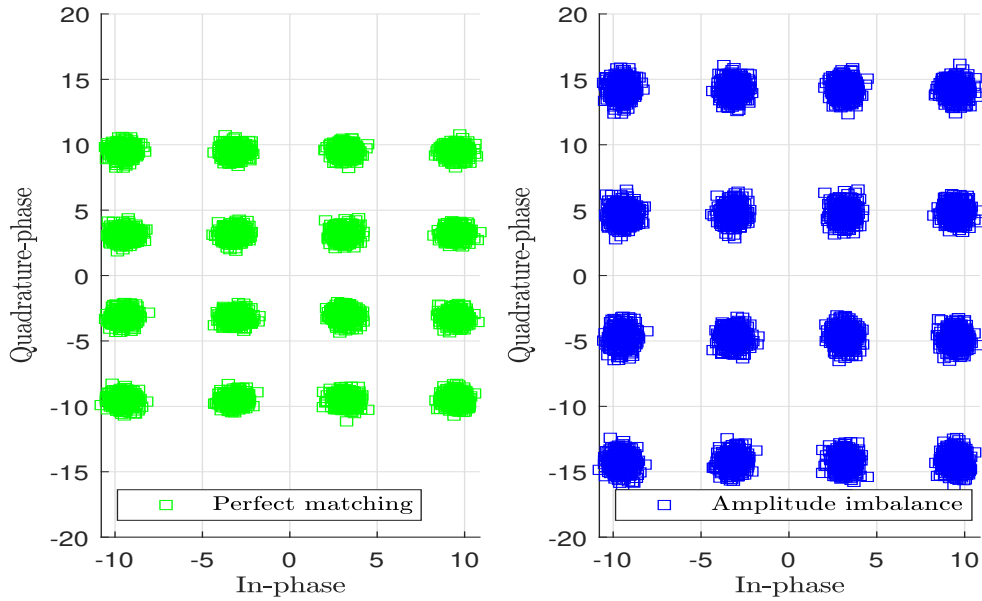


Figure 2.7: The result of amplitude imbalance when  $\beta_{t,r} = 0^\circ$ ,  $\xi_{t,r} = 1.5$ , and SNR=23 dB.

Figs. 2.6 and 2.7 show the effects of the phase and amplitude imbalance on the 16-QAM constellation diagram. The result of the phase imbalance appears as a rotation of the constellation diagram in the I/Q plane. The result of the amplitude imbalance appears as a stretching or shorting of the I component of symbols along the I axis. Fig. 2.8 illustrates the effects of the I/Q applied to the 4-QAM and 64-QAM signal constellation diagrams when  $\beta_{t,r} = 5^\circ$  and  $\xi_{t,r} = 1.2$ . As this figure shows the constellation impaired received symbols overlap with the baseband transmitted symbols when using 64-QAM. This means it may be impractical to obtain the baseband symbols when using the blind receiver to detect signals with higher modulation orders.

## 2.7 IGN Model

A zero mean complex RV is called a proper or circular RV if its pseudo-variance is equal to zero, otherwise it is called non-circular or improper. More details about this topic can be found in Section 2.2. Consequently, zero mean additive white Gaussian noise (AWGN) at the receiver is PGN if its real and imaginary parts are correlated and/or have different

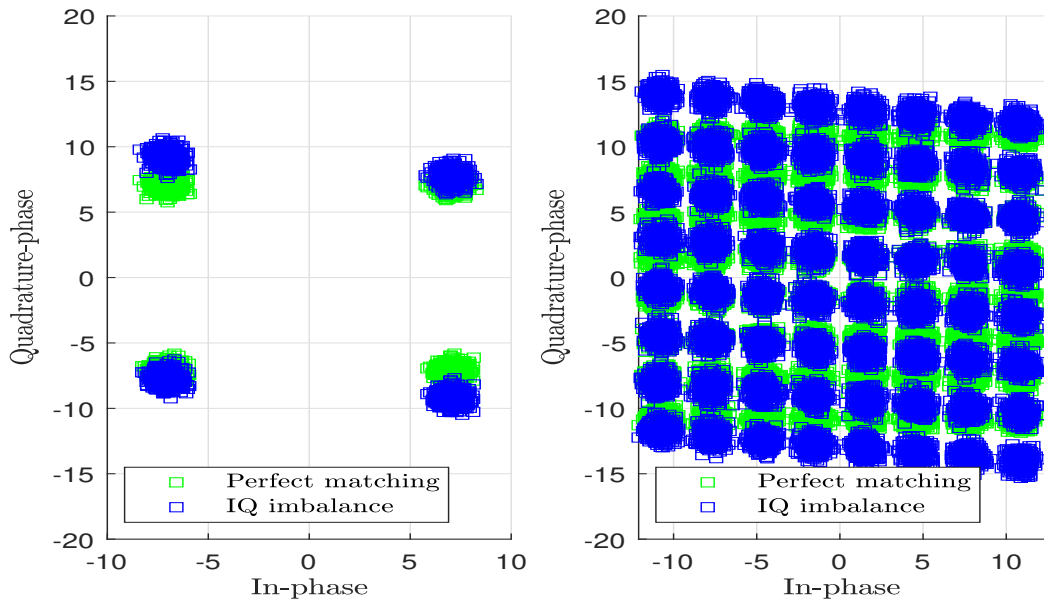


Figure 2.8: The result of transmitter and receiver I/Q imbalances applied to the 4-QAM and 64-QAM signal constellation diagrams when  $\beta_{t,r} = 5^\circ$ ,  $\xi_{t,r} = 1.2$ , and SNR=23 dB.

variances. The scattering diagrams in Fig. 2.9 give more insight information about the relation between the real part ( $x$ ) and imaginary part ( $y$ ) of the complex RV. There are two special cases for IGN. First is when the real and imaginary parts are correlated and have equal variances, case 3 in the figure. Second is when the real and imaginary parts are not correlated but have different variances, case 2. Case 1 represents the PGN while case 4 represents the general case of the IGN.

Examining the effects of HWIs on the system performance and choosing the proper detection designs requires a general model that can represent the wide range of HWIs. HWIs are modeled mostly in the literature as a proper Gaussian term at the transmitter and receiver [15, 57–64]. In several recent works, more general models are used to describe the HWIs. In these models, the HWIs are represented as improper Gaussian RVs [13, 14, 27, 33]. In addition, a more generalize model of AWGN at the receiver where the noise is assumed to be IGN was used in some works in the literature [65–67].

This thesis models the nonlinear effects of HWIs as a combination of I/Q imbalance and IGN. This assumption is justified in our design because, as stated before, I/Q imbalance

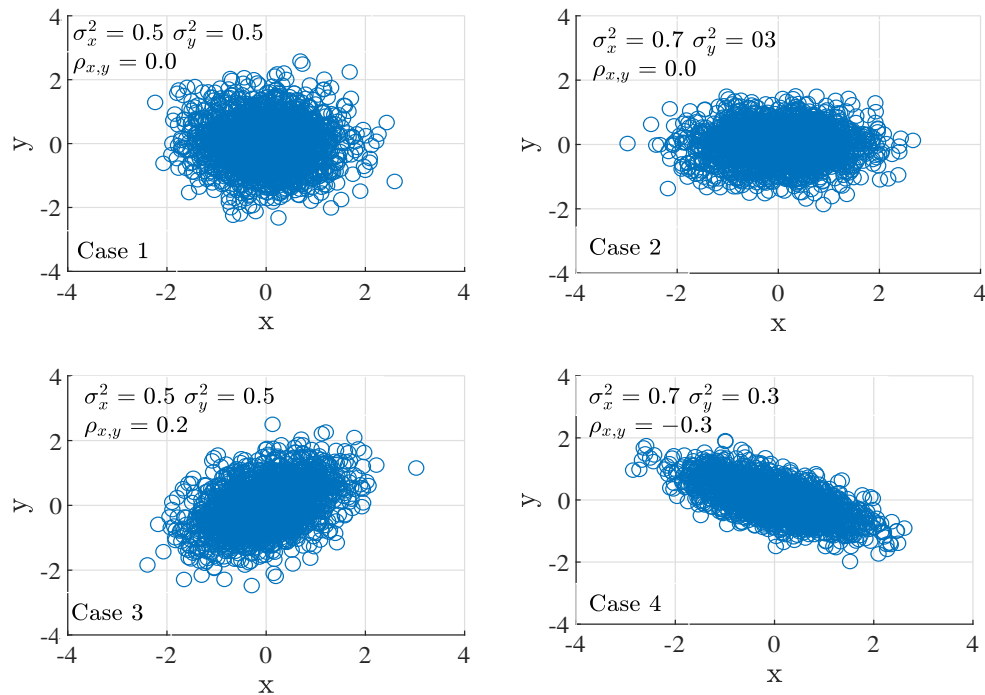


Figure 2.9: The scattering diagrams of zero mean additive white Gaussian noise.  $x$  is the real part and  $y$  is the imaginary part.

is one of the most significant source of nonlinear impairments in modern communication systems and all other impairments can be modeled as IGN with different variances for its real and imaginary parts.

## 2.8 Multiple Access Techniques

Multiple access techniques can be divided into two main schemes: orthogonal multiple access (OMA) and NOMA. When using OMA techniques, a single user is served in each orthogonal resource block. These orthogonal resources can be the time as in the time division multiple access (TDMA), the frequency as in the frequency division multiple access (FDMA), or the code as in the code division multiple access (CDMA). Hence, the maximum number of concurrently supported devices in an OMA scheme is limited by the number of orthogonal resources.

In contrast, NOMA can assign non-orthogonal resources to the users and hence overload the system. The ratio of the total number of users to the total number of orthogonal resources is called the overloading factor. At the receiver, advanced multi-user detection algorithms are required to separate the users. The NOMA schemes can be divided into two main categories: the power domain NOMA and the code domain NOMA [68]. In power domain NOMA, the users are assigned with different power levels based on their channel conditions, which enable them to share the available resources. In code domain NOMA, user specific codes are used as multiple access identities to separate the users. Code domain NOMA is similar to CDMA, but it uses low-density sequences or non-orthogonal sequences having a low cross-correlation.

## 2.9 Space Modulation Techniques (SMTs)

SMTs tackle a novel approach to add a new constellation diagram called spatial constellation diagram. Consequently, this enhances the spectral efficiency (SE) while keeping energy resources and receiver computational complexity. The basic idea of SMTs came from [69], where a binary phase shift keying (BPSK) symbol is used to indicate an active antenna among the set of existing multiple antennas. The receiver detects the transmitted BPSK symbol and the antenna that transmits this symbol. However, the first common SMT was presented in [70, 71] is called SM, and all other SMTs are driven as special or generalized cases from SM. SM extends the conventional two-dimensional complex signal plane to a third dimension, which is called the spatial dimension. This unique approach is based on the idea of using the transmitter antenna (TA) index as an extra information source. SSK was presented as a simple model based on SM where only the antenna index is used during the transmission, rather than the transmitted symbols themselves. This absence of symbol information eliminates the need for amplitude/phase modulation (APM) techniques at the transceivers. Consequently, this reduces the system complexity while keeping almost the same gain as SM [72].

In generalized spatial modulation (GSM), where multiple transmit antenna is activated at each time instant to transmit identical data is proposed in [73]. Similarly, generalized

space shift keying (GSSK) was proposed in [74]. In QSM, spatial constellation symbols of conventional SM are expanded to include two spatial dimensions, each transmits the real and the imaginary parts of a conventional APM data symbol, separately. Since this transmission procedure is realized in an orthogonal manner, ICI is avoided in QSM as well. Additionally, the number of bits conveyed by active TA indices is twice that of SM [75]. Similarly, SSK was expanded to quadrature space shift keying (QSSK). In addition, their generalized parts can be defined as generalized quadrature spatial modulation (GQSM) and generalized quadrature space shift keying (GQSSK).

# Chapter 3

## Cognitive Networks in the Presence of I/Q Imbalance, IGN and Imperfect CSI

### 3.1 Introduction and Related Works

The accelerated developments in wireless communication technology are moving the world toward a fully connected network with new challenges, including the increased demands for the radio spectrum. At the same time, the traditional way of spectrum allocation policy has made the limited spectrum overcrowded. Moreover, the available spectrum has not been utilized sufficiently as reported by the Federal Communications Commission [76]. CR was proposed as a novel solution to alleviate the spectrum scarcity by allowing a secondary user to share the spectrum of a primary user [77]. Intensive research has been done in the spectrum-sharing side of CR, which has revealed many CR models. These can be classified into three main models: underlay, overlay, and interweave networks [78]. This chapter studies the performance of underlay CR networks under the joint effects of I/Q imbalance at the secondary system, and imperfect CSI with IGN at the secondary user.

CR communication systems adapt their transmission to the surrounding radio environment. Accordingly, the performance of CR systems can be significantly affected by

different types of practical imperfections, including noise signal uncertainty, imperfect CSI, transceiver HWIs, and synchronization issues [79]. HWIs, such as I/Q imbalance in the radio frequency front-end, high power amplifier imperfections, and low noise amplifier non-linearity, can dramatically degrade the system performance [13]. Although all HWIs can degrade the system performance, I/Q imbalance represents one of the most significant sources of analog impairments in high-speed wireless communication systems [15]. Specifically, this degradation in performance results from insufficient rejection of the image frequency band [80, 81]. Moreover, taking the effects of I/Q imbalance into account is not only important in the design of the transceiver, but also in choosing coding techniques as well as in resource management of radio communication systems [18]. Furthermore, HWIs have a negative impact on the system secrecy [19].

The effects of I/Q imbalance on the energy detection based spectrum sensing for half-duplex CR were studied in [15] and [57]. In [15], it was shown that the I/Q imbalance can cause the secondary user to interfere with an orthogonal frequency-division multiple access (OFDMA) primary system and destroy the performance of the CR system. The work in [57] concluded that the effects of I/Q imbalance are negligible for single-channel receivers, but are significantly more dramatic for the wide-band multi-channel sensing receivers. The joint effects of I/Q imbalance and self-interference suppression on the energy detection based spectrum sensing of full-duplex CR were studied in [58]. In this study, it was proven that ignoring the effects of I/Q imbalance and partial self-interference suppression can lead to a dramatic degradation in the system performance of single-channel while the energy detection capability can be entirely obliterated in case of multi-channel.

The work in [59] analyzed the performance of cognitive amplify-and-forward (AF) multi-relay networks with active direct link in the presence of relay transceiver HWIs. It was shown that the HWIs have a high impact on the partial relay selection scheme and a worse impact on the opportunistic relay selection scheme. The authors in [60] studied the impact of transceiver HWIs on decode-and-forward (DF) CR networks. In the mentioned work, the authors showed that the effect of transceiver impairments on the outage performance in the high signal-to-noise ratio (SNR) region is more critical than in the low SNR.

The same authors examined the impact of transceiver impairments on the outage probability and throughput of the DF/AF CR relay in [61]. It was shown that HWIs can deteriorate the network performance, and DF CR networks outperforms AF CR networks in terms of both outage probability and throughput but with higher system complexity. The study in [62] considered soft information relaying with transceiver HWIs in CR networks. It was proven that soft information relaying protocol outperforms a hard DF technique, and a ceiling capacity exists even when the transmitter power approaches infinity and it decreases with increasing levels of HWIs.

The joint impact of HWIs and imperfect CSI on CR networks was studied in [63] and [64]. The work in [63] examined this joint impact on cognitive spatial modulation multiple-input multiple-output systems. This work did not propose any receiver designs to mitigate the joint effects of HWIs and imperfect CSI. Furthermore, In [64], the joint effects of HWIs and imperfect CSI on spectrum sharing multiple-relay networks were studied. It was shown that the effects of HWIs limit the system performance and cause various ceiling effects including a relay cooperation ceiling, direct link ceiling, and an overall system ceiling. This work neither studied effects of HWIs or imperfect CSI on the system bit error rate nor proposed any receiver designs to mitigate these effects. It is worth mentioning that all the aforementioned works [15, 57–64] modeled HWIs including I/Q imbalance as additive proper Gaussian noise with different means and variances, which is not accurate at least for I/Q imbalance impairment as will be proven in the following section.

Compared to the existing literature, this chapter studies the performance of the underlay CR secondary system under the joint effects of I/Q imbalance at secondary transmitter (STx)/secondary receiver (SRx) sides, and IGN with imperfect CSI at the SRx side. Subsequently, it is shown that these effects can degrade the system performance and change the noise PDF from proper to improper Gaussian distributions. Besides, receiver designs that can tackle these effects are presented and their computational complexities are calculated. In addition, an exact expression is derived for CRLB of the secondary system channel estimation in the presence of I/Q imbalance at STx/SRx sides and IGN at the receiver side. The obtained results in this chapter have been published in [55].

The rest of this chapter is organized as follows: Section 3.2 describes the system and channel models. Section 3.3 provides the receiver designs and the performance analysis for the presented models. Section 3.4 derives an exact closed-form CRLB expression. Section 3.5 discusses the computational complexity analysis. Section 3.6 discusses the numerical analysis and results. Finally, Section 3.7 concludes this chapter.

## 3.2 System and Channel Models

### 3.2.1 Underlay CR Systems

In an underlay CR model, the STx can use the spectrum of primary users as long as the interference it generates to the most affected primary receiver (PRx) remains below a predefined threshold  $I_p$ . In this work, as can be seen in Fig. 3.1, an underlay spectrum sharing system is considered with secondary user pairs of one STx and one SRx that coexist with another licensed primary transmitter (PTx). Hence, the STx energy ( $E$ ) is constrained as [78]

$$E = \min \left( \frac{I_p}{|f|^2}, E_m \right), \quad (3.1)$$

where  $E_m$  is the maximum available power at the STx, and  $f$  is the channel coefficient between the STx and PRx.  $|f|^2$  has an exponential distribution with a mean equals to  $\lambda$ .

The received signal at the SRx with perfect matching (no I/Q imbalance) is given by

$$y_r = \sqrt{E}hx_i + n, \quad (3.2)$$

where,  $x_i$  represents the transmitted signal,  $i \in [1, 2, \dots, M]$ ,  $M$  is the modulation order, and  $h$  is the fading channel between the STx and SRx, and  $n \sim \mathcal{CN}(\mathbf{0}, \boldsymbol{\sigma}_n^2)$  is the AWGN at the SRx. In this work, the AWGN is modeled as an improper Gaussian RV with zero mean vector and  $\boldsymbol{\sigma}_n^2$  covariance matrix. From 2.7,  $\boldsymbol{\sigma}_n^2$  is given by

$$\boldsymbol{\sigma}_n^2 = \begin{bmatrix} \sigma_{nI}^2 & \rho_n \sigma_n^I \sigma_n^Q \\ \rho_n \sigma_n^I \sigma_n^Q & \sigma_{nQ}^2 \end{bmatrix}.$$

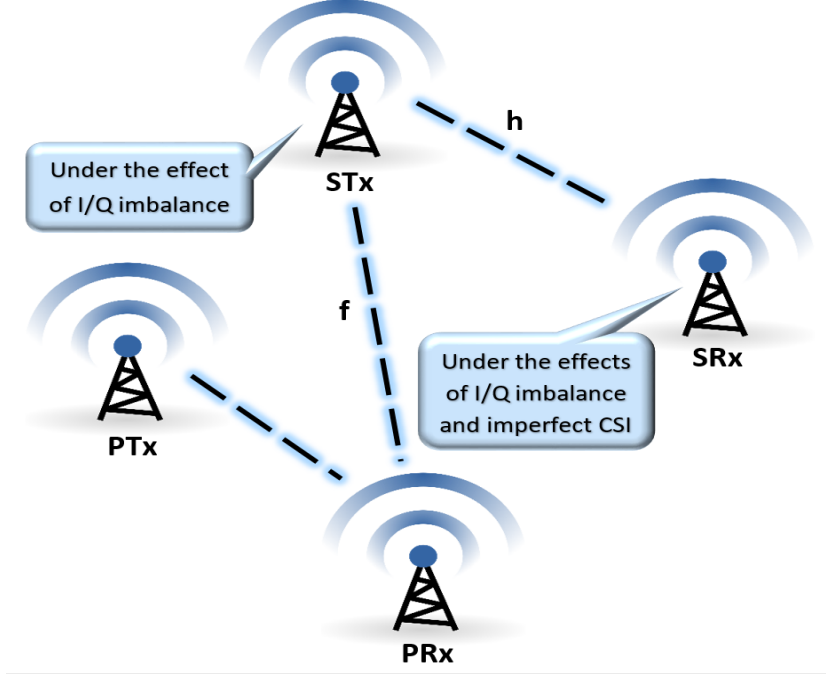


Figure 3.1: Underlay cognitive radio system under the effect of I/Q imbalance.

### 3.2.2 Transceiver I/Q imbalance Model

From Section 2.6, considering the impact of I/Q imbalance at the STx, the transmitted signal can be given as

$$x_i^{IQI} = G_1 x_i + G_2 x_i^*, \quad (3.3)$$

where  $G_1 = \frac{1}{2}(1 + \xi_t e^{j\beta_t})$  and  $G_2 = \frac{1}{2}(1 - \xi_t e^{j\beta_t})$  are I/Q imbalance parameters at the STx. Here,  $\beta_t$  and  $\xi_t$  represent the phase and amplitude imbalance, respectively. Considering the total effects of I/Q imbalance at the STx and SRx sides, the signal  $x_i^{IQI}$  is corrupted and the received signal can be given as

$$\begin{aligned} y &= K_1(\sqrt{E}h x_i^{IQI} + n) + K_2(\sqrt{E}h x_i^{IQI} + n)^* \\ &= K_1(\sqrt{E}h(G_1 x_i + G_2 x_i^*) + n) + K_2(\sqrt{E}h(G_1 x_i + G_2 x_i^*) + n)^*, \end{aligned} \quad (3.4)$$

where  $K_1 = \frac{1}{2}(1 + \xi_r e^{-j\beta_r})$  and  $K_2 = \frac{1}{2}(1 - \xi_r e^{j\beta_r})$  are I/Q imbalance parameters at the SRx. Here,  $\beta_r$  and  $\xi_r$  model the phase and amplitude imbalance, respectively.

The terms  $x_i^*$  and  $(\sqrt{E}h x_i^{IQI} + n)^*$  in (3.3) and (3.4) are the self-interference introduced by the I/Q imbalance at the STx and SRx, respectively. It can be noted that for perfect

I/Q balance, the amplitude imbalance parameters  $\xi_t = \xi_r = 1$  and the phase imbalance parameters  $\beta_t = \beta_r = 0$ . Consequently,  $G_1 = K_1 = 1$  and  $G_2 = K_2 = 0$ .

### 3.2.3 Imperfect CSI Model

In the case of imperfect CSI, there is an estimation error at the receiver. The SRx uses a channel estimator such as a ML or mean square error estimator to get a channel estimate, which can be characterized as follows [49]

$$h = \hat{h} + e, \quad (3.5)$$

where  $\hat{h}$  is the channel estimation and  $e \sim \mathcal{CN}(0, \sigma_e^2)$ , is the channel estimation error. Based on the discussion in Section 2.5, the channel estimation error in the presence of IGN can be modeled as a  $\mathcal{CN}(\mathbf{0}, \boldsymbol{\sigma}_e^2)$  where the covariance matrix  $\boldsymbol{\sigma}_e^2$  is given by

$$\boldsymbol{\sigma}_e^2 = \begin{bmatrix} \sigma_{eI}^2 & \rho_e \sigma_e^Q \sigma_e^I \\ \rho_e \sigma_e^Q \sigma_e^I & \sigma_{eQ}^2 \end{bmatrix},$$

Considering the effect of imperfect CSI at the SRx, (3.4) can be rewritten as

$$\begin{aligned} y &= K_1(\sqrt{E}(\hat{h} + e)(G_1x_i + G_2x_i^*) + n) + K_2(\sqrt{E}(\hat{h} + e)^*(G_1x_i + G_2x_i^*)^* + n^*) \\ &= \underbrace{\sqrt{E}\{K_1\hat{h}G_1 + K_2\hat{h}^*G_2^*\}}_{\tilde{h}_1}x_i + \underbrace{\sqrt{E}\{K_1\hat{h}G_2 + K_2\hat{h}^*G_1^*\}}_{\tilde{h}_2}x_i^* + \underbrace{\sqrt{E}K_1e}_{g_{a_i}}(G_1x_i + G_2x_i^*) \\ &\quad + \underbrace{\sqrt{E}K_2e^*}_{g_{b_i}}(G_1^*x_i^* + G_2^*x_i) + K_1n + K_2n^*. \end{aligned} \quad (3.6)$$

The previous equation shows that the generated noise depends on the noise at the receiver, the channel estimation error, the transmitted symbol, the transmitted energy, and the I/Q imbalance parameters at the STx/SRx. Understanding the characteristics of accumulative resulted noise is the critical factor in designing and analyzing the appropriate receiver.

### 3.2.4 IGN at the SRx

This part discusses how the accumulative noise at the SRx will always be IGN even if the AWGN is PGN. This occurs because of the effects of the I/Q imbalance. The received signal can be separated into two parts: the signal part  $\chi_i$  and the noise part  $\tilde{n}$  as in the following

$$y = \underbrace{\sqrt{E}(\tilde{h}_1 x_i + \tilde{h}_2 x_i^*)}_{\chi_i \text{ (signal)}} + \underbrace{(\sqrt{E}K_1 g_{a_i})e + (\sqrt{E}K_2 g_{b_i})e^* + K_1 n + K_2 n^*}_{\tilde{n}_i \text{ (noise)}}. \quad (3.7)$$

From (3.6), it is easy to show that the real and imaginary components of the signal part ( $\chi_i$ ) can be given as

$$\begin{aligned} \chi_i^I &= (\tilde{h}_1^I + \tilde{h}_2^I)x_i^I + (\tilde{h}_2^Q - \tilde{h}_1^Q)x_i^Q, \\ \chi_i^Q &= (\tilde{h}_1^Q + \tilde{h}_2^Q)x_i^I + (\tilde{h}_1^I - \tilde{h}_2^I)x_i^Q. \end{aligned} \quad (3.8)$$

In addition, the real and imaginary parts of the total resulted noise ( $\tilde{n}$ ) are given by

$$\begin{aligned} \tilde{n}_i^I &= \sqrt{E} \left[ e^I \underbrace{(K_1^I g_{a_i}^I - K_1^Q g_{a_i}^Q)}_{a_i} + \underbrace{(K_2^I g_{b_i}^I - K_2^Q g_{b_i}^Q)}_{b_i} + e^Q \underbrace{(K_2^I g_{b_i}^Q + K_2^Q g_{b_i}^I)}_{c_i} - \underbrace{(K_1^I g_{a_i}^Q - K_1^Q g_{a_i}^I)}_{-d_i} \right] + n^I \\ \tilde{n}_i^I &= \sqrt{E} \{ (a_i + b_i)e^I + (c_i - d_i)e^Q \} + n^I, \\ \tilde{n}_i^Q &= \sqrt{E} \left[ e^I \underbrace{(K_1^I g_{a_i}^Q + K_1^Q g_{a_i}^I)}_{d_i} + \underbrace{(K_2^I g_{b_i}^Q + K_2^Q g_{b_i}^I)}_{c_i} + e^Q \underbrace{(K_1^I g_{a_i}^I - K_1^Q g_{a_i}^Q)}_{a_i} - \underbrace{(K_2^I g_{b_i}^I + K_2^Q g_{b_i}^Q)}_{-b_i} \right] \\ &\quad + n^I K_c + n^Q K_d \\ \tilde{n}_i^Q &= \sqrt{E} \{ (c_i + d_i)e^I + (a_i - b_i)e^Q \} + K_c n^I + K_d n^Q. \end{aligned} \quad (3.9)$$

Here,  $\tilde{n}^I$  and  $\tilde{n}^Q$  are not identical RVs since  $\sigma_{\tilde{n}_i^Q}^2$  and  $\sigma_{\tilde{n}_i^I}^2$  are not equal.  $\sigma_{\tilde{n}_i^Q}^2$  and  $\sigma_{\tilde{n}_i^I}^2$  are given by

$$\begin{aligned} \sigma_{\tilde{n}_i^I}^2 &= E(a_i + b_i)^2 \sigma_e^2 + E(c_i - d_i)^2 \sigma_e^2 + 2E\rho_e(a_i + b_i)(c_i - d_i)\sigma_e^I \sigma_e^Q + \sigma_n^2, \\ \sigma_{\tilde{n}_i^Q}^2 &= E(c_i + d_i)^2 \sigma_e^2 + E(a_i - b_i)^2 \sigma_e^2 + 2E\rho_e(c_i + d_i)(a_i - b_i)\sigma_e^I \sigma_e^Q + K_c^2 \sigma_n^2 + K_d^2 \sigma_n^2 \\ &\quad + 2\rho_n K_c K_d \sigma_n^I \sigma_n^Q, \end{aligned} \quad (3.10)$$

where  $K_c = K_1^Q + K_2^Q$ , and  $K_d = K_1^I - K_2^I$ . In addition,  $\tilde{n}_i^I$  and  $\tilde{n}_i^Q$  are correlated RVs, since  $\mathbb{E}\{\tilde{n}_i^I \tilde{n}_i^Q\} \neq 0$ . The correlation coefficient of  $\tilde{n}_i^I$  and  $\tilde{n}_i^Q$  can be calculated from

$$\varrho_i = \frac{\text{cov}\{\tilde{n}_i^I \tilde{n}_i^Q\}}{\sqrt{\sigma_{\tilde{n}_i^I}^2 \sigma_{\tilde{n}_i^Q}^2}}, \quad (3.11)$$

where  $\mathbb{E}\{\tilde{n}_i^I \tilde{n}_i^Q\}$  is given by

$$\begin{aligned} \mathbb{E}\{\tilde{n}_i^I \tilde{n}_i^Q\} &= E\{(a_i + b_i)(c_i + d_i)\sigma_{e^I}^2 + (c_i - d_i)(a_i - b_i)\sigma_{e^Q}^2\} + K_c \sigma_n^2 + \rho_n K_d \sigma_n^I \sigma_n^Q \\ &\quad + E\rho_e(a_i^2 + c_i^2 - b_i^2 - d_i^2)\sigma_e^I \sigma_e^Q. \end{aligned} \quad (3.12)$$

It can be seen from the previous analysis, as expected, that  $\tilde{n}_i$  is an improper Gaussian RV, since  $\sigma_{\tilde{n}_i^I}^2$  and  $\sigma_{\tilde{n}_i^Q}^2$  are not equal and, in general,  $\tilde{n}_i^I$  and  $\tilde{n}_i^Q$  are correlated. Now, what will be the accumulated noise  $\tilde{n}_i$  if the AWGN is PGN. In this case,  $\sigma_{e^I}^2 = \sigma_{e^Q}^2 = \frac{\sigma_e^2}{2}$ ,  $\rho_e = 0$ ,  $\sigma_n^I = \sigma_n^Q = \frac{\sigma_n^2}{2}$ , and  $\rho_n = 0$ . Consequently,  $\sigma_{\tilde{n}_i^Q}^2$  and  $\sigma_{\tilde{n}_i^I}^2$  are given by

$$\begin{aligned} \sigma_{\tilde{n}_i^I}^2 &= E\frac{\sigma_e^2}{2}\{(a_i + b_i)^2 + (c_i - d_i)^2\} + \frac{\sigma_n^2}{2}. \\ \sigma_{\tilde{n}_i^Q}^2 &= E\frac{\sigma_e^2}{2}\{(c_i + d_i)^2 + E(a_i - b_i)^2\} + (K_c^2 + K_d^2)\frac{\sigma_n^2}{2}, \end{aligned} \quad (3.13)$$

and the correlation coefficient of  $\tilde{n}_i^I$  and  $\tilde{n}_i^Q$  is given by

$$\varrho_i = \frac{\text{cov}\{\tilde{n}_i^I \tilde{n}_i^Q\}}{\sqrt{\sigma_{\tilde{n}_i^I}^2 \sigma_{\tilde{n}_i^Q}^2}}, \quad (3.14)$$

where  $\mathbb{E}\{\tilde{n}_i^I \tilde{n}_i^Q\}$  is given by

$$\mathbb{E}\{\tilde{n}_i^I \tilde{n}_i^Q\} = E\sigma_e^2(a_i c_i + b_i d_i) + K_c \frac{\sigma_n^2}{2}. \quad (3.15)$$

From (3.13) and (3.14), it is clear that,  $\tilde{n}_i$  is improper RV even if  $n$  is proper RV, since  $\sigma_{\tilde{n}_i^I}^2$  and  $\sigma_{\tilde{n}_i^Q}^2$  are not equal and, in general,  $\tilde{n}_i^I$  and  $\tilde{n}_i^Q$  are correlated. This change in noise behavior from proper to improper Gaussian noise demands new requirements in the receiver design.

### 3.3 Receiver Designs and Performance Analysis

The previous section shows how the resulted noise in the presence of I/Q imbalance is IGN regardless of whether the AWGN is proper or improper. In this section, two new receivers

are proposed: an optimal ML and a WLE receiver, and then the blind (traditional) receiver is discussed.

### 3.3.1 Optimal ML Receiver Design

In this section, an optimal ML receiver is proposed for the presented CR wireless communication system, which has I/Q imbalance at STx/SRx and imperfect CSI at SRx. Considering the general signal model in (3.7), and the results in (3.10-3.14), and assuming that the I/Q imbalance parameters are known at the SRx, the joint PDF of the real part,  $y^I$ , and the imaginary part,  $y^Q$ , of the received signal can be written as [32, 41]

$$f_{y^I, y^Q}(y^I, y^Q | x_i) = \frac{1}{2\pi\sigma_{\tilde{n}_i^I}\sigma_{\tilde{n}_i^Q}\sqrt{1-\varrho_i^2}} \exp\left(\frac{-1}{2(1-\varrho_i^2)}\left[\frac{(y^I - \sqrt{E}\chi_i^I)^2}{\sigma_{\tilde{n}_i^I}^2} + \frac{(y^Q - \sqrt{E}\chi_i^Q)^2}{\sigma_{\tilde{n}_i^Q}^2} - \frac{2\varrho_i(y^I - \sqrt{E}\chi_i^I)(y^Q - \sqrt{E}\chi_i^Q)}{\sigma_{\tilde{n}_i^I}\sigma_{\tilde{n}_i^Q}}\right]\right). \quad (3.16)$$

The primary task of the ML receiver is to decide which  $x_i$  was transmitted among  $M$  hypotheses. Assuming that the channel inputs are equally likely, the optimal receiver is designed based on maximizing the following statement

$$\hat{x}_i = \arg \max_{i=1, \dots, M} \{f_{y^I, y^Q}(y^I, y^Q | x_i)\}. \quad (3.17)$$

Maximizing the previous statement is equivalent to

$$\hat{x}_i = \arg \min_{i=1, \dots, M} \left\{ \frac{(y^I - \sqrt{E}\chi_i^I)^2}{\sigma_{\tilde{n}_i^I}^2} + \frac{(y^Q - \sqrt{E}\chi_i^Q)^2}{\sigma_{\tilde{n}_i^Q}^2} - \frac{2\varrho_i(y^I - \sqrt{E}\chi_i^I)(y^Q - \sqrt{E}\chi_i^Q)}{\sigma_{\tilde{n}_i^I}\sigma_{\tilde{n}_i^Q}} \right\}. \quad (3.18)$$

*Conditional PEP<sub>opt</sub>*: From (3.18), the probability of detecting  $\hat{x}_i$  at the SRx given that the STx transmitted  $x_i$ , is given by

$$\text{PEP}_{\text{opt}} = \Pr \left\{ \frac{(y^I - \sqrt{E}\chi_i^I)^2}{\sigma_{\tilde{n}_i^I}^2} + \frac{(y^Q - \sqrt{E}\chi_i^Q)^2}{\sigma_{\tilde{n}_i^Q}^2} - \frac{2\varrho_i(y^I - \sqrt{E}\chi_i^I)(y^Q - \sqrt{E}\chi_i^Q)}{\sigma_{\tilde{n}_i^I}\sigma_{\tilde{n}_i^Q}} > \frac{(y^I - \sqrt{E}\hat{\chi}_i^I)^2}{\sigma_{\tilde{n}_i^I}^2} + \frac{(y^Q - \sqrt{E}\hat{\chi}_i^Q)^2}{\sigma_{\tilde{n}_i^Q}^2} - \frac{2\varrho_i(y^I - \sqrt{E}\hat{\chi}_i^I)(y^Q - \sqrt{E}\hat{\chi}_i^Q)}{\sigma_{\tilde{n}_i^I}\sigma_{\tilde{n}_i^Q}} \right\}. \quad (3.19)$$

After some simplifications, (3.19) can be written as

$$\text{PEP}_{\text{opt}} = \Pr \left\{ \mathcal{N}_i > \frac{E(\chi_i^I - \hat{\chi}_i^I)^2}{\sigma_{\tilde{n}_i^I}^2} + \frac{E(\chi_i^Q - \hat{\chi}_i^Q)^2}{\sigma_{\tilde{n}_i^Q}^2} - \frac{2\varrho_i E(\chi_i^I - \hat{\chi}_i^I)(\chi_i^Q - \hat{\chi}_i^Q)}{\sigma_{\tilde{n}_i^I}\sigma_{\tilde{n}_i^Q}} \right\}, \quad (3.20)$$

where  $\mathcal{N}_i$  is given by

$$\mathcal{N}_i = 2\varrho_i \sqrt{E} \left[ \frac{(\chi_i^I - \hat{\chi}_i^I) \tilde{n}_i^Q + (\chi_i^Q - \hat{\chi}_i^Q) \tilde{n}_i^I}{\sigma_{\tilde{n}_i^I} \sigma_{\tilde{n}_i^Q}} \right] - 2\sqrt{E} \left[ \frac{(\chi_i^I - \hat{\chi}_i^I) \tilde{n}_i^I}{\sigma_{\tilde{n}_i^I}^2} + \frac{(\chi_i^Q - \hat{\chi}_i^Q) \tilde{n}_i^Q}{\sigma_{\tilde{n}_i^Q}^2} \right]. \quad (3.21)$$

From (3.21), it is clear that  $\mathcal{N}_i$  is a Gaussian RV with zero-mean and its variance  $\sigma_{\mathcal{N}_i}^2$  can be expressed as

$$\sigma_{\mathcal{N}_i}^2 = 4E(1 - \varrho_i^2) \left[ \frac{(\chi_i^I - \hat{\chi}_i^I)^2}{\sigma_{\tilde{n}_i^I}^2} + \frac{(\chi_i^Q - \hat{\chi}_i^Q)^2}{\sigma_{\tilde{n}_i^Q}^2} - \frac{(\chi_i^I - \hat{\chi}_i^I) + (\chi_i^Q - \hat{\chi}_i^Q)}{\sigma_{\tilde{n}_i^I} \sigma_{\tilde{n}_i^Q}} \right]. \quad (3.22)$$

Hence, utilizing (3.1), (3.20) and (3.22),  $\text{PEP}_{\text{opt}}$  can also be written by using the well-known  $Q$ -function formula as

$$\begin{aligned} \text{PEP}_{\text{opt}} &= Q \left( \sqrt{\frac{\min\left(\frac{I_p}{|f|^2}, E_m\right) \left[ (\chi_i^I - \hat{\chi}_i^I)^2 + \frac{(\chi_i^Q - \hat{\chi}_i^Q)^2}{\sigma_{\tilde{n}_i^Q}^2} - \frac{2\varrho_i(\chi_i^I - \hat{\chi}_i^I)(\chi_i^Q - \hat{\chi}_i^Q)}{\sigma_{\tilde{n}_i^I} \sigma_{\tilde{n}_i^Q}} \right]}{4(1 - \varrho_i^2)}} \right) \\ &= Q \left( \sqrt{\frac{\min\left(\frac{I_p}{|f|^2}, E_m\right) \gamma_{\text{opt}}}{4(1 - \varrho_i^2)}} \right). \end{aligned} \quad (3.23)$$

*Average PEP<sub>opt</sub>*: Without loss of generality, limited feedback from the PRx is assumed, based on this, the mean-value power allocation (MVPA) method can be exploited [50,82,83]. Relying on MVPA, the interference channel gain between the STx-PRx is usually assumed to be known at the PRx. Therefore, the PRx computes the mean value of this channel gain, instead of the instantaneous CSI. Then, the PRx feeds the calculated mean back to the STx. As a result, sending one value rather than instantaneous CSI feedback for each symbol or block of symbols can significantly reduce the system complexity and decrease the feedback burden. Relying on MVPA,  $E$  in (3.1) is constrained as  $E = \min\left(\frac{I_p}{\sigma_f^2}, E_m\right)$ , where  $\sigma_f^2 = \mathbb{E}\{|f|^2\}$ .

The APEP will be calculated considering the Beckmann fading channels. Making no assumptions on the statistics of the amplitudes and phases of the fading channel (i.e., allowing  $h^I$  and  $h^Q$  to have different means and variances, or being correlated) leads to a more general fading channel model, where most of the well-known fading channel models can be considered as special cases of this general model. More details about Beckmann fading channels can be found in Section 2.4.  $h$  can be modeled as  $\mathcal{CN}(\boldsymbol{\mu}_h, \boldsymbol{\sigma}_h^2)$  where the

mean vector and the covariance matrix of  $h$  are given by  $\boldsymbol{\mu}_h$  and  $\boldsymbol{\sigma}_h^2$  respectively

$$\boldsymbol{\mu}_h = \begin{bmatrix} \mu_{h^I} & \mu_{h^Q} \end{bmatrix}, \quad \boldsymbol{\sigma}_h^2 = \begin{bmatrix} \sigma_{h^I}^2 & \rho_h \sigma_h^Q \sigma_h^I \\ \rho_h \sigma_h^Q \sigma_h^I & \sigma_{h^Q}^2 \end{bmatrix}. \quad (3.24)$$

From (3.23),  $\gamma_{opt}$  can be written using matrix form as  $\gamma_{opt} = \mathbf{x}^T \mathbf{A} \mathbf{x}$ . Here  $\mathbf{x} \sim \mathcal{N}(\boldsymbol{\mu}_x, \boldsymbol{\sigma}_x^2)$  where  $\mathbf{x}^T = [x_1 \ x_2]$ ,  $x_1 = (\chi_i^I - \hat{\chi}_i^I)$ ,  $x_2 = (\chi_i^Q - \hat{\chi}_i^Q)$ , and  $\mathbf{A}$  is the quadratic matrix.

$$\begin{aligned} \mu_{x_1} &= \mu_{\hat{h}}^I([a_i + b_i] - [\hat{a}_i + \hat{b}_i]) + \mu_{\hat{h}}^Q([c_i - d_i] - [\hat{c}_i - \hat{d}_i]), \\ \mu_{x_2} &= \mu_{\hat{h}}^I([c_i + d_i] - [\hat{c}_i + \hat{d}_i]) + \mu_{\hat{h}}^Q([a_i - b_i] - [\hat{a}_i - \hat{b}_i]), \\ \sigma_{x_1}^2 &= \sigma_{\hat{h}^I}^2([a_i + b_i] - [\hat{a}_i + \hat{b}_i])^2 + \sigma_{\hat{h}^Q}^2([c_i - d_i] - [\hat{c}_i - \hat{d}_i])^2 + 2\rho_{\hat{h}} \sigma_{\hat{h}}^Q \sigma_{\hat{h}}^I([a_i + b_i] - [\hat{a}_i + \hat{b}_i]) \\ &\quad \times ([c_i - d_i] - [\hat{c}_i - \hat{d}_i]), \\ \sigma_{x_2}^2 &= \sigma_{\hat{h}^I}^2([c_i + d_i] - [\hat{c}_i + \hat{d}_i])^2 + \sigma_{\hat{h}^Q}^2([a_i - b_i] - [\hat{a}_i - \hat{b}_i])^2 + 2\rho_{\hat{h}} \sigma_{\hat{h}}^I \sigma_{\hat{h}}^Q([c_i + d_i] - [\hat{c}_i + \hat{d}_i]) \\ &\quad \times ([a_i - b_i] - [\hat{a}_i - \hat{b}_i]), \\ \mathbb{E}\{x_1 x_2\} &= \sigma_{\hat{h}^I}^2([a_i + b_i] - [\hat{a}_i + \hat{b}_i])([c_i + d_i] - [\hat{c}_i + \hat{d}_i]) + \sigma_{\hat{h}^Q}^2([c_i - d_i] - [\hat{c}_i - \hat{d}_i]) \\ &\quad \times ([a_i - b_i] - [\hat{a}_i - \hat{b}_i]) + \rho_{\hat{h}} \sigma_{\hat{h}}^I \sigma_{\hat{h}}^Q([a_i + \hat{a}_i]^2 + [c_i + \hat{c}_i]^2 - [b_i + \hat{b}_i]^2 - [d_i + \hat{d}_i]^2), \\ \rho_x &= \text{cov}\{x_1 x_2\} / (\sigma_{x_1} \sigma_{x_2}). \end{aligned} \quad (3.25)$$

Hence,  $\gamma_{opt}$  has the PDF of a quadratic form of two correlated noncentral chi-squared RVs.

From Section 2.3, the MGF of  $\gamma_{opt}$  can be given by

$$M_{\gamma_{opt}}(t) = \frac{\exp\left(\frac{b_1^2 \lambda_1 t}{1 - 2\lambda_1 t}\right)}{\sqrt{1 - 2\lambda_1 t}} \times \frac{\exp\left(\frac{b_2^2 \lambda_2 t}{1 - 2\lambda_2 t}\right)}{\sqrt{1 - 2\lambda_2 t}}, \quad (3.26)$$

where the eigenvalues  $\lambda_1$  and  $\lambda_2$ , and the mean values  $b_1$  and  $b_2$  are calculated as in Section 2.3. In addition, this section shows how other channel models can be considered as a special cases of Beckmann fading model. For example, (3.26) can be used if the fading channels are Rayleigh fading channels. In this case,  $\mu_{x_1} = \mu_{x_2} = 0$ ,  $\sigma_{x_1}^2 = \sigma_{x_2}^2$ , and  $\rho_x = 0$ . Relaxing the condition  $\mu_{x_1} = \mu_{x_2} = 0$  to give the LoS component  $\mu_{x_1} = \mu_{x_2}$  gives the Rician fading channels. Now, from [84], and relying on MVPA a closed-form expression of the  $\text{APEP}_{opt}$  can be calculated by using (3.23)-(3.26) as follows

$$\text{APEP}_{opt} = \frac{1}{\pi} \int_0^{\frac{\pi}{2}} M_{\gamma_{opt}} \left( -\frac{\min\left(\frac{I_p}{\sigma_f^2}, E_m\right)}{8(1 - \varrho_i^2) \sin^2 \theta} \right) d\theta. \quad (3.27)$$

The previous integration can be calculated by using a simple numerical integration technique. Furthermore, (3.27) can be simply upper bounded by

$$\text{APEP}_{\text{opt}} \leq \frac{1}{2} M_{\gamma_{\text{opt}}} \left( -\frac{\min\left(\frac{I_p}{\sigma_f^2}, E_m\right)}{8(1 - \rho_i^2)} \right). \quad (3.28)$$

*Average BER<sub>opt</sub>*: From (3.23), and using the well-known union bound technique [42], the SRx can be calculated as

$$\text{ABER}_{\text{opt}} \leq \sum_{t=1}^M \sum_{\hat{t}=t+1}^M \frac{N(\chi_i, \hat{\chi}_i) \text{APEP}_{\text{opt}}}{M}, \quad (3.29)$$

where  $N(\chi_i, \hat{\chi}_i)$  is the number of bit errors associated with the corresponding pairwise error event.

### 3.3.2 WLE Receiver Design

Here, a WLE receiver is presented at SRx with imperfect CSI when I/Q imbalance exists at STx/SRx. The goal of this filter is to entirely eliminate the I/Q imbalance. The filter parameters are calculated by adding the scaled received signal with its scaled conjugate and then matching the results with the received signal as in the case of perfect I/Q imbalance and perfect CSI. Here, the scaling parameters are calculated assuming that the I/Q imbalance parameters are known at the SRx. After that, the traditional ML detection is applied at the SRx to choose the correct one among  $M$  hypotheses.

The output of the WLE receiver can be given as

$$Y = \sqrt{E}x_i + Z_i, \quad (3.30)$$

*Proof*: See the Appendix A.1.

where  $Z_i \sim \mathcal{CN}(0, \sigma_{Z_i}^2)$  is an improper RV and the variances of its real and imaginary parts are equal to  $\sigma_{Z_i^I}^2$  and  $\sigma_{Z_i^Q}^2$ , respectively, and the correlation factor between  $Z_i^I$  and  $Z_i^Q$  is  $\rho_{Z_i}$ , where  $\rho_{Z_i}$  is calculated as in (A.10).

The traditional ML detection for the proposed WLE receiver, which ignores the improper characteristics of the noise, relies on minimizing the following statement

$$\hat{x}_i = \arg \min_i \{|Y - \sqrt{E}x_i|^2\}. \quad (3.31)$$

*Conditional PEP<sub>wle</sub>* : Considering (3.31) and assuming that  $x_i$  has been sent, the probability of receiving  $\hat{x}_i$  is given as

$$\begin{aligned}
\text{PEP}_{\text{wle}} &= \Pr\{|Y - \sqrt{E}x_i|^2 > |Y - \sqrt{E}\hat{x}_i|^2\} \\
&= \Pr\{|Z_i|^2 > E|(x_i - \hat{x}_i)|^2 + |Z_i|^2 + 2\sqrt{E}\Re[(x_i - \hat{x}_i)Z_i^*]\} \\
&= \Pr\{0 > E|(x_i - \hat{x}_i)|^2 + 2\sqrt{E}\Re[(x_i - \hat{x}_i)Z_i^*]\} \\
&= \Pr\{0 > |E(x_i - \hat{x}_i)|^2 + \zeta_i\}, \tag{3.32}
\end{aligned}$$

where  $\zeta_i = 2\sqrt{E}\Re[(x_i - \hat{x}_i)Z_i^*]$ . Conditioned on  $\hat{x}_i$  and  $x_i$ ,  $\zeta_i$  is a Gaussian RV with zero mean and variance of

$$\begin{aligned}
\sigma_{\zeta_i}^2 &= 4E\mathbb{E}\{[(x_i^I - \hat{x}_i^I)Z_i^I + (x_i^Q - \hat{x}_i^Q)Z_i^Q]^2\} \\
&= 4E(x_i^I - \hat{x}_i^I)^2\mathbb{E}\{Z_i^{I^2}\} + 4E(x_i^Q - \hat{x}_i^Q)^2\mathbb{E}\{Z_i^{Q^2}\} + 8E(x_i^I - \hat{x}_i^I)(x_i^Q - \hat{x}_i^Q)\mathbb{E}\{Z_i^I Z_i^Q\} \\
&= 4E(x_i^I - \hat{x}_i^I)^2\sigma_{Z_i^I}^2 + 4E(x_i^Q - \hat{x}_i^Q)^2\sigma_{Z_i^Q}^2 + 8E(x_i^I - \hat{x}_i^I)(x_i^Q - \hat{x}_i^Q)\sigma_{Z_i^I}\sigma_{Z_i^Q}\rho_{Z_i}. \tag{3.33}
\end{aligned}$$

Considering the mean and variance of  $\zeta_i$ , the closed-form of  $\text{PEP}_{\text{wle}}$  can be given using the  $Q$ -function as

$$\begin{aligned}
\text{PEP}_{\text{wle}} &= Q\left(\sqrt{\frac{\min\left(\frac{I_p}{|f|^2}, E_m\right)|x_i - \hat{x}_i|^4}{4(x_i^I - \hat{x}_i^I)^2\sigma_{Z_i^I}^2 + 4(x_i^Q - \hat{x}_i^Q)^2\sigma_{Z_i^Q}^2 + 8(x_i^I - \hat{x}_i^I)(x_i^Q - \hat{x}_i^Q)\sigma_{Z_i^I}\sigma_{Z_i^Q}\rho_{Z_i}}}\right) \\
&= Q\left(\sqrt{\min\left(\frac{I_p}{|f|^2}, E_m\right)\gamma_{\text{wle}}}\right). \tag{3.34}
\end{aligned}$$

*Average PEP<sub>wle</sub>* : It is clear from (3.34) that the PDF of  $\gamma_{\text{wle}}$  is very complicated and rather difficult, if not impossible, to derive. Thus, the  $\text{APEG}_{\text{wle}}$  is found numerically by averaging the  $\text{PEP}_{\text{wle}}$  over a large number of channel realizations for each SNR value. Finally, the SRx of the WLE receiver ( $\text{ABER}_{\text{wle}}$ ) can be calculated directly using the formula in (3.29).

### 3.3.3 Traditional (Blind) ML Receiver

The blind receiver can be defined as the one that utilizes the traditional ML receiver to detect CR signals as if there is no I/Q imbalance at STx or SRx, even in the case where it

exists at one or both sides. Based on this scenario, and starting from (3.7), the traditional ML receiver for the blind CR receiver depends on minimizing the following statement

$$\hat{x}_i = \arg \min_{i=1, \dots, M} \{ |y - \sqrt{E}hx_i|^2 \}. \quad (3.35)$$

*Conditional PEP<sub>bli</sub>* : The noise  $\tilde{n}$  in (3.7) is an improper RV but it will be treated as if it is proper RV by this blind receiver. The probability of detecting  $\hat{x}_i$  at the SRx given that the STx transmitted  $x_i$ , is given by

$$\begin{aligned} \text{PEP}_{\text{bli}} &= \Pr \{ |y - \sqrt{E}hx_i|^2 > |y - \sqrt{E}h\hat{x}_i|^2 \} \\ &= \Pr \{ |\sqrt{E}\chi_i - \sqrt{E}hx_i|^2 > |\sqrt{E}\chi_i - \sqrt{E}h\hat{x}_i|^2 \}. \end{aligned} \quad (3.36)$$

After some algebraic simplifications, the conditional error probability can be written as

$$\text{PEP}_{\text{bli}} = \Pr \left\{ 0 > \underbrace{E|(\chi_i - h\hat{x}_i)|^2 - E|(\chi_i - hx_i)|^2 + 2\sqrt{E}\Re[(hx_i - h\hat{x}_i)\tilde{n}_i^*]}_{\vartheta_i} \right\}. \quad (3.37)$$

Therefore, after following the same procedure as in (3.33),  $\vartheta_i$  is a Gaussian RV with mean and variance given by

$$\begin{aligned} \mu_{\vartheta_i} &= |\chi_i - hx_i|^2 - |\chi_i - h\hat{x}_i|^2, \\ \sigma_{\vartheta_i}^2 &= 4E[(hx_i)^I - (h\hat{x}_i)^I]^2 \sigma_{\tilde{n}_i^I}^2 + 4E[(hx_i)^Q - (h\hat{x}_i)^Q]^2 \sigma_{\tilde{n}_i^Q}^2 + 8E[(hx_i)^I - (h\hat{x}_i)^I] \\ &\quad \times [(hx_i)^Q - (h\hat{x}_i)^Q] \sigma_{\tilde{n}_i^I} \sigma_{\tilde{n}_i^Q} \rho_i. \end{aligned} \quad (3.38)$$

Based on that,  $\text{PEP}_{\text{bli}}$  can be calculated as in (3.39)

$$\text{PEP}_{\text{bli}} = Q \left( \sqrt{\frac{\min(\frac{I_p}{|f|^2}, E_m) (\mu_{\vartheta_i})^2}{\sigma_{\vartheta_i}^2}} \right) = Q(\sqrt{\gamma_{bli}}). \quad (3.39)$$

*Average PEP<sub>bli</sub>* : It is clear from (3.39) that the PDF of  $\gamma_{bli}$  is more complicated than the PDF of  $\gamma_{wle}$  in (3.34), and it is very difficult to find its average. Based on this, the  $\text{APEP}_{\text{bli}}$  is found through simulation by averaging the  $\text{PEP}_{\text{bli}}$  over a large number of channel realizations for each SNR value. Finally, the SRx of the blind receiver ( $\text{ABER}_{\text{bli}}$ ) can be calculated directly by using (3.29).

### 3.4 CRLB Derivation

In this section, an exact expression is derived for CRLB of the channel estimation in the presence of I/Q imbalance at the STx/SRx and assuming PGN at the SRx. Since CRLB expresses a lower bound on the variance of unbiased estimators, it can be used as a benchmark to predict and evaluate the performance of the estimators in the presence of I/Q imbalance.

To find the CRLB, the received signal in (3.6) can be written as

$$y = \sqrt{E}h \underbrace{(K_1(G_1x_i + G_2x_i^*))}_{Q_1} + \sqrt{E}h^* \underbrace{(x_iK_2(G_1x_i + G_2x_i^*))^*}_{Q_2} + \underbrace{K_1n + K_2n^*}_u. \quad (3.40)$$

To simplify the derivation, let us rewrite  $y$  as

$$y = \sqrt{E}Ah^I + \sqrt{E}Bh^Q + j(\sqrt{E}Ch^I + \sqrt{E}Dh^Q) + u^I + ju^Q, \quad (3.41)$$

where,  $A = Q_1^I + Q_2^I$ ,  $B = Q_2^Q - Q_1^Q$ ,  $C = Q_2^Q + Q_1^Q$ , and  $D = Q_1^I - Q_2^I$ . Noting that  $u$  is an improper Gaussian noise with  $u^I \sim \mathcal{N}(0, \sigma_{n^I}^2)$ , and  $u^Q \sim \mathcal{N}(0, K_c^2\sigma_{n^I}^2 + K_d^2\sigma_{n^Q}^2 + 2\rho_n K_c K_d \sigma_{n^I}^I \sigma_{n^Q}^Q)$  with correlation factor  $\Psi = K_c \sigma_{n^I}^2 + 2\rho_n K_d \sigma_{n^I}^I \sigma_{n^Q}^Q$ .

Now, assuming  $N_P$  is the number of training pilots that used at the SRx to estimate the channel, CRLB matrix can be given as

$$\text{CRLB} = \begin{bmatrix} \text{CRLB}_{(h^I)} & \text{CRLB}_{(h^I, h^Q)} \\ \text{CRLB}_{(h^I, h^Q)} & \text{CRLB}_{(h^Q)} \end{bmatrix}, \quad (3.42)$$

*Proof:* See the Appendix A.2.

where  $\text{CRLB}_{(h^I)}$ ,  $\text{CRLB}_{(h^Q)}$ , and  $\text{CRLB}_{(h^I, h^Q)}$  are given by

$$\text{CRLB}_{(h^I)} = \frac{[A^2\sigma_{u^Q}^2 + C^2\sigma_{u^I}^2 - 2\Psi AC\sigma_u^I\sigma_u^Q]}{N_p E(AD - CB)^2} \quad (3.43)$$

$$\text{CRLB}_{(h^Q)} = \frac{[B^2\sigma_{u^Q}^2 + D^2\sigma_{u^I}^2 - 2\Psi BD\sigma_u^I\sigma_u^Q]}{N_p E(AD - CB)^2} \quad (3.44)$$

$$\text{CRLB}_{(h^I, h^Q)} = \frac{[AB\sigma_{u^Q}^2 + CD\sigma_{u^I}^2 - \Psi AD\sigma_u^I\sigma_u^Q - \Psi BC\sigma_u^I\sigma_u^Q]}{N_p E(AD - CB)^2} \quad (3.45)$$

If the AWGN at the SRx is PGN, then GRLB is given as

$$\text{CRLB} = \begin{bmatrix} \text{CRLB}_{(h^I)} & 0 \\ 0 & \text{CRLB}_{(h^Q)} \end{bmatrix}, \quad (3.46)$$

*Proof:* See the Appendix A.3.

In this case,  $\text{CRLB}_{(h^I, h^Q)} = 0$ , and  $\text{CRLB}_{(h^I)} = \text{CRLB}_{(h^Q)}$  and given by

$$\text{CRLB}_{(h^I)} = \text{CRLB}_{(h^Q)} = \frac{\sigma_n^2}{2N_p E [x_i^{I^2} + x_i^{Q^2} \xi_t^2 - 2x_i^I x_i^Q \xi_t \sin(\beta_t)]}. \quad (3.47)$$

It is worth mentioning, as stated by 3.46, that if the AWGN noise at the SRx is PGN, then the estimation errors of  $h^I$  and  $h^Q$  that reach the CRLB are uncorrelated even though the I/Q imbalance changes the Gaussian noise behavior from a proper to an improper RV. This can be concluded clearly from the diagonal CRLB matrix. Consequently, the quality of estimating  $h^I$  and  $h^Q$  does not degrade when the other one is unknown. In addition, the I/Q imbalance at the STx or SRx does not affect the channel estimation error. For a fair comparison, the transmitted signal energy is normalized by  $(|x_i G_1 + x_i^* G_2|^2)$ . Observing that,  $(|x_i G_1 + x_i^* G_2|^2) = (x_i^{I^2} + x_i^{Q^2} \xi_t^2 - 2x_i^I x_i^Q \xi_t \sin(\beta_t))$ , two results are concluded as follows:

- The first, if the AWGN is proper, then  $\text{CRLB}_{(h^I)} = \text{CRLB}_{(h^Q)} = \frac{\sigma_n^2}{2N_p E}$ , and their values do not depend on the I/Q imbalance parameters at the STx/SRx. Based on this, the optimal channel estimator which exploits the fact that the accumulated noise at the SRx is improper and aware about the I/Q imbalance parameters can reach the CRLB. This is because the noise behavior is affected by the I/Q parameters and the estimator is aware of these parameters.
- The second, if the AWGN is improper then,  $\text{CRLB}_{(h^I)} + \text{CRLB}_{(h^Q)} = \frac{\sigma_n^2}{N_p E}$ , and this values does not depend on the I/Q imbalance parameters at the STx/SRx. Based on this, the optimal channel estimator which exploits the fact that the accumulated noise at the SRx is improper and aware about the I/Q imbalance parameters has a a fixed CRLB for the channel estimate.

Table 3.1: Number of multiplications and summations required for each frame.

	Optimal		WLE		Blind	
	Mul	Sum	Mul	Sum	Mul	Sum
Per received symbol	$6M$	$6M$	$8 + 2M$	$6 + 3M$	$2M$	$3M$
Per coherence time	$4M + 16$	$6M + 12$	24	15	$4M$	$2M$
At preprocessing time	$27M + 16$	$26M + 8$	16	8	—	—

### 3.5 Complexity Analysis

The computational time complexity can be calculated by finding the number of real additions and real multiplications [71, 75, 85–87]. It is widely known that each complex multiplication requires four real multiplications and two real additions, while the square of the absolute value of the complex number requires two real multiplications and one real addition.

The detection process of the proposed receivers requires a few calculations for each received symbol, and several calculations will be repeated  $M$  times depending on the modulation scheme. Moreover, some calculations will be found one time at the preparation phase only, and other calculations will be found for each coherence time (i.e., time duration over which the channel impulse response is not varying).

It is easy to show that the blind receiver given in (3.35) needs four real multiplications and two real summations to calculate the term  $\sqrt{E}hx_i$ . This term is calculated  $M$  times for each coherence time. After that, the square of the absolute value is calculated  $M$  times, and this needs two real multiplications and three real summations.

On the other hand, the WLE receiver given in (3.31) needs eight real multiplications and four real summations at the preprocessing phase to compute  $K_1G_1$ ,  $K_2G_2^*$ ,  $K_1G_2$ , and  $K_2G_1^*$ . Then, it calculates  $w_1$  and  $w_2$  in (A.5), and  $Y$  in (A.6). The variables  $w_1$  and  $w_2$  are required to be calculated once for each coherence time, which takes twenty-four real

multiplications and fifteen real summations. Moreover,  $Y$  is required to be calculated once for each received symbol, and this takes eight real multiplications and six real summations. Finally, the square of the absolute value takes two real multiplications and three real summations and it is calculated  $M$  times for each received symbols.

Following the same logic, the optimal receiver detects  $\hat{x}_i$  in (3.18) by calculating  $\tilde{h}_1$ , and  $\tilde{h}_2$  in (3.7) once for each coherence time, and this takes sixteen real multiplications and twelve real summations. After that  $\sigma_{\tilde{n}_i I}^2$ , and  $\sigma_{\tilde{n}_i Q}^2$  in (3.10), and  $\varrho_i$  in (3.11) are calculated  $M$  times at the preprocessing phase, and this takes twenty-seven real multiplications and twenty-six real summations. At the end,  $\hat{x}_i$  can be detected after doing six real multiplications and six real summations  $M$  times. Assuming that  $I$  is the number of symbols per coherence time, the total number of real multiplications and summations for all receivers can be seen in Table. 3.1.

## 3.6 Numerical Analysis and Results

Considering the aforementioned CR receivers designs, comprehensive computer simulations were carried out to validate the analytical results and assess the performance of a STx/SRx that has I/Q imbalance with imperfect CSI and IGN at the SRx. More specifically and unless specified otherwise, a single-input single-output (SISO) system scenario is assumed, and 4-QAM modulation is used. The computer simulations are performed under Rayleigh fading channel conditions and the receiver is affected by proper Gaussian noise  $n \sim \mathcal{CN}(0, 1)$ . Moreover, for a fair comparison, the transmitted signal energy is normalized by  $(|x_i G_1 + x_i^* G_2|^2)$ . All the comparisons are made against a system with perfect I/Q balance. In addition, we assume the predefined threshold is  $I_p = 30$  dB and  $f$  is the channel coefficient between the STx and PRx where  $f \sim \mathcal{CN}(0, 1)$ . Finally, the SRx for all figures is plotted versus the SNR  $E/\sigma_n^2$  using (3.29).

Fig. 3.2 shows the simulation and numerical results where the conditional PEP averaging of a large number of channel realizations for the optimal, WLE, and blind receivers. In addition, the closed form APEP of the optimal receiver relying on MVPA [equation (3.27)] is presented in this figure. It is clear that the simulation results match with the analytical

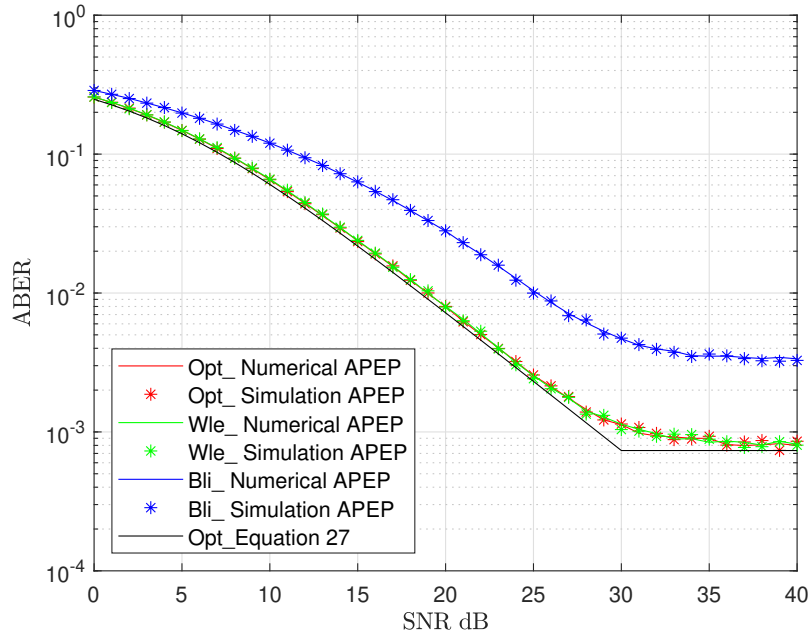


Figure 3.2: APEP at 3 dB amplitude mismatch and  $5^\circ$  phase imbalance at both STx/SRx and assuming PGN and perfect CSI at SRx.

analysis for all receivers which validates our results.

Fig. 3.3 considers the performance the SRx at different values of  $\sigma_{nI}^2$ ,  $\sigma_{nQ}^2$  and  $\rho_n$  assuming perfect I/Q matching at the STx/SRx sides and assuming perfect CSI. Two main points can be concluded from this figure. First, the proposed optimal ML detector is superior to the WLE and blind receivers which have the same performance. Second, increasing the imperpness level (i.e more differences between  $\sigma_{nI}^2$  and  $\sigma_{nQ}^2$  values or higher  $\rho_n$  values) of the noise does not provide any performance enhancement for the WLE and blind receivers while it noticeably increases the performance of the optimal one; for instance, approximately 7 dB improvement is ensured on the performance of the optimal receiver for  $\sigma_{nI}^2 = 0.1$  and  $\rho_n = 0.7$  case when  $\text{ABER} = 10^{-3}$ .

The results in Fig. 3.3 can be interpreted from (3.23), (3.34), and (3.39). From (3.23), it is clear that the term inside the Q-function goes to  $Q(\infty)$  and the error probability goes to zero in two cases; *case 1*, when the correlation factor  $\rho_n$  goes to one, because in this case, the denominator goes to zero, *case 2*, when one of the variances ( $\sigma_{nI}^2$  or  $\sigma_{nQ}^2$ ) goes to

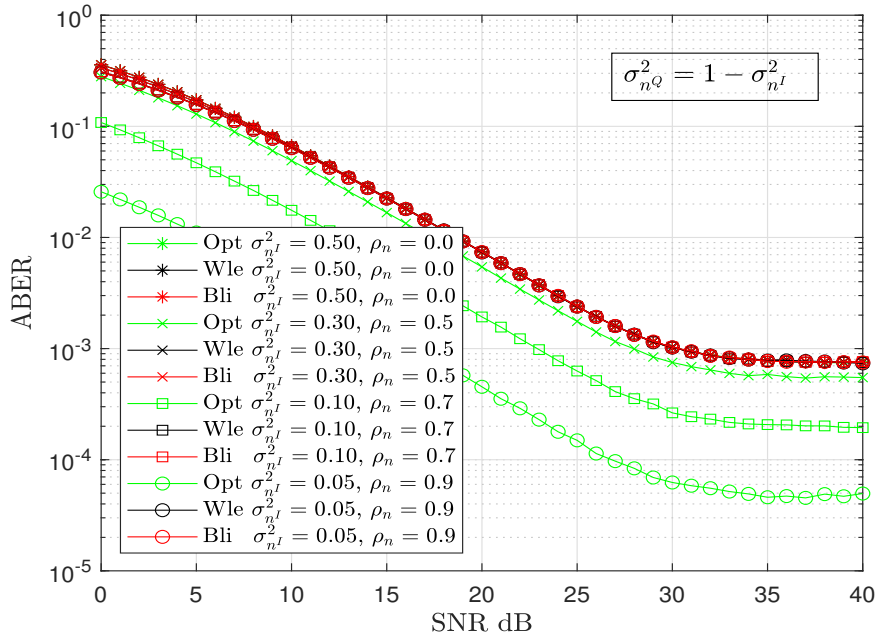


Figure 3.3: ABER performance at different values of  $\sigma_{nI}^2$ ,  $\sigma_{nQ}^2$  and  $\rho_n$  assuming perfect I/Q matching and perfect CSI.

zero because in this case, the numerator goes to  $\infty$ ). This trend is not valid in (3.34) where any change in  $\sigma_{nI}^2$  is cancelled by the apposite change in  $\sigma_{nQ}^2$  (note:  $\sigma_{nI}^2 + \sigma_{nQ}^2 = 1$ ). The behavior of the blind receiver is similar to the behavior of the WLE one in this case for the same explained reasons. Note that changing the sign of  $\rho_n$  will not affect the value APEP for all receivers. Consequently, this will not affect the performance of the receivers.

Figs 3.4 and 3.5 show the effects of the I/Q imbalance at STx only, with perfect CSI at the SRx. Fig. 3.4 shows the results of fixing the phase mismatch at  $10^\circ$  while varying the amplitude imbalance between 2, 4, and 6 dB. It shows that the performance of all receivers decreases when the level of the amplitude mismatching increases. In addition, the optimal receiver outperforms the WLE and blind receivers at all levels of SNR while the WLE receiver outperforms the blind receiver at higher values of SNR. Finally, it is clear that in the higher SNR region, the SRx performance saturates due to the power constraint limitation, leading to an error floor and zero power gain.

In Fig. 3.5, the ABER is plotted by fixing the amplitude mismatch to 3 dB while the

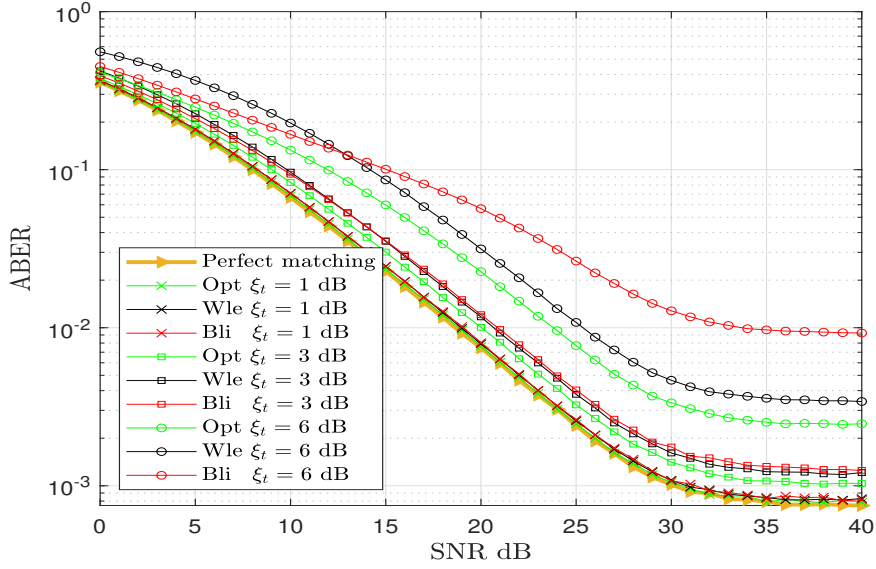


Figure 3.4: Effect of amplitude mismatching at STx side and assuming perfect CSI ( $\beta_t = 10^\circ$ ).

phase imbalance changes between  $5^\circ$ ,  $10^\circ$ , and  $15^\circ$ . It shows that the optimal receiver yields the best performance and it can completely resist the phase mismatching effect at the STx. In addition, the WLE and blind receivers have approximately the same performance at low and intermediate levels of phase mismatching while the WLE receiver exceeds the blind receiver at high level of phase mismatching. Even more, in the high SNR region, the SRx performance saturates, leading to an error floor and zero power gain due energy constraint limitation.

Figs 3.6 and 3.7 study the effects of the I/Q imbalance at SRx only and assuming perfect CSI. Fig. 3.6 shows the results of fixing the phase mismatch at  $10^\circ$  while varying the amplitude imbalance between 2, 4, and 6 dB, and Fig. 3.7 illustrates the ABER at the SRx by fixing the amplitude mismatch to 3 dB while the phase imbalance changes between  $0^\circ$ ,  $10^\circ$  and  $20^\circ$ . It can be seen from these figures that the optimal and the WLE receivers have the same performance exactly and that they outperform the blind receiver. In addition, the optimal and WLE receivers can resist the amplitude and phase mismatching effects completely. Finally, the blind receiver has an extremely poor performance at high values of the amplitude mismatching. For example, noting the 6 dB amplitude mismatching, 14

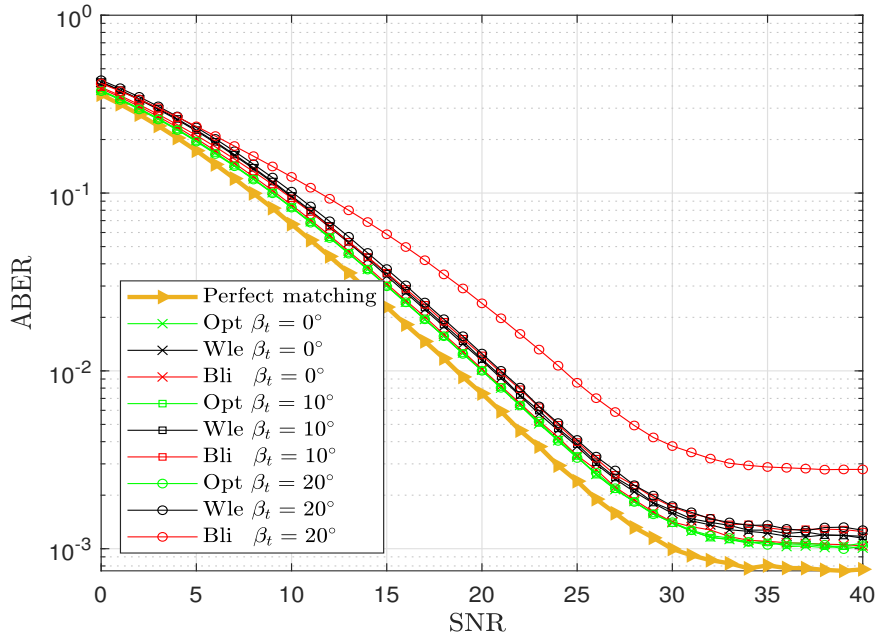


Figure 3.5: Effect of phase imbalance at STx side and assuming perfect CSI ( $\xi_t = 3$  dB).

dB of gain decrease between the blind receiver and the others can be seen at 0.03 ABER.

Fig. 3.8 illustrates the performance of the receivers in the presence of low, average and high levels of I/Q imbalance at STx/SRx with perfect CSI. This figure emphasizes the conclusions of the previous discussion where the optimal receiver has the best performance and the WLE receiver outperforms the blind receiver at high SNR. Moreover, the optimal and WLE receivers have approximately the same performance at low level I/Q imbalance.

Figs 3.9 and 3.10 illustrate the performance of the receivers in the presence of different levels of I/Q imbalance at STx/SRx with perfect CSI when higher modulation orders are used. The results in Figs 3.9 show 16-QAM modulation when using the same levels of I/Q imbalance as in Fig. 3.8. This figure shows how a low level of I/Q imbalance degrades the performance of the blind receiver. In Fig. 3.10, lower levels of I/Q imbalance are studied when using 256-QAM. The results in this figure emphasize that the proposed receiver has almost the same performance and can mitigate the I/Q imbalance when using higher modulation orders while this is not the case for the WLE and the blind receivers.

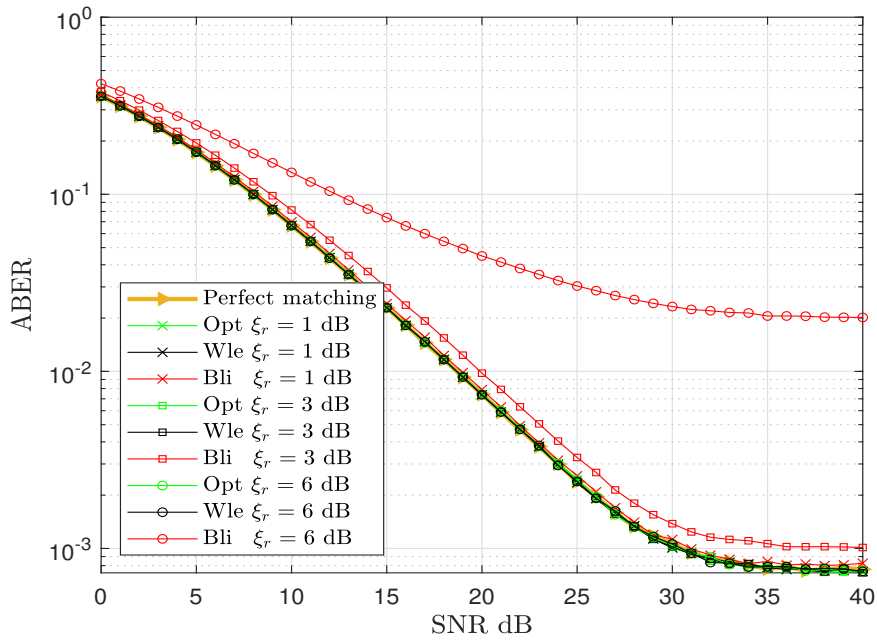


Figure 3.6: Effect of amplitude mismatching at SRx side and assuming perfect CSI ( $\beta_r = 10^\circ$ ).

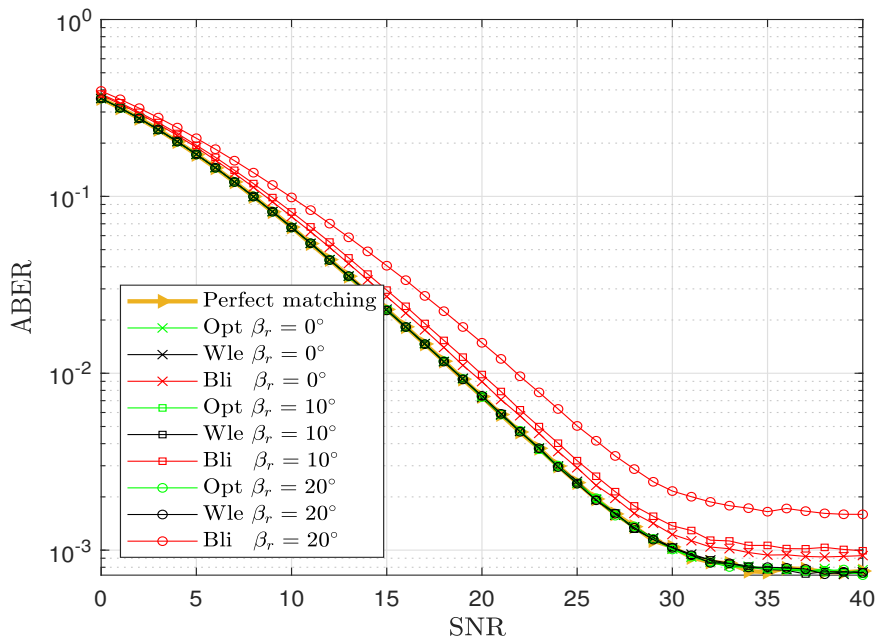


Figure 3.7: Effect of phase imbalance at SRx side and assuming perfect CSI ( $\xi_r = 3$  dB).

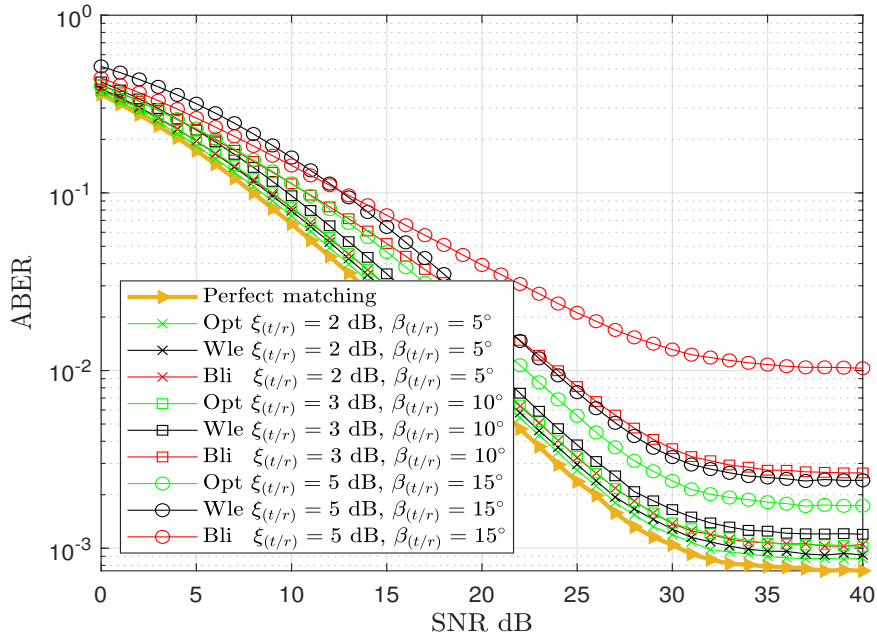


Figure 3.8: SRx in the presence of low, average and high levels of I/Q imbalance at STx/SRx with perfect CSI and PGN at the SRx (4-QAM).

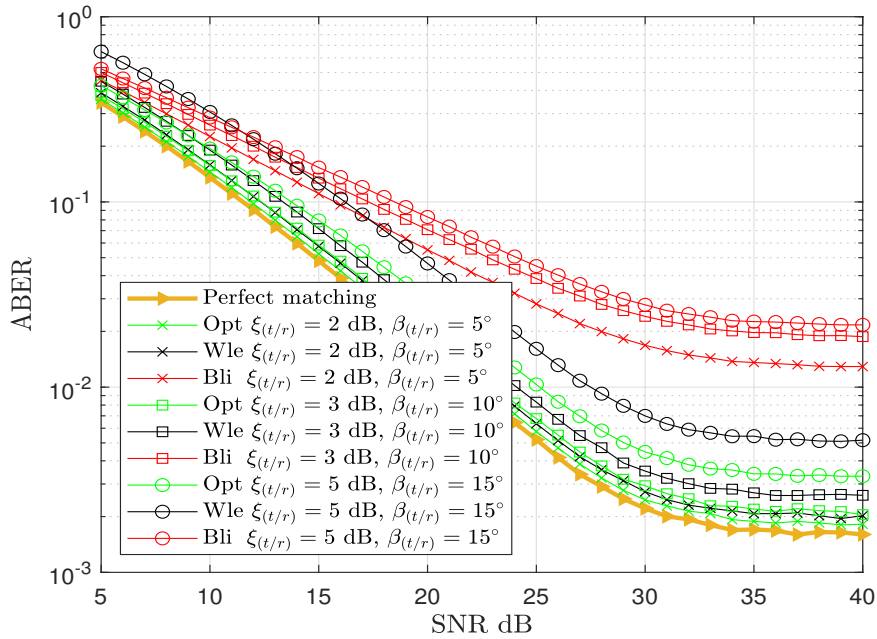


Figure 3.9: SRx in the presence of low, average and high levels of I/Q imbalance at STx/SRx with perfect CSI and PGN at the SRx (16-QAM).

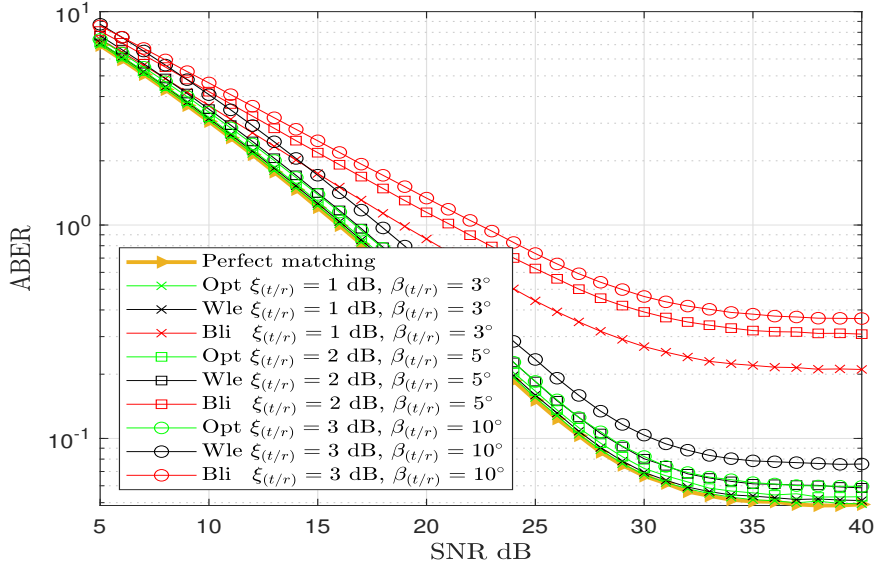


Figure 3.10: SRx in the presence of low, average and high levels of I/Q imbalance at STx/SRx with perfect CSI and PGN at the SRx (256-QAM).

Fig. 3.11 investigates the effect of channel estimation errors on the ABER, where it is assumed that the channel estimation error has real and imaginary variances equal to the CRLB values that were calculated in Section IV. This figure shows, as expected, how channel estimation errors can degrade the system performance of all the receivers even if it is assumed that the estimator has the best estimated real and imaginary channel values.

Figs. 3.12 and 3.13 discuss the effect of the number of pilots on the channel estimation error for both perfect and imperfect I/Q matching. In Fig. 3.12, the power gain between the perfect CSI and imperfect CSI for the optimal receiver when using one pilot equals 3 dB at ABER=0.02, the same power gain can be noticed for each receiver in Fig. 3.13. This clearly means that if the estimator reaches the CRLB, then the channel estimation error will not maximize the effect of the I/Q imbalance. Note that we normalize the transmitted power to get a fair comparison as it is shown in Appendix A.2.

Fig. 3.14 studies the effects of channel parameters (more details about these parameters can be found in Section 2.4). For a fair comparison,  $\Omega = 1$  for all channels.  $\Omega = \mu_{hI}^2 + \mu_{hQ}^2 + \sigma_{hI}^2 + \sigma_{hQ}^2$ , and indicates the average power of the fading channel. As the figure shows, the Rician fading channel has the best performance, and this is because of the

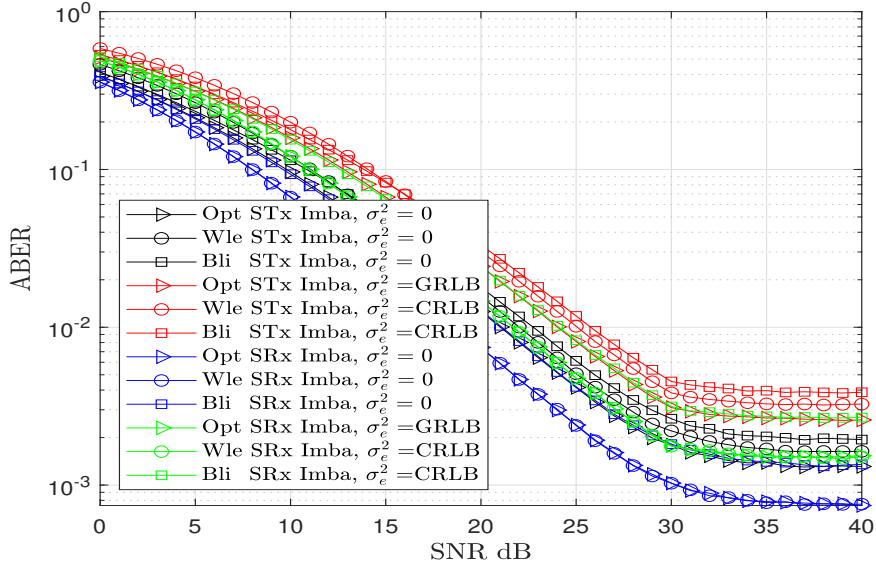


Figure 3.11: ABER at 4 dB amplitude mismatch and  $10^\circ$  phase imbalance at STx or SRx alone with perfect CSI or channel estimation errors that has CRLB variance.

LoS component. Here, the parameter  $K$  indicates the ratio between the LoS and non-LoS power. In addition, there is about a 3 dB reduction at  $10^{-3}$  ABER in the power gain for the Beckmann channel-1 that has the same Rician parameters except that it has correlated I and Q components. The same thing can be noticed between the Rayleigh channel and the Beckmann-2 channel that has the same Rayleigh parameters except that it has correlated I and Q components. The result in this figures indicates the importance of studying the performance of the more general fading channel model (Beckmann) where most of the well-known fading channel models can be considered as special cases of this one.

Figs. 3.15 and 3.16 illustrate the computational complexities of the proposed receivers for 4-QAM, 8-QAM, 16-QAM, 32-QAM, and 64-QAM modulation schemes. These figures demonstrate the number of real multiplications and summations which were calculated by assuming that the frame time is equal to the coherence time, and the number of symbols per frame is 1000. As expected, the blind receiver requires the minimum numbers of real multiplications and summations while the optimal one requires the largest numbers. Another interesting result from this figure is that the WLE receiver has almost the same complexity as the blind one even though there is a noticeable difference in their performances.

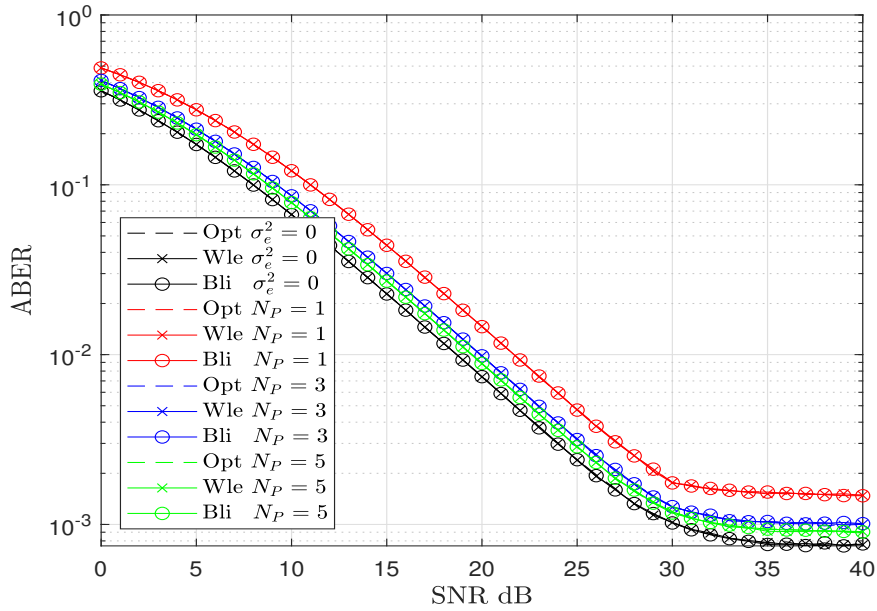


Figure 3.12: The effect of number of pilots on the channel estimation error at Perfect I/Q matching condition assuming  $\sigma_e^2 = \text{CRLB}$  and PGN at the SRx.

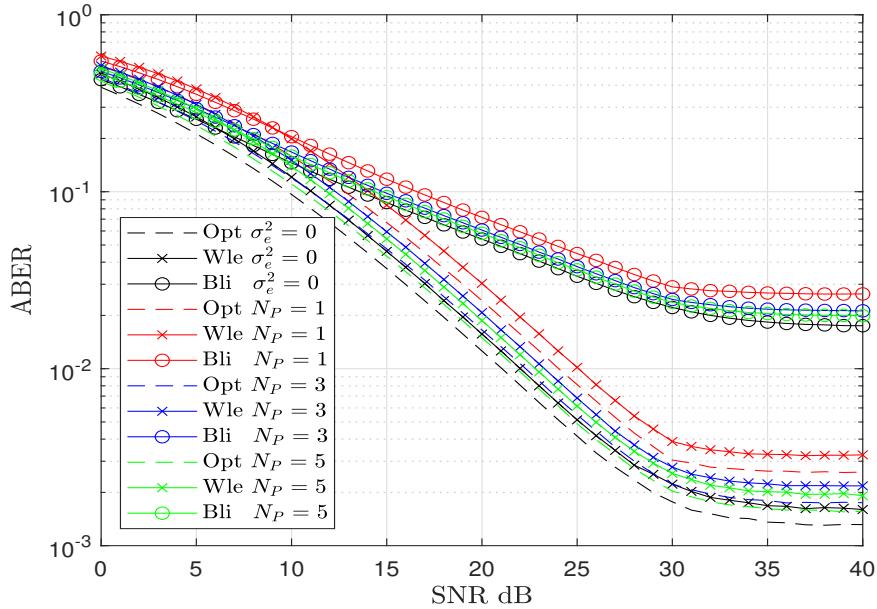


Figure 3.13: The effect of number of pilots on the channel estimation error with imperfect I/Q matching ( $\beta_{t,r} = 10^\circ$ ,  $\xi_{t,r} = 4$  dB), PGN, and assuming  $\sigma_e^2 = \text{CRLB}$ .

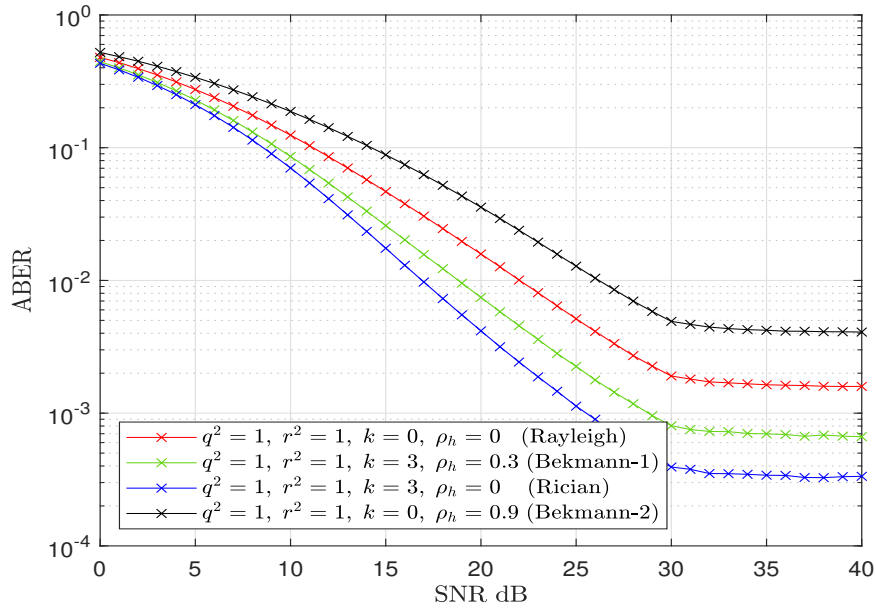


Figure 3.14: The effect of channel parameters assuming  $\sigma_e^2 = \text{CRLB}$ , PGN, and I/Q impaired transmitter and receiver where  $\xi_{t,r}=2$  dB and  $\beta_{t,r} = 5^\circ$ .

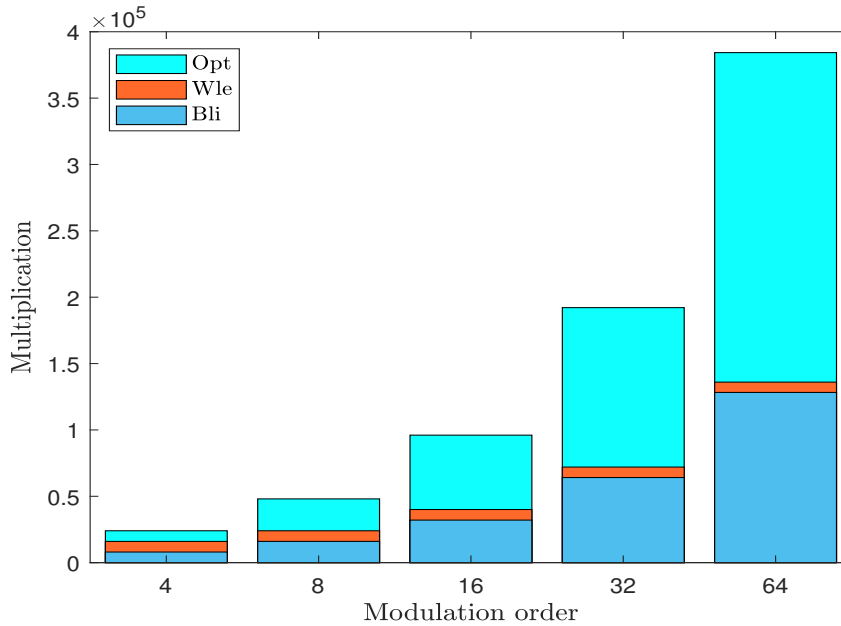


Figure 3.15: Number of multiplications of the proposed receivers assuming that the frame size is 1000 symbols.

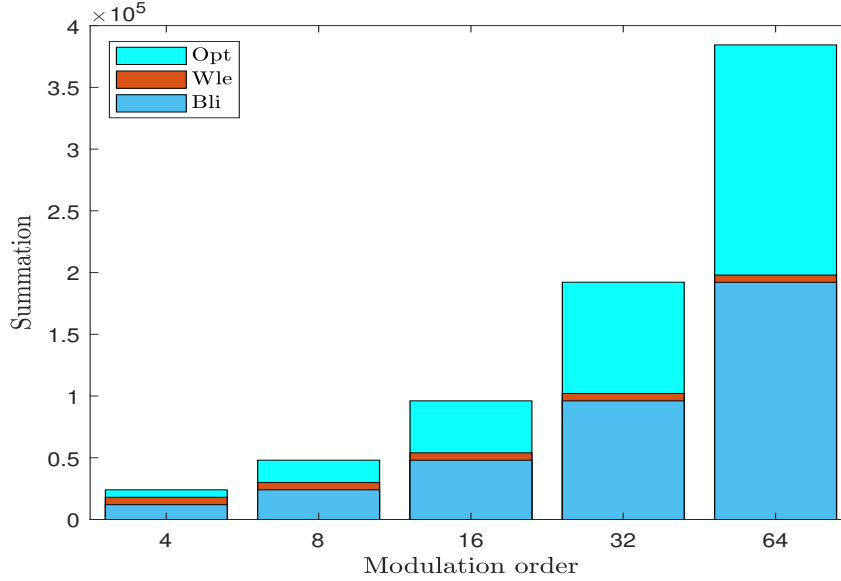


Figure 3.16: Number of summations of the proposed receivers assuming that the frame size is 1000 symbols.

### 3.7 Conclusion

This chapter presented an analytical framework to study the performance of a CR secondary system that has I/Q imbalance, imperfect CSI and IGN. The performance of the system was studied assuming Beckmann fading channels where most of the well-known fading channel models can be considered as special cases of this assumption. It was shown that the I/Q imbalance affects the system performance and this effect is maximized in case of imperfect CSI. Two receivers were designed: an optimal receiver and a widely linear one, where their performance was compared with the traditional ML receiver using different scenarios. It was proven that the optimal receiver has the best performance, while the widely linear one also out-performed the traditional one in all scenarios. Moreover, this work calculated the exact PEP of these receivers and APEP for the optimal one. Exact Fisher information matrix (FIM) and CRLB matrices were also calculated, proving that if the noise at the SRx is PGN, then the CRLB elements are not correlated even if the I/Q imbalance changes the Gaussian noise behavior from proper to improper.

# Chapter 4

## QSM Under the Effects of I/Q Imbalance, IGN and Imperfect CSI

### 4.1 Introduction and Related Works

The accelerated developments in mobile communication systems technology are moving the world toward a fully connected network with new challenges, including an inevitable trade-off between spectral efficiency and energy efficiency [88]. One of the key solutions for this problem is MIMO techniques [89]. Since MIMO techniques ensure a remarkable capacity gain, depending on the number of antennas, and provide high data rates as well, they have played a major role in recent standards such as LTE, LTE-advanced, and worldwide interoperability for microwave access (WiMAX) [90]. MIMO systems, which enable new deployments and architectures, will also be one of the key technologies in achieving 5G demands [1,91]. Significant challenges of next-generation MIMO technology can be summarized as follows: 1) design of multi-antenna transmission schemes with reduced complexity and number of RF chains, 2) avoiding inter-antenna synchronization and ICI, 3) improving energy efficiency (EE) [89].

In this context, SM has been introduced as a flexible solution to solve the main problems of traditional MIMO communications [92]. SM extends the conventional two-dimensional complex signal plane to a third dimension, which is called the spatial dimension. This

unique approach is based on the idea of using the TA index as an extra information source. Since only one TA is activated at each transmission time instant, *i.e.*, only one RF chain is operated; SM not only provides high EE but also eliminates the ICI and the requirement for the synchronization of TAs. Moreover, a high SE is achieved as the transmitted symbol carries a higher number of information bits at the same time duration [92]. A general survey of the SM design framework and of its limitations were presented in [93].

SSK was presented as a simple model based on SM where only the antenna index is used during the transmission, rather than the transmitted symbols themselves. This absence of symbol information eliminates the need for APM techniques at the transceivers. Consequently, this reduces the system complexity with keeping almost the same gain as SM [72].

QSM has been recently proposed in [75] to further enhance the SE of SM. The receiver complexity of SM and QSM schemes are equal and depends on the considered SE [75]. On the other hand, in QSM, spatial constellation symbols of conventional SM are expanded to include two spatial dimensions, each transmits the real and the imaginary parts of a conventional APM data symbol, separately. Since this transmission procedure is realized in an orthogonal manner, ICI is avoided in QSM as well. Additionally, the number of bits conveyed by active TA indices is twice that of SM [75].

Several schemes based on the unique manner of SSK have been investigated in the literature. For instance, an accurate framework for evaluating the performance of SSK over Rayleigh fading channels in the presence of imperfect CSI was presented in [47], and a simple asymptotic approximation for the error probability was also defined. The joint impact of imperfect CSI and co-channel interference (CCI) on the performance of SSK MIMO systems was investigated in [94]. Most recently, a general analytical SSK MIMO system scheme, which considers the effects of HWIs and CCI, was introduced in [95], and the deterioration effects of HWIs on SSK were proven. ML detector behavior in the presence of IGN was considered for the first time in [65] and [66]. The work in [65] confirmed that, exploiting the improperness of the Gaussian noise using the ML detector leads to decreasing the error probability when detecting the binary signals. In [66], a general likelihood test

was considered to detect the target patterns in multi-band spectral images. The results showed that more computational time is required to detect the patterns when the system is under the effect of IGN. In [96], the optimal ML receiver of single-input multiple-output (SIMO) system is used to detect the quadrature amplitude modulation symbols affected by IGN. It was shown that the ML receiver, under the assumption of IGN, outperforms the one under the assumption of PGN.

The work in [97] proposed a low-complexity compensation scheme to tackle the impact of I/Q imbalance at the base station for a massive MIMO system. In addition, the compensation method was used to mitigate I/Q imbalance encountered in wideband mmWave transmitters. Nevertheless, the effects of I/Q imbalance on SM techniques have not been investigated adequately, yet. Surprisingly, I/Q imbalance effects on QSM transmission were discussed in only one study in the literature. In [98], the performance of a QSM receiver under the effects of I/Q imbalance was examined and the PEP and the ABER performance were analyzed. However, this study was realized by utilizing a non-optimal solution under the assumption of perfect CSI.

The performance of the QSM was evaluated over small-scale fading channels in [99] and generalized fading scenarios in [100]. The issue of CCI and its negative impact on the performance of the QSM system was studied in [101], and the obtained results proved that QSM is superior to SM in the presence of CCI for the same system setup. The effect of imperfect CSI on the overall system performance of the QSM receiver was discussed in [102], and it was emphasized that the QSM system is considerably more robust to channel estimation errors than the conventional SM system while achieving higher SE. In addition to this, the results showed that, in the presence of imperfect CSI, QSM requires 3-5 decibel (dB) less signal power than the conventional SM for the same SE and error performance without any additional receiver complexity.

Recent studies also focused on extending QSM communications to CR systems [48, 103], cooperative relaying systems [104], and exploring low-complexity detectors [105]. All these studies converge on the point that QSM is a promising candidate for future wireless communication systems [100]-[105]. Additionally, because future wireless standards are

expected to be based on mmWave and large scale MIMO technologies, the combination of mmWave and QSM schemes was studied in [106], and significant performance enhancements were achieved under different system and channel configurations. In [107], capacity analysis for the QSM scheme over a three-dimensional mmWave MIMO wireless communication system was provided. The adoption of QSM for large-scale MIMO configurations was presented in [108], where a low-complexity decoder was proposed and analyzed.

To the best of our knowledge, no work in the literature proposed an ideal receiver design that can mitigate the effects of I/Q imbalance on QSM systems and accurately treat the IGN at the receiver. Therefore, in this chapter, the traditional ML detector design is accurately adapted for QSM systems that suffer from I/Q imbalance at the transmitter and receiver sides in the presence of imperfect CSI at the receiver side. In addition, the AWGN at the receiver is assumed to be IGN. An optimum ML detection method is proposed to tackle the effects of self-interference and signal distortion caused by I/Q imbalance and to treat the impact of IGN at the receiver in the proper way. Average PEP and ABER are defined, and an asymptotic approximation is presented. The simulation results match the analytical derivations which prove the presented analysis. At the end of this chapter, we discuss the effect of IGN on the SSK receiver and propose the appropriate design that accurately treat the IGN. The given results prove that the proposed optimal ML detector design is superior to the traditional ML detector and successfully makes QSM robust against the I/Q imbalance. Parts of the results in this chapter have been published in [32, 54, 109].

The rest of this chapter is organized as follows: Section 4.2 describes the QSM system and channel models. Section 4.3 discusses the accumulative noise at the receiver. Section 4.4 provides the receiver design and performance analysis for the presented model. Section 4.6 describes the SSK system under the effect of IGN. Section 4.7 discusses the numerical analysis and results. Finally, Section 4.8 concludes this chapter.

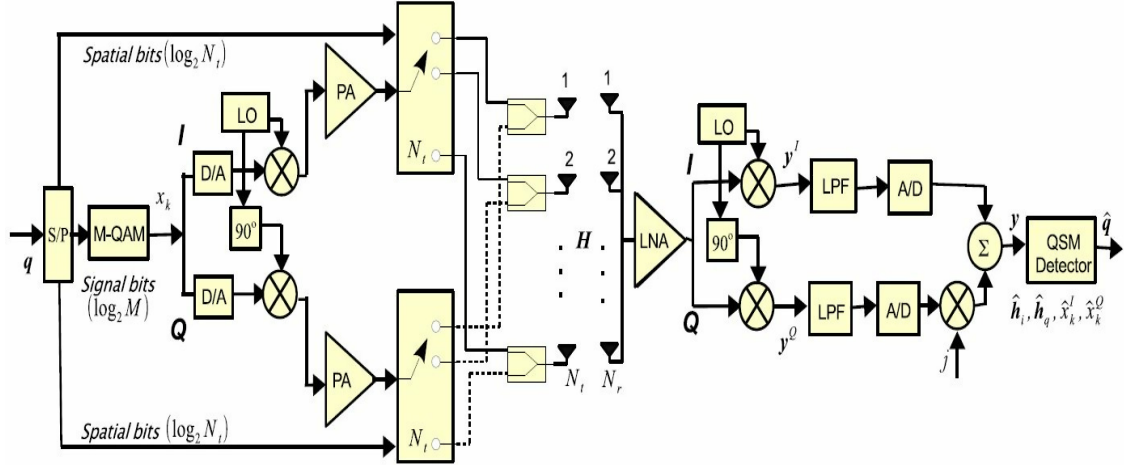


Figure 4.1: The scheme of QSM wireless communication system employing a homodyne architecture transceiver.

## 4.2 System and Channel Models

Consider a QSM wireless communication system employing a direct down-conversion (DDC), also referred to as homodyne architecture transceiver in the RF front-end as given in Fig. 4.1. First of all, the incoming data stream  $\mathbf{q}$  is partitioned into groups, each of which has  $m = \log_2(N_t^2 M)$  bits at the transmitter side ( $M$  is modulation order of complex constellations and  $N_t$  is the number of TAs). These groups are further divided into three blocks of bits, where two of these blocks are used for spatial mapping and the remaining one is used for ordinary signal mapping. Each signal bit block has  $\log_2(M)$  bits and modulates a conventional amplitude/phase modulation symbol, e.g.,  $M$ -QAM.

During this homodyne up-conversion stage, the baseband digital signal  $x_k$ ,  $k = [1, \dots, M]$ , is first converted to an analog signal. Then,  $x_k^I$  modulates the I part (cosine) of the carrier, whereas  $x_k^Q$  modulates the Q part (sine) of the carrier. After amplifying the I and Q parts of the signal with power amplifiers (PAs), they are mapped into transmitter indices by using spatial bits, which act as controllers to enable or disable the TAs at each specific time instant by QSM demultiplexer. The RF signal goes through an  $N_r \times N_t$  sized fading channel characterized by  $\mathbf{H}$  ( $N_r$  is the number of receiver antennas). The columns of the channel matrix,  $\mathbf{h}_i$ , represents the complex fading coefficients between the  $i^{th}$  transmitter

and all receiver antennas, and  $h_{l,i}$  represents the complex fading coefficients between the  $i^{\text{th}}$  transmitter and  $l^{\text{th}}$  receiver antennas.

At the receiver side, the received signal is first amplified by a low-noise amplifier (LNA) and then, quadrature mixing is applied by LO. Afterwards, the signal on each branch passes through a LPF and an ADC converter, respectively. After all these operations, the QSM detector recovers the whole information block (activated antenna indices and the transmitted symbol). The noise vector  $\mathbf{n} = [n_1, \dots, n_{N_r}]^T$  at the receiver antennas has uncorrelated and identical components at each receiver. Here, being identical means that they have the same mean vector and covariance matrix. The noise at each receiver is improper and follows  $\mathcal{CN}(\mathbf{0}, \boldsymbol{\sigma}_{\mathbf{n}_l}^2)$ , where the covariance matrix  $\boldsymbol{\sigma}_{\mathbf{n}_l}^2$  is given by

$$\boldsymbol{\sigma}_{\mathbf{n}_l}^2 = \begin{bmatrix} \sigma_{n_l^I}^2 & \rho_{n_l} \sigma_{n_l^I} \sigma_{n_l^Q} \\ \rho_{n_l} \sigma_{n_l^I} \sigma_{n_l^Q} & \sigma_{n_l^Q}^2 \end{bmatrix}.$$

### 4.2.1 Imperfect CSI Model

In practical MIMO systems, the channel matrix  $\mathbf{H}$  is not known at the receiver side, and a channel estimation algorithm is used to obtain the estimated channel matrix  $\hat{\mathbf{H}}$ . In the presence of estimation error, one can write

$$\mathbf{H} = \hat{\mathbf{H}} + \mathbf{H}_e, \quad (4.1)$$

where  $\mathbf{H}_e$  is the channel estimation error matrix. However, as shown in Section 2.5, it is assumed that the fading channel component  $h_{l,i}$  and the estimated version of it  $\hat{h}_{l,i}$  are jointly ergodic and stationary. Therefore, the related channel estimation error  $e_{l,i}$  can be modeled as  $\mathcal{CN}(\mathbf{0}, \boldsymbol{\sigma}_{e_{l,i}}^2)$  where the covariance matrix  $\boldsymbol{\sigma}_{e_{l,i}}^2$  is given by

$$\boldsymbol{\sigma}_{e_{l,i}}^2 = \begin{bmatrix} \sigma_{e_{l,i}^I}^2 & \rho_{e_{l,i}} \sigma_{e_{l,i}^Q} \sigma_{e_{l,i}^I} \\ \rho_{e_{l,i}} \sigma_{e_{l,i}^Q} \sigma_{e_{l,i}^I} & \sigma_{e_{l,i}^Q}^2 \end{bmatrix}.$$

Here, it is worth noting that  $\boldsymbol{\sigma}_{e_{l,i}}^2$  indicates the quality of the estimation and can be chosen depending on the channel dynamics and estimation methods.

## 4.2.2 Transceiver I/Q Imbalance Model

Considering the frequency-independent I/Q imbalance model as shown in Section 2.6, the transmitted signal can be given as

$$\tilde{x}_k = G_1 x_k + G_2 x_k^*, \quad (4.2)$$

where  $G_1 = \frac{1}{2}(1 + \xi_t e^{j\beta_t})$  and  $G_2 = \frac{1}{2}(1 - \xi_t e^{j\beta_t})$  are I/Q imbalance parameters at the transmitter. Here,  $\xi_t$  and  $\beta_t$  represent the amplitude and the phase mismatches in the up-conversion process, respectively. Now, denoting that  $G_c = (G_1^Q - G_2^Q)$  and  $G_d = (G_1^I - G_2^I)$ , and noting that  $G_1^I + G_2^I = 1$  and  $G_1^Q + G_2^Q = 0$ ,  $\tilde{x}_k^I$  and  $\tilde{x}_k^Q$  can be given as

$$\tilde{x}_k^I = x_k^I - x_k^Q G_c, \quad \tilde{x}_k^Q = x_k^Q G_d. \quad (4.3)$$

Considering the effects of the I/Q imbalance model at the receiver side, the received baseband signal at  $l^{\text{th}}$  receiver antenna is

$$y_l = K_1 \left[ \sqrt{E} (h_{l,i} \tilde{x}_k^I + j h_{l,q} \tilde{x}_k^Q) + n_l \right] + K_2 \left[ \sqrt{E} (h_{l,i} \tilde{x}_k^I + j h_{l,q} \tilde{x}_k^Q) + n_l \right]^*, \quad (4.4)$$

where  $\{i, q\} \in \{1, \dots, N_t\}$  and denote the indices of the activated QSM TAs,  $l = \{1, \dots, N_r\}$ . Here  $h_{l,i}$  and  $h_{l,q}$  are the corresponding complex channel coefficients,  $E$  is the transmitted signal energy and  $K_1 = \frac{1}{2}(1 + \xi_r e^{-j\beta_r})$  and  $K_2 = \frac{1}{2}(1 - \xi_r e^{j\beta_r})$  are I/Q imbalance coefficients at the receiver. Here, where  $\xi_r$  and  $\beta_r$  represent the amplitude and the phase mismatches in the down-conversion process, respectively.

Now, denoting  $K_c = K_1^Q + K_2^Q$  and  $K_d = K_1^I - K_2^I$ , and noting that  $K_1^I + K_2^I = 1$  and  $K_1^Q - K_2^Q = 0$ , (4.4) can be rewritten after some mathematical operations by using (4.1) as

$$\begin{aligned} y_l = & \sqrt{E} \{ \tilde{h}_{l,i}^I (x_k^I - x_k^Q G_c) - \tilde{h}_{l,q}^Q x_k^Q G_d \} + n_l^I + \sqrt{E} \{ e_{l,i}^I (x_k^I - x_k^Q G_c) - e_{l,q}^Q x_k^Q G_d \} \\ & + j \sqrt{E} \{ \tilde{h}_{l,i}^I (x_k^I - x_k^Q G_c) K_c + \tilde{h}_{l,i}^Q (x_k^I - x_k^Q G_c) K_d - \tilde{h}_{l,q}^Q x_k^Q G_d K_c + \tilde{h}_{l,q}^I x_k^Q G_d K_d \} \\ & + j \sqrt{E} \{ e_{l,i}^I (x_k^I - x_k^Q G_c) K_c + e_{l,i}^Q (x_k^I - x_k^Q G_c) K_d - e_{l,q}^Q x_k^Q G_d K_c + e_{l,q}^I x_k^Q G_d K_d \} \\ & + j \{ n_l^I K_c + n_l^Q K_d \}. \end{aligned} \quad (4.5)$$

*Proof:* See the Appendix B.1.

### 4.3 Accumulative Noise at the Receiver

The accumulative noise is affected by the I/Q parameters at the transmitter and receiver, the channel estimation error, and the noise at the receiver. If the noise at the receiver is improper (which is the more general case), then the channel estimation error is assumed to be improper as well. From (4.5), the noise component of  $y_l$ , which is a zero-mean complex Gaussian RV, is given by

$$\begin{aligned} \tilde{n}_l = & n_l^I + \sqrt{E}\{e_{l,i}^I(x_k^I - x_k^Q G_c) - e_{l,q}^Q x_k^Q G_d\} + j\{n_l^I K_c + n_l^Q K_d\}. \\ & + j\sqrt{E}\{e_{l,i}^I(x_k^I - x_k^Q G_c)K_c + e_{l,i}^Q(x_k^I - x_k^Q G_c)K_d - e_{l,q}^Q x_k^Q G_d K_c + e_{l,q}^I x_k^Q G_d K_d\}. \end{aligned} \quad (4.6)$$

As explained in Section 2.2, the improper characteristics of a complex RV variable are based on the existence of at least one of these two conditions: i) the real and imaginary parts are correlated or ii) the real and imaginary parts do not have the same variance (non-identical). In order to analyze the improper characteristics of  $\tilde{n}_l$ , these two conditions need to be checked. It can be directly concluded that the accumulative noise is improper because we assumed in our model that the noise  $\tilde{n}_l$  is improper. Based on this, the variances of the real and imaginary parts of  $n_l$  are calculated as follows

$$\begin{aligned} \sigma_{\tilde{n}_l^I}^2 = & \sigma_{n_l^I}^2 + E(x_k^I - x_k^Q G_c)^2 \sigma_{e_{l,i}^I}^2 + E(x_k^Q G_d)^2 \sigma_{e_{l,q}^Q}^2, \\ \sigma_{\tilde{n}_l^Q}^2 = & \sigma_{n_l^I}^2 K_c^2 + \sigma_{n_l^Q}^2 K_d^2 + 2\rho_{n_l} K_c K_d \sigma_{n_l}^I \sigma_{n_l}^Q \\ & + E(x_k^I - x_k^Q G_c)^2 \sigma_{e_{l,i}^I}^2 K_c^2 + E(x_k^I - x_k^Q G_c)^2 \sigma_{e_{l,i}^Q}^2 K_d^2 + 2E\rho_{l,i}^e K_c K_d (x_k^I - x_k^Q G_c)^2 \sigma_{e_{l,i}^I}^Q \sigma_{e_{l,i}^I}^I \\ & + E(x_k^Q G_d)^2 \sigma_{e_{l,q}^Q}^2 K_c^2 + E(x_k^Q G_d)^2 \sigma_{e_{l,q}^I}^2 K_d^2 + 2E\rho_{l,q}^e K_c K_d (x_k^Q G_d)^2 \sigma_{e_{l,q}^Q}^I \sigma_{e_{l,q}^Q}^I. \end{aligned} \quad (4.7)$$

The correlation coefficient can be calculated using (4.7) as

$$\rho_l = \frac{\text{cov}\{\tilde{n}_l^I \tilde{n}_l^Q\}}{\sqrt{\sigma_{\tilde{n}_l^I}^2 \sigma_{\tilde{n}_l^Q}^2}}, \quad (4.8)$$

where  $\mathbb{E}\{\tilde{n}_l^I \tilde{n}_l^Q\}$  is given by

$$\begin{aligned} \mathbb{E}\{\tilde{n}_l^I \tilde{n}_l^Q\} = & \sigma_{n_l^I}^2 K_c + \rho_{n_l} \sigma_{n_l}^I \sigma_{n_l}^Q K_d + E(x_k^I - x_k^Q G_c)^2 \sigma_{e_{l,i}^I}^2 K_c + E(x_k^I - x_k^Q G_c)^2 \rho_{l,i}^e \sigma_{e_{l,i}^I}^Q \sigma_{e_{l,i}^I}^I K_d \\ & + E(x_k^Q G_d)^2 \sigma_{e_{l,q}^Q}^2 K_c - E(x_k^Q G_d)^2 \rho_{l,q}^e \sigma_{e_{l,q}^Q}^I \sigma_{e_{l,q}^Q}^I K_d. \end{aligned} \quad (4.9)$$

Now, noting that the channel estimation errors  $e_{l,i}$  and  $e_{l,q}$  are uncorrelated and identical, (4.7) and (4.9) can be rewritten as (4.10) and (4.11) respectively by

$$\begin{aligned}\sigma_{\tilde{n}_l^I}^2 &= \sigma_{n_l^I}^2 + E(x_k^I - x_k^Q G_c)^2 \sigma_{e^I}^2 + E(x_k^Q G_d)^2 \sigma_{e^Q}^2, \\ \sigma_{\tilde{n}_l^Q}^2 &= E\sigma_{e^I}^2 [(x_k^I - x_k^Q G_c)^2 K_c^2 + (x_k^Q G_d)^2 K_d^2] + E\sigma_{e^Q}^2 [(x_k^I - x_k^Q G_c)^2 K_d^2 + (x_k^Q G_d)^2 K_c^2] \\ &\quad + 2E\rho_e K_c K_d [(x_k^I - x_k^Q G_c)^2 + (x_k^Q G_d)^2] \sigma_e^I \sigma_e^Q + \sigma_{n_l^I}^2 K_c^2 + \sigma_{n_l^Q}^2 K_d^2.\end{aligned}\quad (4.10)$$

$$\begin{aligned}\mathbb{E}\{\tilde{n}_l^I \tilde{n}_l^Q\} &= \sigma_{n_l^I}^2 K_c + \rho_{n_l} \sigma_{n_l}^I \sigma_{n_l}^Q K_d + EK_c [\sigma_{e^I}^2 (x_k^I - x_k^Q G_c)^2 + \sigma_{e^Q}^2 (x_k^Q G_d)^2] \\ &\quad + E\rho_e \sigma_e^Q \sigma_e^I K_d [(x_k^I - x_k^Q G_c)^2 - (x_k^Q G_d)^2].\end{aligned}\quad (4.11)$$

To understand the effects of I/Q imbalance on the accumulated noise at each receiver antenna, it would be well worth considering a special case when the AWGN is PGN. In this case,  $\sigma_{\tilde{n}_l^I}^2$ ,  $\sigma_{\tilde{n}_l^Q}^2$ , and  $\mathbb{E}\{\tilde{n}_l^I \tilde{n}_l^Q\}$  are given by

$$\begin{aligned}\sigma_{\tilde{n}_l^I}^2 &= \frac{\sigma_n^2}{2} + E\frac{\sigma_e^2}{2} [(x_k^I - x_k^Q G_c)^2 + (x_k^Q G_d)^2], \\ \sigma_{\tilde{n}_l^Q}^2 &= (K_c^2 + K_d^2) \left\{ \frac{\sigma_n^2}{2} + E\frac{\sigma_e^2}{2} [(x_k^I - x_k^Q G_c)^2 + (x_k^Q G_d)^2] \right\}, \\ \mathbb{E}\{\tilde{n}_l^I \tilde{n}_l^Q\} &= K_c \left\{ \frac{\sigma_n^2}{2} + E\frac{\sigma_e^2}{2} [(x_k^I - x_k^Q G_c)^2 + (x_k^Q G_d)^2] \right\}.\end{aligned}\quad (4.12)$$

As can be noted from the previous equations, the resulting accumulated noise is improper noise even though the AWGN is proper. This means the traditional ML detector that ignores the fact that the accumulated noise is improper can not work efficiently. Consequently, there is a need to design an optimal receiver that can tackle this fact.

On the other hand, the useful signal part of (4.5) along with the I/Q imbalance effects and fading characteristics is given by

$$\begin{aligned}\tilde{\chi}_p &= \{\tilde{\mathbf{h}}_{l,i}^I (x_k^I - x_k^Q G_c) - \tilde{\mathbf{h}}_{l,q}^Q x_k^Q G_d\} \\ &\quad + j\{\tilde{\mathbf{h}}_{l,i}^I (x_k^I - x_k^Q G_c) K_c + \tilde{\mathbf{h}}_{l,i}^Q (x_k^I - x_k^Q G_c) K_d - \tilde{\mathbf{h}}_{l,q}^Q x_k^Q G_d K_c + \tilde{\mathbf{h}}_{l,q}^I x_k^Q G_d K_d\},\end{aligned}\quad (4.13)$$

where  $p \in \{1, \dots, N_t^2 M\}$ . Considering the received useful signal component vector  $\tilde{\chi}_p$  and the complex IGN vector  $\tilde{\mathbf{n}}$ , (4.5) can be rewritten as

$$\mathbf{y} = \sqrt{E} \tilde{\chi}_p + \tilde{\mathbf{n}}.\quad (4.14)$$

## 4.4 Optimal ML Receiver Design

It has been shown in the previous section that the accumulative noise at the receiver is improper. In this section, an optimal ML detector is proposed for the presented QSM wireless communication system operating under this practical condition.

Considering the general signal model in (4.14), the joint multivariate PDF of the real part,  $\mathbf{y}^I$ , and the imaginary part,  $\mathbf{y}^Q$ , of the received signal can be derived that the I/Q imbalance parameters are known at the receiver side as

$$f_{\mathbf{y}^I, \mathbf{y}^Q}(\mathbf{y}^I, \mathbf{y}^Q | \tilde{\chi}_p) = \left( \frac{1}{2\pi\sigma_{\tilde{n}_I}\sigma_{\tilde{n}_Q}\sqrt{1-\varrho_l^2}} \right)^{N_r} \times \exp \left( \frac{-1}{2(1-\varrho_l^2)} \left[ \frac{\|\mathbf{y}^I - \sqrt{E}\tilde{\chi}_p^I\|^2}{\sigma_{\tilde{n}_I}^2} + \frac{\|\mathbf{y}^Q - \sqrt{E}\tilde{\chi}_p^Q\|^2}{\sigma_{\tilde{n}_Q}^2} - \frac{2\varrho_l(\mathbf{y}^I - \sqrt{E}\tilde{\chi}_p^I)^T(\mathbf{y}^Q - \sqrt{E}\tilde{\chi}_p^Q)}{\sigma_{\tilde{n}_I}\sigma_{\tilde{n}_Q}} \right] \right). \quad (4.15)$$

The optimal ML detector is designed based on maximizing the following conditional probability for equiprobable symbols

$$\hat{p} = \arg \max_p \{f_{\mathbf{y}^I, \mathbf{y}^Q}(\mathbf{y}^I, \mathbf{y}^Q | \tilde{\chi}_p)\}. \quad (4.16)$$

Using (4.15) and (4.16), a decision rule for optimal ML which jointly accounts the errors in transmitter indices and symbols detection can be defined by

$$\hat{p} = \arg \min_p \left\{ \frac{\|\mathbf{y}^I - \sqrt{E}\tilde{\chi}_p^I\|^2}{\sigma_{\tilde{n}_I}^2} + \frac{\|\mathbf{y}^Q - \sqrt{E}\tilde{\chi}_p^Q\|^2}{\sigma_{\tilde{n}_Q}^2} - \frac{2\varrho_l(\mathbf{y}^I - \sqrt{E}\tilde{\chi}_p^I)^T(\mathbf{y}^Q - \sqrt{E}\tilde{\chi}_p^Q)}{\sigma_{\tilde{n}_I}\sigma_{\tilde{n}_Q}} \right\}, \quad (4.17)$$

At this point, it is worth noting that the traditional (blind) ML detector, which neglects the improper characteristics of the accumulative noise and ignores the I/Q imbalance effects under ideal hardware assumption, cannot provide an optimal solution for our system model as we need to consider the amplitude imbalance  $\xi_r$  and the phase impairment  $\beta_r$ . In the case of using traditional ML detection, a non-optimal detector can be given by assuming that  $\tilde{\chi}_p$ , which is under the effects of I/Q imbalance, has been sent and  $K_1$  and  $K_2$  are unknown at the receiver side:

$$[\hat{i}, \hat{q}, \hat{x}_k^I, \hat{x}_k^Q] = \arg \min_{i, q, x_k} \|\mathbf{y} - \sqrt{E}(\tilde{\mathbf{h}}_i x_k^I + j\tilde{\mathbf{h}}_q x_k^Q)\|^2. \quad (4.18)$$

## 4.5 Error Performance Analysis

### 4.5.1 Average Pairwise Error Probability

Considering the optimal ML detection rule given in (4.17), the PEP can be calculated from (4.19) under the assumption of that  $\tilde{\boldsymbol{\chi}}_p$  has been transmitted, while  $\hat{\boldsymbol{\chi}}_p$  is detected erroneously at the receiver as

$$\begin{aligned} \Pr(\tilde{\boldsymbol{\chi}}_p \rightarrow \hat{\boldsymbol{\chi}}_p | \tilde{\mathbf{H}}) &= \\ \Pr\left( \frac{\|\mathbf{y}^I - \sqrt{E}\tilde{\boldsymbol{\chi}}_p^I\|^2}{\sigma_{\tilde{n}_l^I}^2} + \frac{\|\mathbf{y}^Q - \sqrt{E}\tilde{\boldsymbol{\chi}}_p^Q\|^2}{\sigma_{\tilde{n}_l^Q}^2} - \frac{2\varrho_l(\mathbf{y}^I - \sqrt{E}\tilde{\boldsymbol{\chi}}_p^I)^T(\mathbf{y}^Q - \sqrt{E}\tilde{\boldsymbol{\chi}}_p^Q)}{\sigma_{\tilde{n}_l^I}\sigma_{\tilde{n}_l^Q}} \right. \\ &> \left. \frac{\|\mathbf{y}^I - \sqrt{E}\hat{\boldsymbol{\chi}}_p^I\|^2}{\sigma_{\tilde{n}_l^I}^2} + \frac{\|\mathbf{y}^Q - \sqrt{E}\hat{\boldsymbol{\chi}}_p^Q\|^2}{\sigma_{\tilde{n}_l^Q}^2} - \frac{2\varrho_l(\mathbf{y}^I - \sqrt{E}\hat{\boldsymbol{\chi}}_p^I)^T(\mathbf{y}^Q - \sqrt{E}\hat{\boldsymbol{\chi}}_p^Q)}{\sigma_{\tilde{n}_l^I}\sigma_{\tilde{n}_l^Q}} \right). \end{aligned} \quad (4.19)$$

Here,  $\hat{\boldsymbol{\chi}}_p = \{\hat{\mathbf{h}}_{l,i}^I(\hat{x}_k^I - \hat{x}_k^Q G_c) - \hat{\mathbf{h}}_{l,q}^Q \hat{x}_k^Q G_d\} + j\{\hat{\mathbf{h}}_{l,i}^I(\hat{x}_k^I - \hat{x}_k^Q G_c)K_c + \hat{\mathbf{h}}_{l,i}^Q(\hat{x}_k^I - \hat{x}_k^Q G_c)K_d - \hat{\mathbf{h}}_{l,q}^Q \hat{x}_k^Q G_d K_c + \hat{\mathbf{h}}_{l,q}^I \hat{x}_k^Q G_d K_d\}$ , while  $\hat{\mathbf{h}}_i$  and  $\hat{\mathbf{h}}_q$  are the complex channel coefficients related to detected TAs that transmit the real and imaginary parts of the detected signal  $\hat{x}_k$ . After some algebraic simplifications, it is determined that

$$\begin{aligned} \text{PEP} &= \\ \Pr\left( \frac{2\varrho_l \sqrt{E} \{(\tilde{\boldsymbol{\chi}}_p^I - \hat{\boldsymbol{\chi}}_p^I)^T \tilde{\mathbf{n}}_l^Q (\tilde{\boldsymbol{\chi}}_p^Q - \hat{\boldsymbol{\chi}}_p^Q)^T \tilde{\mathbf{n}}_l^I\}}{\sigma_{\tilde{n}_l^I} \sigma_{\tilde{n}_l^Q}} - \frac{2\sqrt{E}(\tilde{\boldsymbol{\chi}}_p^I - \hat{\boldsymbol{\chi}}_p^I)^T \tilde{\mathbf{n}}_l^I}{\sigma_{\tilde{n}_l^I}^2} - \frac{2\sqrt{E}(\tilde{\boldsymbol{\chi}}_p^Q - \hat{\boldsymbol{\chi}}_p^Q)^T \tilde{\mathbf{n}}_l^Q}{\sigma_{\tilde{n}_l^Q}^2} \right. \\ &\left. - \frac{E\|\tilde{\boldsymbol{\chi}}_p^I - \hat{\boldsymbol{\chi}}_p^I\|^2}{\sigma_{\tilde{n}_l^I}^2} - \frac{E\|\tilde{\boldsymbol{\chi}}_p^Q - \hat{\boldsymbol{\chi}}_p^Q\|^2}{\sigma_{\tilde{n}_l^Q}^2} + \frac{2\varrho_l E (\tilde{\boldsymbol{\chi}}_p^I - \hat{\boldsymbol{\chi}}_p^I)^T (\tilde{\boldsymbol{\chi}}_p^Q - \hat{\boldsymbol{\chi}}_p^Q)}{\sigma_{\tilde{n}_l^I} \sigma_{\tilde{n}_l^Q}} > 0 \right) = \Pr(\mathcal{K} > 0), \end{aligned} \quad (4.20)$$

where  $\mathcal{K}$ , conditioned on  $\tilde{\boldsymbol{\chi}}_p$ , is a Gaussian RV. The mean and variance values of  $\mathcal{K}$  are obtained respectively as

$$\mu_{\mathcal{K}} = \left( \frac{E\|\tilde{\boldsymbol{\chi}}_p^I - \hat{\boldsymbol{\chi}}_p^I\|^2}{\sigma_{\tilde{n}_l^I}^2} + \frac{E\|\tilde{\boldsymbol{\chi}}_p^Q - \hat{\boldsymbol{\chi}}_p^Q\|^2}{\sigma_{\tilde{n}_l^Q}^2} - \frac{2\varrho_l E (\tilde{\boldsymbol{\chi}}_p^I - \hat{\boldsymbol{\chi}}_p^I)^T (\tilde{\boldsymbol{\chi}}_p^Q - \hat{\boldsymbol{\chi}}_p^Q)}{\sigma_{\tilde{n}_l^I} \sigma_{\tilde{n}_l^Q}} \right), \quad (4.21)$$

$$\sigma_{\mathcal{K}}^2 = 4E(1 - \varrho_l^2) \times \left( \frac{\|\tilde{\boldsymbol{\chi}}_p^I - \hat{\boldsymbol{\chi}}_p^I\|^2}{\sigma_{\tilde{n}_l^I}^2} + \frac{\|\tilde{\boldsymbol{\chi}}_p^Q - \hat{\boldsymbol{\chi}}_p^Q\|^2}{\sigma_{\tilde{n}_l^Q}^2} - \frac{2\varrho_l (\tilde{\boldsymbol{\chi}}_p^I - \hat{\boldsymbol{\chi}}_p^I)^T (\tilde{\boldsymbol{\chi}}_p^Q - \hat{\boldsymbol{\chi}}_p^Q)}{\sigma_{\tilde{n}_l^I} \sigma_{\tilde{n}_l^Q}} \right). \quad (4.22)$$

PEP can also be defined by using the well-known  $Q$ -function as follows

$$\text{PEP} = Q\left(\frac{\mathbb{E}\{\mathcal{K}\}}{\sqrt{\text{var}(\mathcal{K})}}\right) = Q\left(\frac{\mu_{\mathcal{K}}}{\sqrt{\sigma_{\mathcal{K}}^2}}\right). \quad (4.23)$$

By substituting (4.21) and (4.22) in (4.23), considering (4.7), PEP is given as

$$\begin{aligned} \text{PEP} &= Q\left(\sqrt{\frac{E}{2(1-\varrho_l^2)}\left(\frac{\|\tilde{\mathbf{x}}_p^I - \hat{\mathbf{x}}_p^I\|^2}{\sigma_{\tilde{n}_l^I}^2} + \frac{\|\tilde{\mathbf{x}}_p^Q - \hat{\mathbf{x}}_p^Q\|^2}{\sigma_{\tilde{n}_l^Q}^2} - \frac{2\varrho_l(\tilde{\mathbf{x}}_p^I - \hat{\mathbf{x}}_p^I)^T(\tilde{\mathbf{x}}_p^Q - \hat{\mathbf{x}}_p^Q)}{\sigma_{\tilde{n}_l^I}\sigma_{\tilde{n}_l^Q}}\right)}\right) \\ &= Q\left(\sqrt{E_s\gamma}\right). \end{aligned} \quad (4.24)$$

where  $E_s = \frac{E}{4(1-\varrho_l^2)}$  and  $\gamma = \left(\frac{\|\tilde{\mathbf{x}}_p^I - \hat{\mathbf{x}}_p^I\|^2}{\sigma_{\tilde{n}_l^I}^2} + \frac{\|\tilde{\mathbf{x}}_p^Q - \hat{\mathbf{x}}_p^Q\|^2}{\sigma_{\tilde{n}_l^Q}^2} - \frac{2\varrho_l(\tilde{\mathbf{x}}_p^I - \hat{\mathbf{x}}_p^I)^T(\tilde{\mathbf{x}}_p^Q - \hat{\mathbf{x}}_p^Q)}{\sigma_{\tilde{n}_l^I}\sigma_{\tilde{n}_l^Q}}\right)$ . Based on this expression, it can be said that PEP mainly depends on the Euclidean distance between the transmitted and detected signal components, I/Q imbalance distortions, energy of the signal, and the variance of the estimation error.

The APEP will be derived for Beckmann fading channels. Making no assumptions on the statistics of the amplitudes and phases of the fading channel (i.e., allowing the real and imaginary parts of the channel matrix elements to have different means and variances, or being correlated) leads to a more general fading channel model, where most of the well-known fading channel models can be considered as special cases. More details about Beckmann fading channels can be found in Section 2.4. The elements of the channel matrix  $\mathbf{H}$  can be modeled as  $\mathcal{CN}(\boldsymbol{\mu}_h, \boldsymbol{\sigma}_h^2)$  where the mean vector and the covariance matrix of each element are given by  $\boldsymbol{\mu}_h$  and  $\boldsymbol{\sigma}_h^2$  respectively

$$\boldsymbol{\mu}_h = \begin{bmatrix} \mu_{h^I} & \mu_{h^Q} \end{bmatrix}, \quad \boldsymbol{\sigma}_h^2 = \begin{bmatrix} \sigma_{h^I}^2 & \rho_h \sigma_h^Q \sigma_h^I \\ \rho_h \sigma_h^Q \sigma_h^I & \sigma_{h^Q}^2 \end{bmatrix}. \quad (4.25)$$

Here, we assume that channel matrix elements are identical and independent. The columns of the channel matrix,  $\mathbf{h}_i$ , represent the complex fading coefficients between the  $i^{\text{th}}$  transmitter and all receiver antennas. The received signal experiences improper AWGN  $\mathbf{n} = [n_1, \dots, n_{N_r}]^T$  as well.

Although the APEP can be defined by using the expected value of PEP expression of (4.24) as given in (4.26), it is not relatively easy to find  $f_\gamma(\gamma)$ , which is the PDF of  $\gamma$ , in

this expression

$$\text{APEP} = \mathbb{E} \left\{ Q \left( \sqrt{E_s \gamma} \right) \right\} = \int_{-\infty}^{\infty} Q \left( \sqrt{E_s \gamma} \right) f_{\gamma}(\gamma) d\gamma. \quad (4.26)$$

From (4.26),  $\gamma$  can be written using matrix form as  $\gamma = \mathbf{x}^T \mathbf{A} \mathbf{x}$ . Here  $\mathbf{x} \sim \mathcal{N}(\boldsymbol{\mu}_x, \boldsymbol{\sigma}_x^2)$  where  $\mathbf{x}^T = [x_1 \ x_2]$ ,  $x_1 = (\tilde{\boldsymbol{\chi}}_p^I - \hat{\boldsymbol{\chi}}_p^I)$ ,  $x_2 = (\tilde{\boldsymbol{\chi}}_p^Q - \hat{\boldsymbol{\chi}}_p^Q)$ , and  $\mathbf{A}$  is the quadratic matrix. Assume, without loss of generality that the indices  $\hat{i} \neq q$  and  $\hat{q} \neq i$ , the parameters of  $x_1$  and  $x_2$  can be given by

$$\begin{aligned} \mu_{x_1} &= k_c \mu_{\hat{h}}^I (\tilde{x}_k^I - \hat{x}_k^I) + k_d \mu_{\hat{h}}^Q (\tilde{x}_k^I - \hat{x}_k^I) - k_c \mu_{\hat{h}}^Q (\tilde{x}_k^Q - \hat{x}_k^Q) + k_d \mu_{\hat{h}}^I (\tilde{x}_k^Q - \hat{x}_k^Q). \\ \mu_{x_2} &= \mu_{\hat{h}}^I (\tilde{x}_k^I - \hat{x}_k^I) - \mu_{\hat{h}}^Q (\tilde{x}_k^Q - \hat{x}_k^Q), \end{aligned} \quad (4.27)$$

$$\sigma_{x_1}^2 = \left\{ \begin{array}{l} (i \neq \hat{i}, q \neq \hat{q}) \\ K_c^2 \sigma_{\hat{h}^I}^2 [(\tilde{x}_k^I)^2 + (\hat{x}_k^I)^2] + K_d^2 \sigma_{\hat{h}^Q}^2 [(\tilde{x}_k^I)^2 + (\hat{x}_k^I)^2] + 4\rho_{\hat{h}} K_c K_d \sigma_{\hat{h}}^I \sigma_{\hat{h}}^Q [(\tilde{x}_k^I)^2 + (\hat{x}_k^I)^2] \\ + K_d^2 \sigma_{\hat{h}^I}^2 [(\tilde{x}_k^Q)^2 + (\hat{x}_k^Q)^2] + K_c^2 \sigma_{\hat{h}^Q}^2 [(\tilde{x}_k^Q)^2 + (\hat{x}_k^Q)^2] - 4\rho_{\hat{h}} K_c K_d \sigma_{\hat{h}}^I \sigma_{\hat{h}}^Q [(\tilde{x}_k^Q)^2 + (\hat{x}_k^Q)^2] \\ \\ (i = \hat{i}, q \neq \hat{q}) \\ K_c^2 \sigma_{\hat{h}^I}^2 [(\tilde{x}_k^I - \hat{x}_k^I)^2] + K_d^2 \sigma_{\hat{h}^Q}^2 [(\tilde{x}_k^I - \hat{x}_k^I)^2] + 2\rho_{\hat{h}} K_c K_d \sigma_{\hat{h}}^I \sigma_{\hat{h}}^Q [(\tilde{x}_k^I - \hat{x}_k^I)^2] \\ + K_d^2 \sigma_{\hat{h}^I}^2 [(\tilde{x}_k^Q)^2 + (\hat{x}_k^Q)^2] + K_c^2 \sigma_{\hat{h}^Q}^2 [(\tilde{x}_k^Q)^2 + (\hat{x}_k^Q)^2] - 4\rho_{\hat{h}} K_c K_d \sigma_{\hat{h}}^I \sigma_{\hat{h}}^Q [(\tilde{x}_k^Q)^2 + (\hat{x}_k^Q)^2] \\ \\ (i \neq \hat{i}, q = \hat{q}) \\ K_c^2 \sigma_{\hat{h}^I}^2 [(\tilde{x}_k^I)^2 + (\hat{x}_k^I)^2] + K_d^2 \sigma_{\hat{h}^Q}^2 [(\tilde{x}_k^I)^2 + (\hat{x}_k^I)^2] + 4\rho_{\hat{h}} K_c K_d \sigma_{\hat{h}}^I \sigma_{\hat{h}}^Q [(\tilde{x}_k^I)^2 + (\hat{x}_k^I)^2] \\ + K_d^2 \sigma_{\hat{h}^I}^2 [(\tilde{x}_k^Q - \hat{x}_k^Q)^2] + K_c^2 \sigma_{\hat{h}^Q}^2 [(\tilde{x}_k^Q - \hat{x}_k^Q)^2] - 2\rho_{\hat{h}} K_c K_d \sigma_{\hat{h}}^I \sigma_{\hat{h}}^Q [(\tilde{x}_k^Q - \hat{x}_k^Q)^2] \\ \\ (i = \hat{i}, q = \hat{q}) \\ K_c^2 \sigma_{\hat{h}^I}^2 [(\tilde{x}_k^I - \hat{x}_k^I)^2] + K_d^2 \sigma_{\hat{h}^Q}^2 [(\tilde{x}_k^I - \hat{x}_k^I)^2] + 2\rho_{\hat{h}} K_c K_d \sigma_{\hat{h}}^I \sigma_{\hat{h}}^Q [(\tilde{x}_k^I - \hat{x}_k^I)^2] \\ + K_d^2 \sigma_{\hat{h}^I}^2 [(\tilde{x}_k^Q - \hat{x}_k^Q)^2] + K_c^2 \sigma_{\hat{h}^Q}^2 [(\tilde{x}_k^Q - \hat{x}_k^Q)^2] - 2\rho_{\hat{h}} K_c K_d \sigma_{\hat{h}}^I \sigma_{\hat{h}}^Q [(\tilde{x}_k^Q - \hat{x}_k^Q)^2] \end{array} \right. \quad (4.28)$$

$$\sigma_{x_2}^2 = \begin{cases} \sigma_{\hat{h}^I}^2 [(\tilde{x}_k^I)^2 + (\hat{x}_k^I)^2] + \sigma_{\hat{h}^Q}^2 [(\tilde{x}_k^Q)^2 + (\hat{x}_k^Q)^2] & (i \neq \hat{i}, q \neq \hat{q}) \\ \sigma_{\hat{h}^I}^2 [(\tilde{x}_k^I - \hat{x}_k^I)^2] + \sigma_{\hat{h}^Q}^2 [(\tilde{x}_k^Q)^2 + (\hat{x}_k^Q)^2] & (i = \hat{i}, q \neq \hat{q}) \\ \sigma_{\hat{h}^I}^2 [(\tilde{x}_k^I)^2 + (\hat{x}_k^I)^2] + \sigma_{\hat{h}^Q}^2 [(\tilde{x}_k^Q - \hat{x}_k^Q)^2] & (i \neq \hat{i}, q = \hat{q}) \\ \sigma_{\hat{h}^I}^2 [(\tilde{x}_k^I - \hat{x}_k^I)^2] + \sigma_{\hat{h}^Q}^2 [(\tilde{x}_k^Q - \hat{x}_k^Q)^2] & (i = \hat{i}, q = \hat{q}). \end{cases} \quad (4.29)$$

$$\mathbb{E}\{x_1 x_2\} = \begin{cases} (i \neq \hat{i}, q \neq \hat{q}) \\ K_c \sigma_{\hat{h}^I}^2 [(\tilde{x}_k^I)^2 + (\hat{x}_k^I)^2] + K_d \rho_{\hat{h}} \sigma_{\hat{h}^I}^I \sigma_{\hat{h}^Q}^Q [(\tilde{x}_k^I)^2 + (\hat{x}_k^I)^2] + K_c \sigma_{\hat{h}^Q}^2 [(\tilde{x}_k^Q)^2 + (\hat{x}_k^Q)^2] \\ - K_d \rho_{\hat{h}} \sigma_{\hat{h}^I}^I \sigma_{\hat{h}^Q}^Q [(\tilde{x}_k^Q)^2 + (\hat{x}_k^Q)^2] \\ (i = \hat{i}, q \neq \hat{q}) \\ K_c \sigma_{\hat{h}^I}^2 [(\tilde{x}_k^I - \hat{x}_k^I)^2] + K_d \rho_{\hat{h}} \sigma_{\hat{h}^I}^I \sigma_{\hat{h}^Q}^Q [(\tilde{x}_k^I - \hat{x}_k^I)^2] + K_c \sigma_{\hat{h}^Q}^2 [(\tilde{x}_k^Q)^2 + (\hat{x}_k^Q)^2] \\ - K_d \rho_{\hat{h}} \sigma_{\hat{h}^I}^I \sigma_{\hat{h}^Q}^Q [(\tilde{x}_k^Q)^2 + (\hat{x}_k^Q)^2] \\ (i \neq \hat{i}, q = \hat{q}) \\ K_c \sigma_{\hat{h}^I}^2 [(\tilde{x}_k^I)^2 + (\hat{x}_k^I)^2] + K_d \rho_{\hat{h}} \sigma_{\hat{h}^I}^I \sigma_{\hat{h}^Q}^Q [(\tilde{x}_k^I)^2 + (\hat{x}_k^I)^2] + K_c \sigma_{\hat{h}^Q}^2 [(\tilde{x}_k^Q - \hat{x}_k^Q)^2] \\ - \rho_{\hat{h}} K_c K_d \sigma_{\hat{h}^I}^I \sigma_{\hat{h}^Q}^Q [(\tilde{x}_k^Q - \hat{x}_k^Q)^2] \\ (i = \hat{i}, q = \hat{q}) \\ K_c \sigma_{\hat{h}^I}^2 [(\tilde{x}_k^I - \hat{x}_k^I)^2] + K_d \rho_{\hat{h}} \sigma_{\hat{h}^I}^I \sigma_{\hat{h}^Q}^Q [(\tilde{x}_k^I - \hat{x}_k^I)^2] + K_c \sigma_{\hat{h}^Q}^2 [(\tilde{x}_k^Q - \hat{x}_k^Q)^2] \\ - \rho_{\hat{h}} K_c K_d \sigma_{\hat{h}^I}^I \sigma_{\hat{h}^Q}^Q [(\tilde{x}_k^Q - \hat{x}_k^Q)^2] \end{cases} \quad (4.30)$$

$$\rho_x = \text{cov}\{x_1 x_2\} / (\sigma_{x_1} \sigma_{x_2}). \quad (4.31)$$

Hence,  $\gamma$  has the PDF of a quadratic form of two correlated noncentral chi-squared RVs.

From Section 2.3, the MGF of  $\gamma$  can be given by

$$M_\gamma(t) = \left( \frac{\exp\left(\frac{b_1^2 \lambda_1 t}{1-2\lambda_1 t}\right)}{\sqrt{1-2\lambda_1 t}} \times \frac{\exp\left(\frac{b_2^2 \lambda_2 t}{1-2\lambda_2 t}\right)}{\sqrt{1-2\lambda_2 t}} \right)^{N_r}, \quad (4.32)$$

where the eigenvalues  $\lambda_1$  and  $\lambda_2$ , and the mean values  $b_1$  and  $b_2$  are calculated as in Section 2.3. In addition, this section shows how other channel models can be considered as a special cases of Beckmann fading model. For example, (3.26) can be used if the fading channels are Rayleigh fading channels. In this case,  $\mu_{x1} = \mu_{x2} = 0$ ,  $\sigma_{x1}^2 = \sigma_{x2}^2$ , and  $\rho_x = 0$ . Relaxing the condition  $\mu_{x1} = \mu_{x2} = 0$  to give the LoS competent  $\mu_{x1} = \mu_{x2}$  gives the Rician fading channels. In light of this information, an exact closed-form expression of the APEP can be calculated by using (4.24)-(4.32)

$$\text{APEP} = \Pr(\tilde{\mathbf{X}}_p \rightarrow \hat{\mathbf{X}}_p) = \frac{1}{\pi} \int_0^{\frac{\pi}{2}} M_\gamma\left(-\frac{E_s}{2\sin^2\theta}\right) d\theta. \quad (4.33)$$

The above integration can be calculated by using a simple numerical integration technique. Furthermore, (3.27) can be simply upper bounded by

$$\text{APEP}_{\text{opt}} \leq \frac{1}{2} M_{\gamma_{\text{opt}}}\left(-\frac{E_s}{2}\right). \quad (4.34)$$

## 4.5.2 Asymptotic Analysis

Even though the exact expression of APEP given in (4.33) provides numerical evaluation of the system performance; it does not present the effects of key parameters on the system's behavior. Hence, assuming that  $E_s \gg 1$ , an asymptotic APEP is introduced by using (4.32) and (4.33) as follows

$$\text{APEP}_{\text{asy}} = \frac{1}{\pi} \left( \frac{\exp\left(-\frac{b_1^2+b_2^2}{2}\right)}{(E_s/\sigma_{\tilde{n}_l}^2)\sqrt{1-\varrho_l^2}} \right)^{N_r} \int_0^{\frac{\pi}{2}} (\sin\theta)^{2N_r} d\theta. \quad (4.35)$$

In this case, considering that  $\int_0^{\frac{\pi}{2}} (\sin\theta)^{2N_r} d\theta = \frac{\sqrt{\pi} \Gamma(N_r + \frac{1}{2})}{2\Gamma(N_r + 1)}$ , where  $\Gamma(\cdot)$  is the Gamma function, and applying some mathematical operations,  $\text{APEP}_{\text{asy}}$  can be given in a simpler form as [110]

$$\text{APEP}_{\text{asy}} = \frac{(2N_r - 1)!!}{2^{N_r+1} N_r!} \left( \frac{\exp\left(-\frac{b_1^2+b_2^2}{2}\right)}{\sqrt{1-\varrho_l^2}} \right)^{N_r} (E_s/\sigma_{\tilde{n}_l}^2)^{-N_r}, \quad (4.36)$$

It is clear from (4.36) that APEP depends on the number of receiver antennas, the mean value of the received signal, energy of the transmitted signal and the variance of the noise. In addition, the diversity gain  $g$  is equal to the number of receiver antennas as in the case of perfect I/Q balance, and it can be calculated from the following expression

$$g = - \lim_{\text{SNR} \rightarrow \infty} \frac{\log(\text{APEP}_{\text{asy}})}{\log(\text{SNR})} = N_r. \quad (4.37)$$

## 4.6 Imperfect CSI and IGN Effects on SSK

In SSK, only the antennas indices are used as the source of information, which means that it can be treated as a special case of SM. However, the lack of a signal constellation grants SSK substantial advantages over other SM techniques. The system complexity of SSK is reduced, while the performance is almost the same as the traditional SM. The phase and amplitude do not convey any data, which means it has a natural immunity to I/Q imbalance effects. This section studies the joint effects of IGN and imperfect CSI on the performance of SSK receiver. Particularly, an optimal ML detector is discussed, and a PEP expression is derived. Additionally, an exact expression for CRLB is derived for evaluating the channel estimation accuracy under the effect of IGN.

### 4.6.1 System and Channel Models

SSK transceiver model is basically defined as an  $N_t \times N_r$  MIMO system, where  $N_t$  and  $N_r$  are the numbers of transmitter and receiver antennas, respectively. First of all, the transmitter maps  $m = \log_2 N_t$  of equiprobable incoming bits into the index of a single transmit antenna, which is activated for data transmission while all other transmit antennas are kept silent [47]. Then, the signal is conveyed over an  $N_r \times N_t$  complex wireless channel  $\mathbf{H}$ . Each element of  $\mathbf{H}$ , shown by  $h_{i,j}$ , stands for a complex fading channel gain between the  $i^{\text{th}}$  receive antenna and  $j^{\text{th}}$  transmit antenna ( $i \in \{1, \dots, N_r\}$ ,  $j \in \{1, \dots, N_t\}$ ). Considering that only one transmit antenna can be activated, the channel output can be given by

$$\mathbf{y} = \sqrt{E} \mathbf{h}_j + \mathbf{n}, \quad (4.38)$$

where  $\mathbf{h}_j$  is the  $j^{\text{th}}$  column of the channel coefficients matrix  $\mathbf{H}$ , i.e.,  $\mathbf{h}_j = [h_{1,j}, \dots, h_{N_r,j}]^T$ , while  $E$  is the transmitted signal energy. In addition to this,  $\mathbf{n} = [n_1, \dots, n_{N_r}]^T$  is the IGN vector that has independent improper Gaussian RVs. Besides, the estimated channel coefficients at the receiver can be characterized as follows

$$\mathbf{h}_j = \hat{\mathbf{h}}_j + \mathbf{e}_j, \quad (4.39)$$

where  $\hat{\mathbf{h}}_j$  is the  $j^{\text{th}}$  column of the estimated channel coefficients matrix,  $\hat{\mathbf{h}}_j = [\hat{h}_{1,j}, \dots, \hat{h}_{N_r,j}]^T$ , and  $\mathbf{e}_j$  is the  $j^{\text{th}}$  column of the channel estimation error vector,  $\mathbf{e}_j = [e_{1,j}, \dots, e_{N_r,j}]^T$ . In addition,  $e_{i,j}$  is the channel estimation error between the  $i^{\text{th}}$  receive antenna and  $j^{\text{th}}$  transmit antenna,  $e_{i,j}$  is also assumed to have improper Gaussian RVs.

## 4.6.2 Optimal ML Receiver

From (4.38) and (4.39), the received signal  $\mathbf{y}$  can be expressed as

$$\mathbf{y} = \sqrt{E}\hat{\mathbf{h}}_j + \underbrace{\sqrt{E}\mathbf{e}_j + \mathbf{n}}_{\mathbf{z}}. \quad (4.40)$$

From (4.40), it clear that  $\mathbf{z}$  is a zero-mean improper RV and the variances of its real part  $\mathbf{z}^I$  and imaginary part  $\mathbf{z}^Q$  are  $\delta_I^2 = E\sigma_{e_I}^2 + \sigma_I^2$  and  $\delta_Q^2 = E\sigma_{e_Q}^2 + \sigma_Q^2$ , respectively. Based on that, the conditional joint PDF of the real part,  $\mathbf{y}^I$ , and the imaginary part,  $\mathbf{y}^Q$ , of the received signal can be given as

$$f_{\mathbf{y}^I, \mathbf{y}^Q}(\mathbf{y}^I, \mathbf{y}^Q | \mathbf{h}_j) = \left( \frac{1}{2\pi\delta_I\delta_Q\sqrt{1-\rho^2}} \right)^{N_r} \exp \left( \frac{-1}{2(1-\rho^2)} \left[ \frac{\|\mathbf{y}^I - \sqrt{E}\hat{\mathbf{h}}_j^I\|^2}{\delta_I^2} + \frac{\|\mathbf{y}^Q - \sqrt{E}\hat{\mathbf{h}}_j^Q\|^2}{\delta_Q^2} - \frac{2\rho(\mathbf{y}^I - \sqrt{E}\hat{\mathbf{h}}_j^I)^T(\mathbf{y}^Q - \sqrt{E}\hat{\mathbf{h}}_j^Q)}{\delta_I\delta_Q} \right] \right), \quad (4.41)$$

where  $\hat{\mathbf{h}}_j^I$  and  $\hat{\mathbf{h}}_j^Q$  are the real and imaginary parts of  $\hat{\mathbf{h}}_j$ , respectively, and  $\rho = \text{cov}\{\mathbf{z}^I, \mathbf{z}^Q\}/(\delta_I\delta_Q)$ .

Assuming that the channel inputs are equiprobable, the optimal ML detector is defined based on maximizing the joint PDF given in (4.41) as follows

$$\hat{j} = \arg \max_j \left\{ \left( \frac{1}{2\pi\delta_I\delta_Q\sqrt{1-\rho^2}} \right)^{N_r} \exp \left( -\frac{1}{2(1-\rho^2)} \left[ \frac{\|\mathbf{y}^I - \sqrt{E}\hat{\mathbf{h}}_j^I\|^2}{\delta_I^2} + \frac{\|\mathbf{y}^Q - \sqrt{E}\hat{\mathbf{h}}_j^Q\|^2}{\delta_Q^2} - \frac{2\rho(\mathbf{y}^I - \sqrt{E}\hat{\mathbf{h}}_j^I)^T(\mathbf{y}^Q - \sqrt{E}\hat{\mathbf{h}}_j^Q)}{\delta_I\delta_Q} \right] \right) \right\}. \quad (4.42)$$

By following the same steps as in Section 4.5, the conditional PEP of the proposed receiver can be obtained as

$$\begin{aligned} \text{PEP}_{\text{opt}} &= Q \left( \sqrt{\frac{E}{4(1-\rho^2)} \left( \frac{\|\hat{\mathbf{h}}_j^I - \hat{\mathbf{h}}_k^I\|^2}{\delta_I^2} + \frac{\|\hat{\mathbf{h}}_j^Q - \hat{\mathbf{h}}_k^Q\|^2}{\delta_Q^2} - \frac{2\rho(\hat{\mathbf{h}}_j^I - \hat{\mathbf{h}}_k^I)^T(\hat{\mathbf{h}}_j^Q - \hat{\mathbf{h}}_k^Q)}{\delta_I\delta_Q} \right)} \right) \\ &= Q \left( \sqrt{\frac{E\lambda}{4(1-\rho^2)}} \right) \end{aligned} \quad (4.43)$$

where  $\lambda = \left( \frac{\|\hat{\mathbf{h}}_j^I - \hat{\mathbf{h}}_k^I\|^2}{\delta_I^2} + \frac{\|\hat{\mathbf{h}}_j^Q - \hat{\mathbf{h}}_k^Q\|^2}{\delta_Q^2} - \frac{2\rho(\hat{\mathbf{h}}_j^I - \hat{\mathbf{h}}_k^I)^T(\hat{\mathbf{h}}_j^Q - \hat{\mathbf{h}}_k^Q)}{\delta_I\delta_Q} \right)$ . The accuracy of the proposed analysis in this section can be proved by assuming perfect CSI and PGN, i.e.,  $\delta_I^2 = \delta_Q^2 = \sigma_n^2/2$  and  $\rho = 0$ . In this case, the error probability in (4.43) can be simplified to the well-known detection formula [47]

$$\text{PEP} = Q \left( \sqrt{\frac{E\|\mathbf{h}_j - \mathbf{h}_k\|^2}{2\sigma_n^2}} \right). \quad (4.44)$$

The APEP of the SSK receiver can also be found in the same way as QSM was in Section 4.5. From (4.43),  $\lambda$  can be written using matrix form as  $\lambda = \mathbf{v}^T \mathbf{B} \mathbf{v}$ . Here  $\mathbf{v} \sim \mathcal{N}(\mathbf{0}, \boldsymbol{\sigma}_v^2)$ , where  $\mathbf{v}^T = [v_1 \ v_2]$ ,  $v_1 = (\hat{\mathbf{h}}_j^I - \hat{\mathbf{h}}_k^I)$ ,  $v_2 = (\hat{\mathbf{h}}_j^Q - \hat{\mathbf{h}}_k^Q)$ , and  $\mathbf{B}$  is a quadratic matrix. Here,  $\sigma_{v_1}^2 = 2\sigma_{\hat{h}^I}^2$  and  $\sigma_{v_2}^2 = 2\sigma_{\hat{h}^Q}^2$ , and  $\rho_v = \text{cov}\{v_1 v_2\}/(\sigma_{v_1}^2 \sigma_{v_2}^2)$ . The MGF of  $\lambda$  is

$$M_{\lambda_{\text{opt}}}(t) = \left( \frac{1}{\sqrt{1-2\psi_1 t}} \times \frac{1}{\sqrt{1-2\psi_2 t}} \right)^{N_r}, \quad (4.45)$$

where the eigenvalues  $\psi_1$  and  $\psi_2$  are calculated as in Section 2.3. If the fading channels are Rayleigh channels with  $\sigma_h^2 = 1$ , then  $\psi_1$  and  $\psi_2$  are calculated from

$$\psi_{1,2} = \frac{1}{2\delta_I^2} + \frac{1}{2\delta_Q^2} \pm \sqrt{\left( \frac{1}{2\delta_I^2} + \frac{1}{2\delta_Q^2} \right)^2 - \frac{(1-\rho^2)}{\delta_I^2\delta_Q^2}}. \quad (4.46)$$

Now, an exact closed-form expression of the APEP can be given by using (4.43) and (4.45) as follows

$$\text{APEP}_{\text{opt}} = \frac{1}{\pi} \int_0^{\frac{\pi}{2}} M_{\lambda_{\text{opt}}} \left( -\frac{E}{8(1-\rho^2)\sin^2\theta} \right) d\theta. \quad (4.47)$$

The integration in (4.47) can be calculated by simple numerical integration techniques. Furthermore, (4.47) can be simply upper bounded by

$$\text{APEP}_{\text{opt}} \leq \frac{1}{2} M_{\lambda_{\text{opt}}} \left( -\frac{E}{8(1-\rho^2)} \right). \quad (4.48)$$

Asymptotic error probability (when the energy  $E$  has a high value) can be approximated as

$$\text{APEP}_{\text{opt}} \approx \frac{1}{2} \left( \frac{1}{\sqrt{\frac{E^2}{16(1-\rho^2)\delta_I^2\delta_Q^2}}} \right)^{N_r}. \quad (4.49)$$

Two interesting results can be drawn from (4.49). First, it is clear that the diversity gain equals to the number of receive antennas ( $N_r$ ). Second, the results match the results when the noise at the receiver is PGN under the assumption of perfect CSI (i.e.,  $\rho = 0$ ,  $\sigma_I^2 = \sigma_Q^2 = \sigma_n^2/2$  and  $\sigma_e^2 = 0$ ). In this case,  $\text{APEP}_{\text{opt}} \approx \frac{1}{2} \left( \frac{1}{E/2\sigma_n^2} \right)^{N_r}$ , validating the consequent analysis.

### 4.6.3 CRLB Derivation

The CRLB provides a lower bound for the variance of an unbiased estimator of a parameter. In this section, an exact expression is derived for CRLB of the channel estimation in the presence of IGN at the receiver side. This expression can be used as a benchmark to predict and evaluate any estimator performance in the presence of IGN.

Assuming  $N_P$  is the number of training pilots that used to estimate the channel, the CRLB at each SSK receiver can be given as

$$\text{CRLB} = \begin{bmatrix} \text{CRLB}_{(h^I)} = \frac{\sigma_I^2}{N_P E} & \text{CRLB}_{(h^I, h^Q)} = \frac{\sigma_I \sigma_Q \rho}{N_P E} \\ \text{CRLB}_{(h^I, h^Q)} = \frac{\sigma_I \sigma_Q \rho}{N_P E} & \text{CRLB}_{(h^Q)} = \frac{\sigma_I \sigma_Q \rho}{N_P E} \end{bmatrix}, \quad (4.50)$$

*Proof:* See the Appendix B.2.

### 4.6.4 Traditional (Blind) ML Receiver

The traditional ML detector is defined by using the traditional ML detection method which ignores the improper characteristics of the noise. In this case, the traditional ML detector for the SSK system is given as

$$\hat{j} = \arg \max_j \left\{ \frac{1}{(\sqrt{2\pi}\delta_n^2)^{N_r}} \exp \left( -\frac{1}{2} \|\mathbf{y} - \sqrt{E}\hat{\mathbf{h}}_j\|^2 \right) \right\}. \quad (4.51)$$

(4.51) can also be maximized by

$$\hat{j} = \arg \min_j \left\{ \|\mathbf{y} - \sqrt{E}\hat{\mathbf{h}}_j\|^2 \right\}. \quad (4.52)$$

The PEP of the traditional ML detector can be written under the assumption of equally likely information as follows (note that  $\mathbf{y} = \sqrt{E}\mathbf{h}_j + \mathbf{n}$ )

$$P(\mathbf{h}_j \rightarrow \mathbf{h}_k)_{\text{tra}} = \Pr \left\{ \|\mathbf{y} - \sqrt{E}\hat{\mathbf{h}}_j\|^2 > \|\mathbf{y} - \sqrt{E}\hat{\mathbf{h}}_k\|^2 \right\}, \quad (4.53)$$

and it can be simplified to

$$\text{APEP}_{\text{tra}} = \Pr \left\{ E\|(\hat{\mathbf{h}}_j - \hat{\mathbf{h}}_k)\|^2 + D < 0 \right\}, \quad (4.54)$$

where  $D = 2\sqrt{E}\Re\{\mathbf{n}^T(\hat{\mathbf{h}}_j - \hat{\mathbf{h}}_k)\}$  is a Gaussian RV with zero mean and a variance of

$$\sigma_D^2 = 4\|\hat{\mathbf{h}}_j^I - \hat{\mathbf{h}}_k^I\|^2\delta_I^2 + 4\|\hat{\mathbf{h}}_j^Q - \hat{\mathbf{h}}_k^Q\|^2\delta_Q^2 + 8\rho(\hat{\mathbf{h}}_j^I - \hat{\mathbf{h}}_k^I)^T(\hat{\mathbf{h}}_j^Q - \hat{\mathbf{h}}_k^Q)\delta_I\delta_Q. \quad (4.55)$$

Therefore, after some simplifications, the APEP of traditional SSK receiver can also be written as

$$\begin{aligned} \text{APEP}_{\text{tra}} &= Q \left( \sqrt{\frac{E\|\hat{\mathbf{h}}_j - \hat{\mathbf{h}}_k\|^4}{4\|\hat{\mathbf{h}}_j^I - \hat{\mathbf{h}}_k^I\|^2\delta_I^2 + 4\|\hat{\mathbf{h}}_j^Q - \hat{\mathbf{h}}_k^Q\|^2\delta_Q^2 + 8\rho(\hat{\mathbf{h}}_j^I - \hat{\mathbf{h}}_k^I)^T(\hat{\mathbf{h}}_j^Q - \hat{\mathbf{h}}_k^Q)\delta_I\delta_Q}} \right) \\ &= Q \left( \sqrt{\lambda_{\text{tra}}} \right) \end{aligned} \quad (4.56)$$

However, it is not easy to find the PDF of  $\lambda_{\text{tra}}$ . Therefore, the APEP for the traditional case can be calculated by averaging the instantaneous PEP values over a large number of channel realizations.

## 4.7 Numerical Analysis and Results

In this section, the effects of I/Q imbalance at transmitter and receiver, imperfect CSI, IGN, channel model, diversity gain, and modulation order on the performance of the QSM wireless communication system are studied and analyzed. Considering the aforementioned QSM receiver design, comprehensive computer simulations were carried out to validate

the analytical results and assess the system performance. Unless specified otherwise, 4-QAM modulation is used. The computer simulations are performed under Rayleigh fading channel conditions and the receiver is affected by PGN  $n \sim \mathcal{CN}(0, 1)$ . Moreover, for a fair comparison, the transmitted signal energy is normalized by  $(|x_i G_1 + x_i^* G_2|^2)$ . All the comparisons are made against a system with perfect I/Q balance. In addition, the ABER is presented for the SNR values between 0-30 dB, and computer simulations are realized using at least  $10^6$  symbols transmitted for each SNR value.

Fig. 4.2 shows the simulation and numerical results where APEP of the optimal receiver were calculated using (4.32) and (4.33) with simulation parameters  $\mu_{hI} = .001$ ,  $\mu_{hQ} = .05$ ,  $\sigma_{hI}^2 = 0.4$ ,  $\sigma_{hQ}^2 = 0.6$ ,  $\rho_h = -0.3$ ,  $\sigma_{nI}^2 = 0.7$ ,  $\sigma_{nQ}^2 = 0.3$ ,  $\rho_n = 0.3$ ,  $\sigma_{eI}^2 = 0.001$ ,  $\sigma_{eQ}^2 = 0.002$ ,  $\rho_e = 0.3$ ,  $\xi_{t,r} = -1.5$  dB, and  $\beta_{t,r} = 5^\circ$ . These parameters were chosen using general fading channel model (Beckmann model) with imperfect CSI, general Gaussian noise conditions (IGN), and I/Q impaired transmitter and receiver. Four cases were considered which match with the four channel transmitted and detected channels indices possibilities in (4.27)-(4.31). It is clear that the simulation results match with the analytical results in all cases which validates the analysis.

Figs. 4.3 and 4.4 show the performance of a  $2 \times 2$  QSM system affected by I/Q imbalance at the transmitter side only, with perfect CSI and PGN at the receiver side. Fig. 4.3 shows the results of fixing the phase mismatch at  $5^\circ$  while varying the amplitude imbalance between 0.6, 1.2, and 2 dB. It shows a minor impact of I/Q imbalance on the optimal receiver while this impact is very dramatic for the blind one. In addition, it is clear that, in the higher SNR region, the blind receiver performance saturates, leading to an error floor and zero power gain. In Fig. 4.4, the ABER is plotted by fixing the amplitude mismatch at 0.3 dB while the phase imbalance changes between  $5^\circ$ ,  $10^\circ$ , and  $15^\circ$ . It shows that the optimal receiver can completely resist phase mismatching effect at the transmitter side. In addition, as in the amplitude imbalance case, in the high SNR region, the blind receiver's performance saturates, leading to an error floor and zero power gain.

Figs. 4.5 and 4.6 show the performance of  $2 \times 2$  QSM system affected by I/Q imbalance at the receiver side only and assuming perfect CSI and PGN. Fig. 4.5 shows the results of

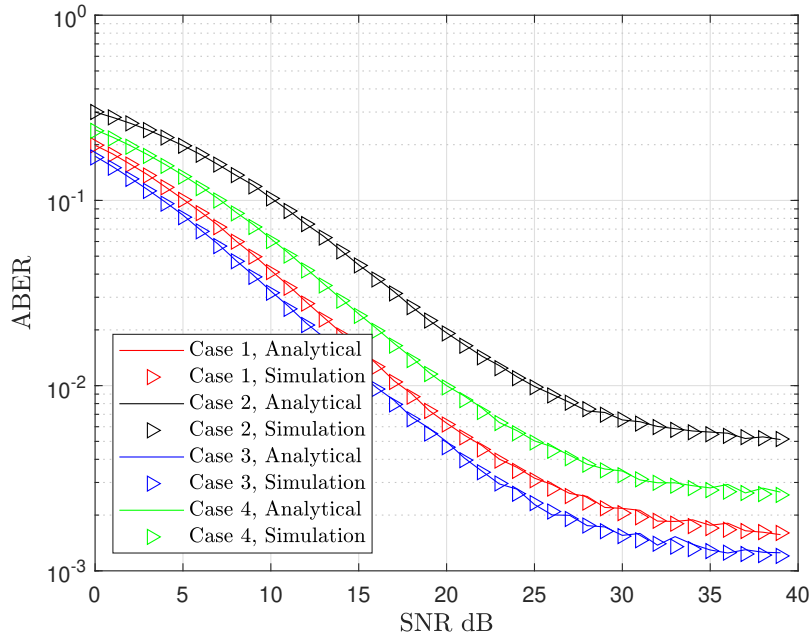


Figure 4.2: APEP of QSM system over Beckmann channels conditions with perfect CSI, PGN, and I/Q impaired transmitter and receiver.

fixing the phase mismatch at  $5^\circ$  while varying the amplitude imbalance between 0.6, 1.2, and 2 dB, and Fig. 4.6 illustrates the results of fixing the amplitude mismatch to 0.3 dB while the phase imbalance changes between  $5^\circ$ ,  $10^\circ$  and  $15^\circ$ . It can be seen from these figures that the optimal receiver outperforms the blind one and can resist the amplitude and phase mismatching effects completely. Finally, the blind receiver has an extremely poor performance at high values of the amplitude or phase mismatching. This can be noticed in the higher SNR regions of both figures, where the performance saturates, leading to an error floor and zero power gain. From Figs. 4.3-4.6, phase imbalance at the transmitter and receiver sides have almost the same impact on the QSM system when using 4-QAM modulation. While the amplitude imbalance has more effect at the transmitter side.

Figs. 4.7 and 4.8 illustrate two QSM configurations. One configuration considers  $2 \times 2$  MIMO setup with 16-QAM modulation achieving a spectral efficiency of 6 bps/Hz. Similar spectral efficiency is also achieved with  $4 \times 2$  MIMO setup and 4-QAM modulation. The results in these figures have patterns similar to the previous figures and confirm the superiority of the proposed receiver. The remarkable finding here is that, the effects of I/Q

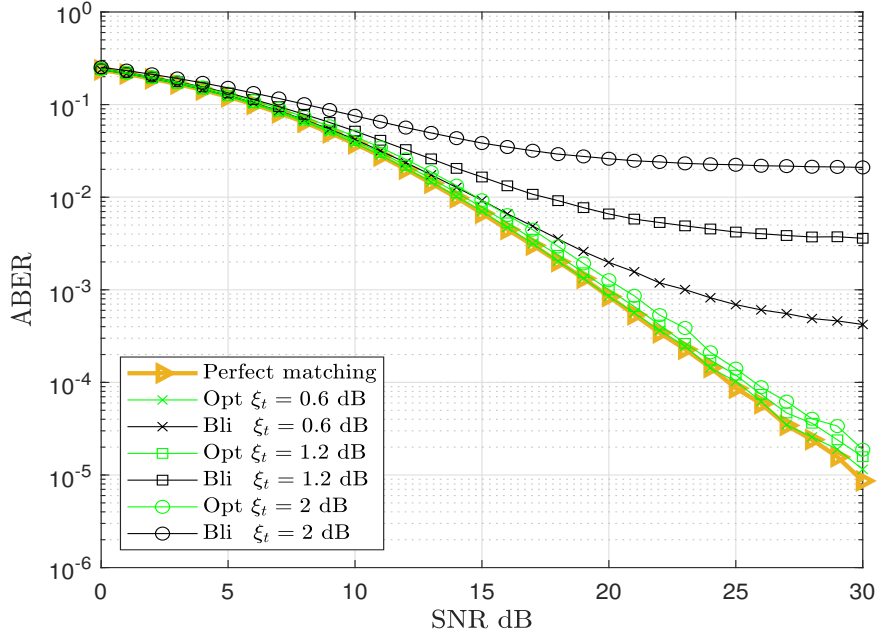


Figure 4.3:  $2 \times 2$  QSM MIMO system with 4-QAM modulation in the presence of different levels of amplitude imbalance at the transmitter side with fixed  $\beta_t = 5^\circ$ .

imbalance are more critical in case of  $2 \times 2$  even though the receivers in both figures achieve the same spectral efficiencies. This appears as 1 dB gain difference of the optimal receiver performance at  $10^{-3}$  ABER when  $\xi_{t,r} = 1$  dB.

Fig. 4.9 illustrates the ABER performance of  $4 \times 1$ ,  $4 \times 2$ , and  $4 \times 4$  QSM MIMO systems with 4-QAM modulation in the presence of  $\xi_{t,r}=0.3$  dB and  $\beta_{t,r}=5^\circ$  I/Q imbalance parameters. As this figure shows, the diversity order in the case of optimal receiver is  $N_r$ , and increasing the SNR enhances the system performance. This gain can be seen where the ABER results at high SNR have gains of 1, 2, and 3 for  $N_r=1$ ,  $N_r=2$ , and  $N_r=3$ , respectively. On the other hand, increasing the SNR has no impact on the ABER in the case of the blind receiver, which leads to an error floor and a diversity order of zero.

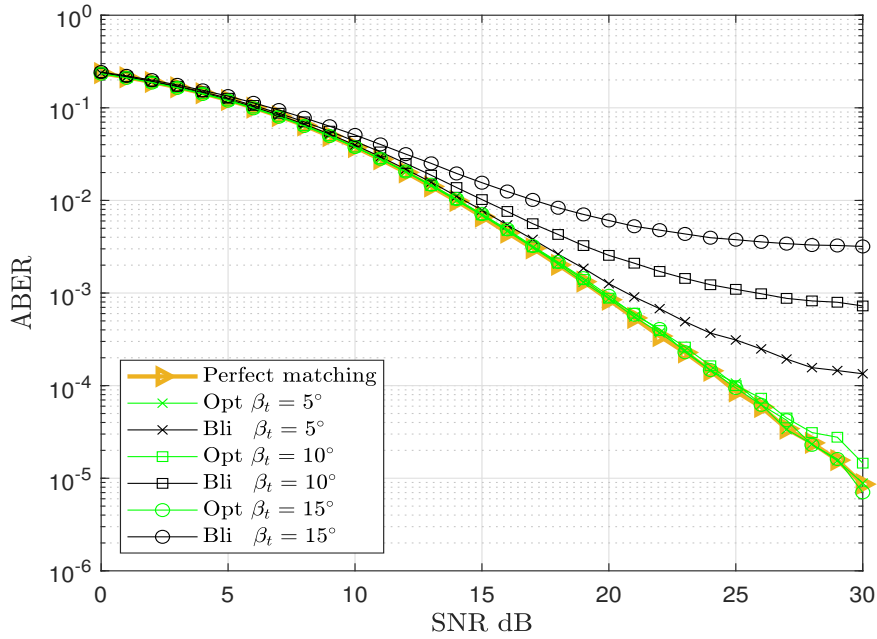


Figure 4.4:  $2 \times 2$  QSM MIMO system with 4-QAM modulation in the presence of different levels of angle mismatches at the transmitter side with fixed  $\xi_t=0.3$  dB.

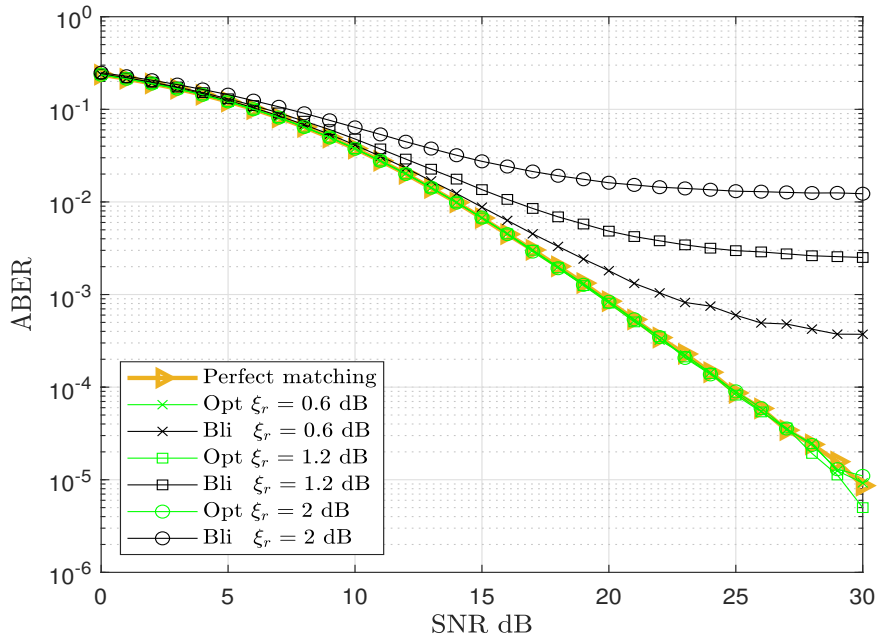


Figure 4.5:  $2 \times 2$  QSM MIMO system with 4-QAM modulation in the presence of different levels of amplitude imbalance at the receiver side with fixed  $\beta_r = 5^\circ$ .

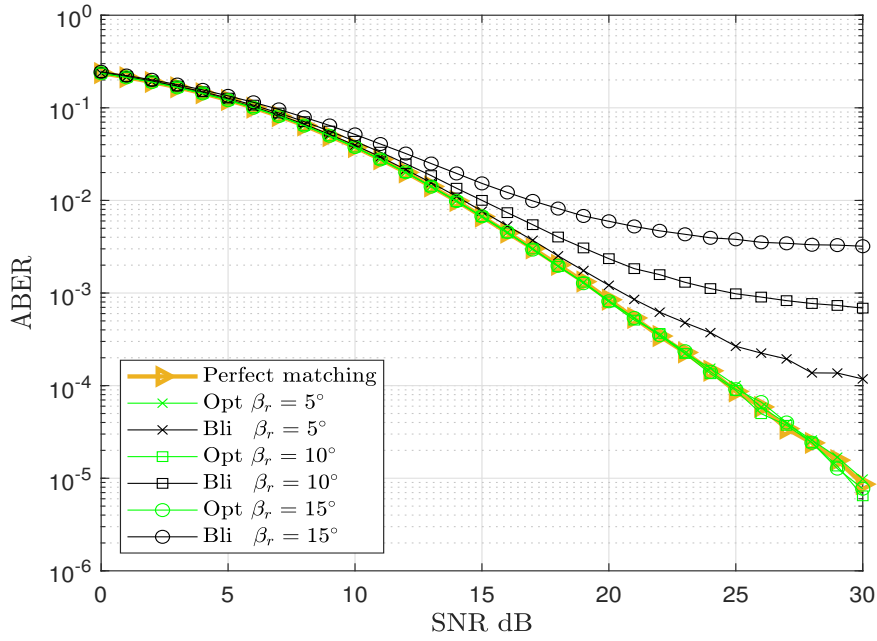


Figure 4.6:  $2 \times 2$  QSM MIMO system with 4-QAM modulation in the presence of different levels of angle mismatches at the receiver side with fixed  $\xi_r=0.3$  dB.

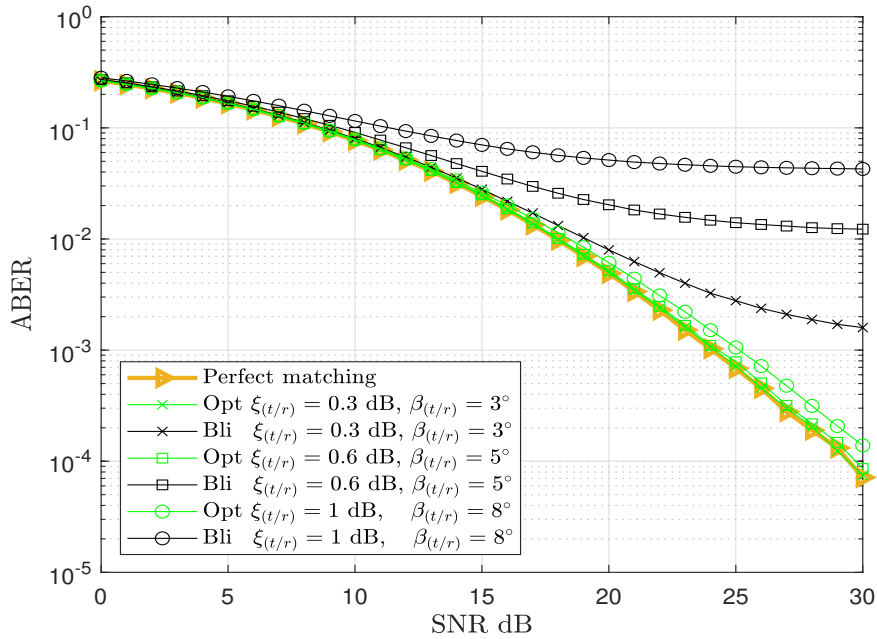


Figure 4.7:  $2 \times 2$  QSM MIMO system with 16-QAM modulation in the presence of different levels of I/Q imbalance.

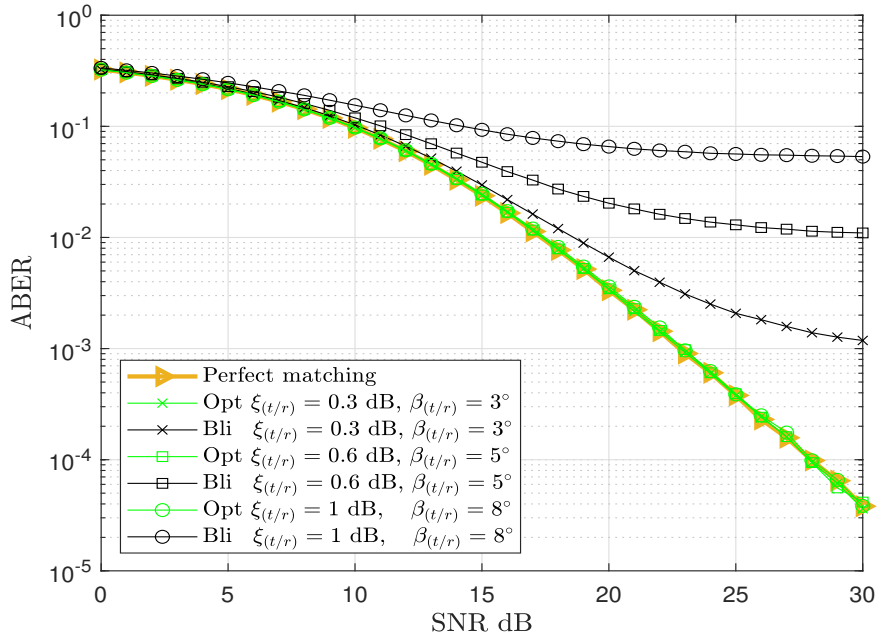


Figure 4.8:  $4 \times 2$  QSM MIMO system with 4-QAM modulation in the presence of different levels of I/Q imbalance.

Fig. 4.10 shows the effects of channel parameters (more details about these parameters can be found in Section 2.4). For a fair comparison,  $\Omega = 1$  for all channels.  $\Omega = \mu_{hI}^2 + \mu_{hQ}^2 + \sigma_{hI}^2 + \sigma_{hQ}^2$ , and indicates the average power of the fading channel. As the figure shows, the channel parameters have the same effects on both receivers. Here, Rician fading channel has the worst performance, and this is because it has the minimum variance and the QSM system relies strongly on the difference in the channel conditions to transmit the spatial bits. Here, the parameter  $K$  indicates the ratio between the LoS and non-LoS power. There is about a 5 dB difference at  $10^{-3}$  ABER in the power gain between the Rayleigh channel and the Beckmann-2 channel that has the same Rayleigh parameters except that it has correlated I and Q components. On the other hand, the correlation has less effect when there is a strong LoS channel path as can be seen by the very small reduction in the power gain for the Beckmann channel-1 that has the same Rician parameters except that it has correlated I and Q components.

Fig. 4.11 illustrates the performance of  $2 \times 2$  QSM MIMO system under the effects of

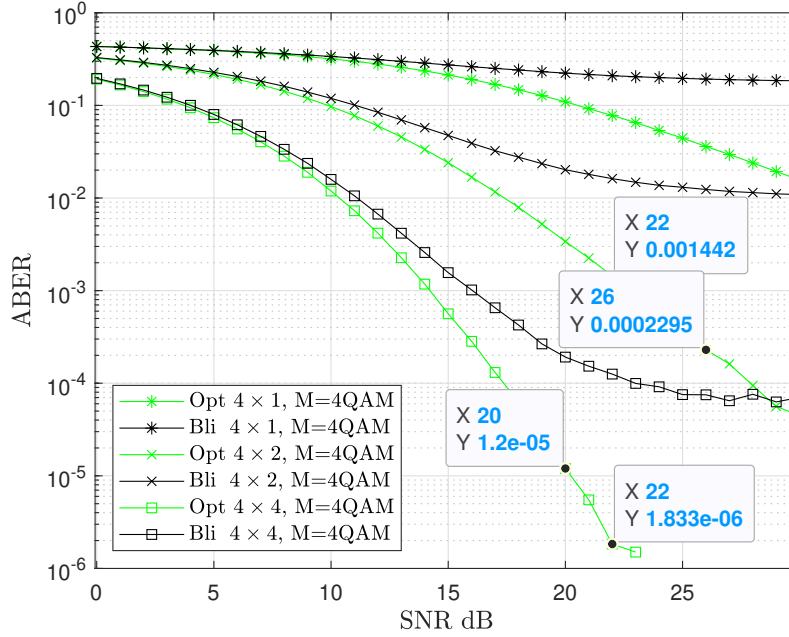


Figure 4.9:  $4 \times 1$ ,  $4 \times 2$ , and  $4 \times 4$  QSM MIMO systems with 4-QAM modulation in the presence of I/Q imbalance where  $\xi_{t,r}=0.3$  dB and  $\beta_{t,r} = 5^\circ$ .

different levels of imperfect CSI when  $\xi_{t,r} = 0.3$  dB and  $\beta_{t,r} = 5^\circ$ . This figure shows that the imperfect CSI has a big impact on both receivers, where the performance saturates in the high SNR region, leading to an error floor and zero power gain. Comparing the results here with the previous one shows that small values of  $\sigma_e^2$  has a significant effect on the performance of the optimal receiver and its performance become as worse as the blind one with higher values of  $\sigma_e^2$ .

Fig. 4.12 shows the effect of IGN on  $2 \times 2$  QSM MIMO system. Here, the I/Q components are perfect matching. The results in this figure agree with the one in Section. 3.6 and can be interpreted from (4.24) where term inside the Q-function goes to  $Q(\infty)$  and the error probability goes to zero in two cases; *case 1*, when the correlation factor  $\rho_n$  goes to one, because in this case, the denominator goes to zero, *case 2*, when one of the variances ( $\sigma_{n^I}^2$  or  $\sigma_{n^Q}^2$  goes to zero because in this case, the numerator goes to  $\infty$ ). This trend is not valid for the blind receiver.

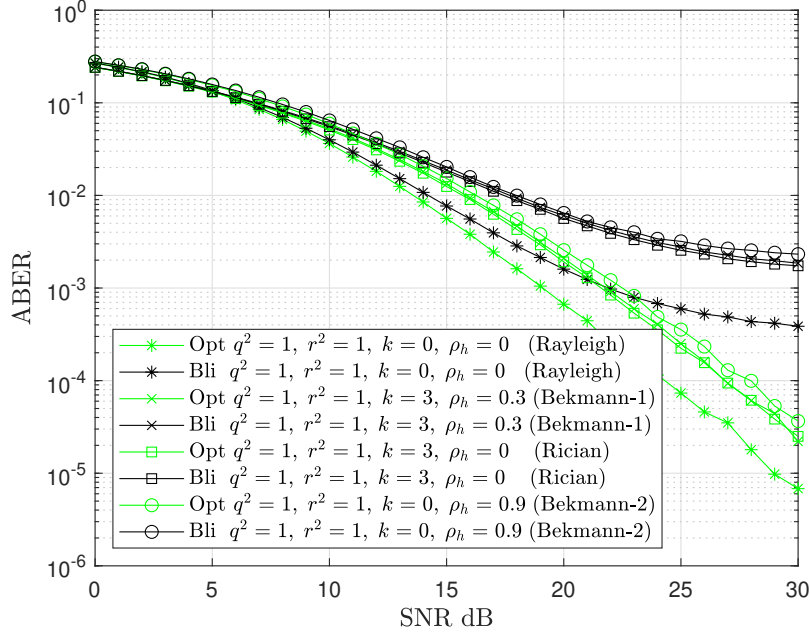


Figure 4.10: ABER performance of  $2 \times 2$  QSM system over Beckmann channels when the transmitter and receiver under the effect of I/Q imbalance ( $\xi_{t,r}=0.3$  dB and  $\beta_{t,r}=5^\circ$ ).

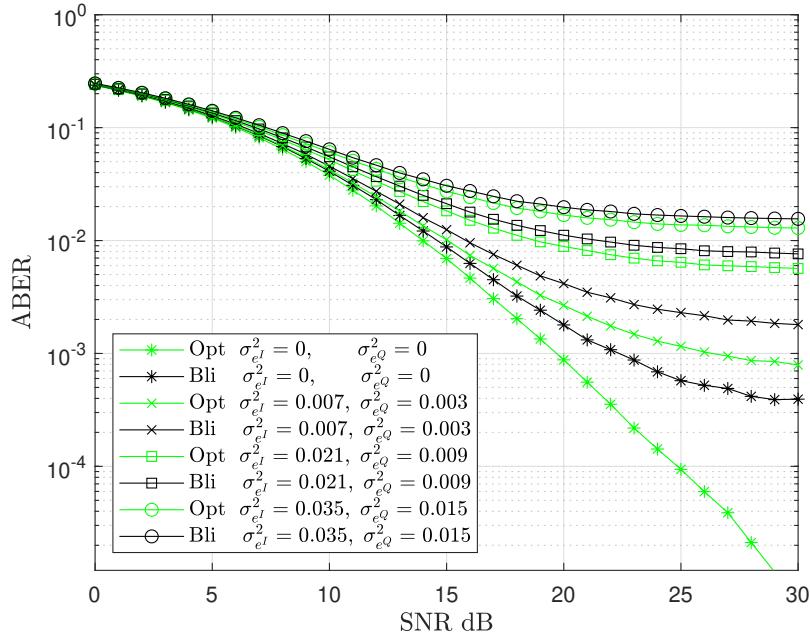


Figure 4.11: ABER performance of  $2 \times 2$  QSM with different levels of improper channel estimation errors when  $\xi_{t,r}=0.3$  dB and  $\beta_{t,r}=5^\circ$ .

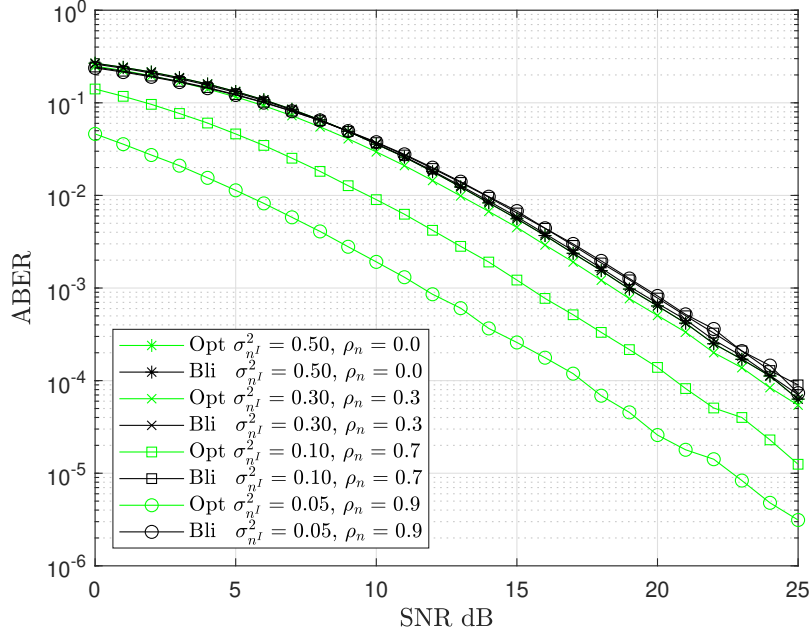


Figure 4.12: ABER performance of  $2 \times 2$  QSM with different levels of IGN assuming that  $\sigma_I^2 + \sigma_Q^2 = 1$ .

In Fig. 4.13, the ABER performance of two  $2 \times 2$  SSK MIMO system receivers are given in the presence of imperfect CSI with  $\sigma_{e_I}^2 = \sigma_I^2/E$  and  $\sigma_{e_Q}^2 = \sigma_Q^2/E$  at different values of  $\sigma_I^2$ ,  $\sigma_Q^2$  and  $\rho$  (note that  $\sigma_n^2 = \sigma_I^2 + \sigma_Q^2 = 1$ ). This result in this figures agrees with the one in Fig. 4.12 where increasing the imperpness (i.e more the difference between  $\sigma_I^2$  and  $\sigma_Q^2$  values or higher  $\rho$  values) of the noise does not provide considerable performance enhancement for the sub-optimal detector, it noticeably increases the performance of the optimal one; for instance, approximately 4 dB improvement is ensured on the performance of the optimal receiver design for  $\sigma_I^2 = 0.2$  and  $\rho = 0.7$  case when  $\text{ABER} = 10^{-3}$ .

Finally, the ABER performance evaluation of the optimal  $2 \times 2$  SSK MIMO receiver under the effect of imperfect CSI employing the CRLB variances of  $\sigma_{e_I}^2$  and  $\sigma_{e_Q}^2$  in (4.50) at different numbers of pilots (1, 3, 5, 7 and 10) is presented in Fig. 4.14. This figure helps not only to evaluate the system performance but also predict the estimator performance. The perfect CSI is also included to the figure for comparison. It can be noticed that increasing number of pilots enhances the system performance. This estimator can work as

a benchmark to find the CRLB variances of  $\sigma_{e_I}^2$  and  $\sigma_{e_Q}^2$  under the effect of IGN.

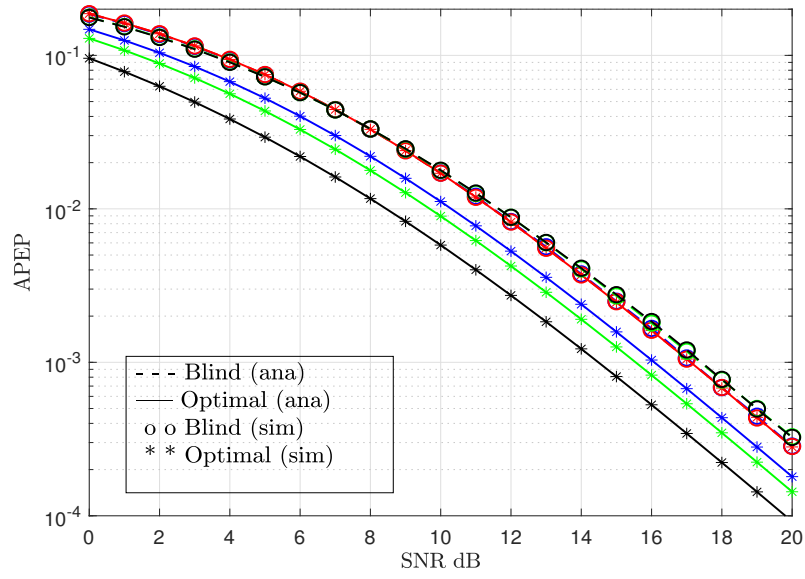


Figure 4.13: ABER performance of the SSK-MIMO system in the presence of imperfect CSI and IGN: red, blue, green and black curves represent the cases of  $\sigma_I^2 = 0.5, \rho = 0$ ;  $\sigma_I^2 = 0.2, \rho = 0$ ;  $\sigma_I^2 = 0.5, \rho = 0.7$  and  $\sigma_I^2 = 0.2, \rho = 0.7$ , respectively.

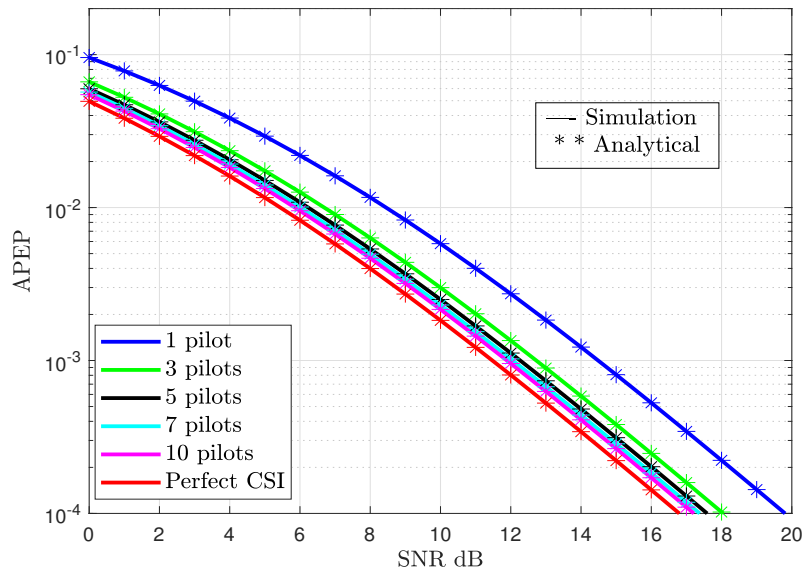


Figure 4.14: ABER performance of the optimal  $2 \times 2$  SSK MIMO system under the effect of IGN using CRLB at different number of pilots ( $N_p$ ) where  $\sigma_I^2 = 0.2, \rho = 0.7$ , respectively.

## 4.8 Conclusion

The importance of considering the I/Q imbalance effects, channel estimation errors, and IGN for the future QSM wireless communication systems has been pointed out in this chapter. An optimal ML detector design has been proposed to make QSM systems effective against the deterioration effects of I/Q imbalance in the presence of IGN and imperfect CSI. Besides, the effect of IGN on SSK systems which have a natural immunity to I/Q imbalance effects has been studied. Specifically, exact closed-form of APEPs have been derived and asymptotic bounds have been provided for both systems. In addition, an exact closed form CRLB expression is calculated for evaluating the channel estimation accuracy in the presence of IGN

The systems performances have been evaluated over Beckmann channels via analytical derivations as well as computer simulations. The obtained results have shown that the proposed optimal receiver of QSM successfully reduces the effects of I/Q imbalance to the minimum. The results also showed that the optimal SSK receiver outperforms the sub-optimal one in the presence of IGN and the performance difference is noteworthy in some cases.

# Chapter 5

## Down-link NOMA Networks in the Presence of I/Q imbalance, IGN and Imperfect SIC

### 5.1 Introduction and Related Works

NOMA has recently attracted a significant amount of attention from researchers because its performance eclipses that of OMA. By serving multiple users at the same time and with the same frequency, NOMA effectively increases the spectral efficiency. This in turn allows a massive number of connections to be granted, hence fulfilling 5G communication requirements. In addition, NOMA maintains user fairness through flexible power control between strong and weak users. NOMA also offers low transmission latency without the prerequisite of scheduling time from users to the base station [111]. Alongside academia, NOMA has received remarkable attention from industry [112].

Hardware impairments, such as in-phase and I/Q imbalance in the RF front-end, imperfect high-power amplifiers manufacturing, and the low noise amplifier non-linearities can dramatically degrade the communication system's performance [13, 14]. The impact of hardware impairments on cooperative NOMA systems was studied in [113, 114]. It was observed that residual interferences caused by full-duplex and non-ideal hardware can

decrease the system capacity and severely degrade the system performance. The results in [114] showed that the loop self interference caused by the relay has a big impact on the ergodic rate performance. It also proposed a full duplex cooperative NOMA system which can improve the ergodic rate performance of the users compared with the half duplex cooperative NOMA system. The work in [115] considered a simultaneous wireless information and power transfer NOMA network. The results also showed that the performance of system is limited by imperfect SIC and HWIs. In particular, it causes error floor for the outage probability and zero diversity order.

The performance of NOMA systems under the effects of transmitter/receiver I/Q imbalance was considered in [116] and [117]. It was shown that in multi-carrier NOMA systems both the SIC and the orthogonality of the subcarriers are compromised, leading to significant performance degradation. Moreover, it was shown that I/Q imbalance can change the optimum power splitting ratio and hence compromise the efficiency of multi-carrier NOMA systems. In [118], it was shown that I/Q imbalance leads to a considerable degradation on the system bit error rate (BER). Moreover, the degradation level depends on the power allocation ratio, the total number of users, and the users' orders. However, this work depended only on Monte Carlo simulations without presenting any mathematical models or performance analysis.

The works in [119] and [120] investigated the joint effects of I/Q imbalance and imperfect SIC on NOMA systems. The work in [119] showed that a noticeable decrease in the BER can result from I/Q imbalance. Besides, the diversity order achieved by NOMA users is preserved under certain I/Q imbalance scenarios. Even though this work offered an interesting analysis but it was assumed that the NOMA users are unaware of the I/Q imbalance parameters. The work in [120] showed that for cooperative NOMA systems I/Q imbalance has a noticeable effect on their outage probability, as well as on the ergodic sum rate in moderate and high SNR regions.

To the best of our knowledge, no work in the literature proposed an ideal receiver design that can mitigate the effects of I/Q imbalance on NOMA systems. Therefore, this chapter studies the performance of two user power-domain down-link NOMA systems under the

joint effects of receiver I/Q imbalance and imperfect SIC. In particular, an optimal receiver design that can mitigate the effects of I/Q imbalance is presented and examined. A closed-form expression for the PEP of both users is also derived. The simulation results validate the presented analysis and prove that the proposed design outperforms the traditional one. The obtained results in this chapter have been published in [121].

The rest of this chapter is organized as follows: Section 5.2 describes the system and channel models. Section 5.3 provides the receiver designs and the performance analysis for the presented models. Section 5.4 discusses the numerical analysis and results. Finally, Section 5.5 concludes this chapter.

## 5.2 System and Channel Models

### 5.2.1 Power-domain NOMA System

Power-domain NOMA systems separate the users in the power domain by allocating different power levels for them according to their channel conditions. On the transmitter side, superposition coding can be applied. On the other hand, the receiver side exploits the difference between power levels by utilizing SIC [5, 6].

This work focuses on power-domain down-link NOMA systems with one base station and two users ( $U_1$  and  $U_2$ ) as shown in Fig. 5.1. The channel coefficients between the users and the base station are  $h_1$  and  $h_2$ , and the allocated powers for the users are  $P_1 = (1 - \alpha)P_t$  and  $P_2 = \alpha P_t$ , where  $P_t$  represents the total transmitted power. Based on NOMA conventions and assuming, without loss of generality, that  $|h_1|^2 > |h_2|^2$  (i.e.,  $U_1$  has a stronger channel condition than  $U_2$ ),  $U_2$  is granted a higher transmitted power than  $U_1$  (i.e.,  $P_2 > P_1$ ). Here,  $h_1 = g_1 d_1^\kappa$  and  $h_2 = g_2 d_2^\kappa$ , where  $d_1$  and  $d_2$  are the distances between the base station and the users,  $\kappa$  is the path loss exponent, and  $g_1$  and  $g_2$  are modeled as independently distributed Rayleigh flat fading channels.

$U_1$  can decode its desired signal after canceling the decoded signal of  $U_2$  using SIC. On the other hand, decoding  $U_2$ 's desired signal is straightforward, as the interference imposed by  $U_1$  is minimal and can be considered as noise. Assuming that perfect I/Q balance at  $U_1$

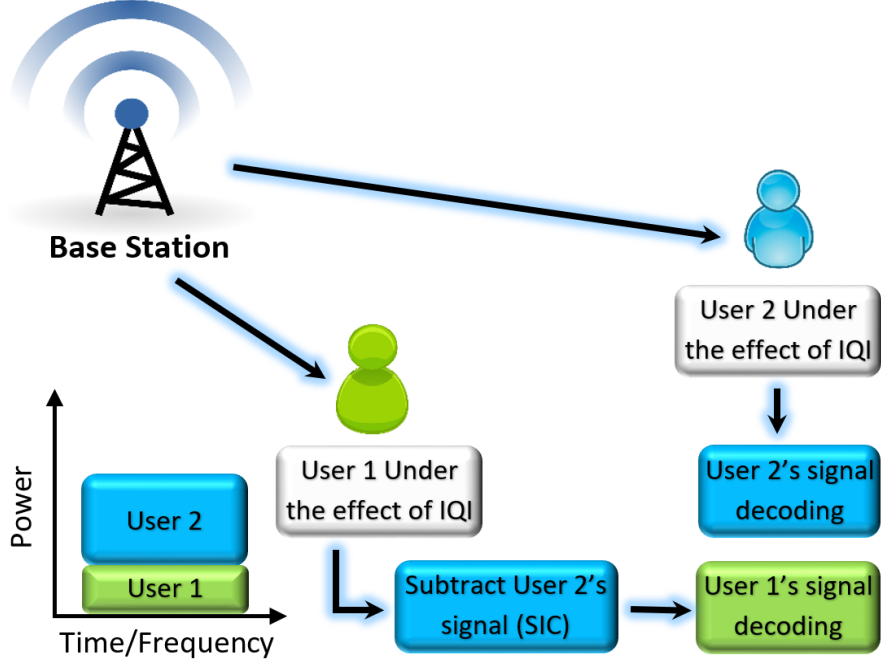


Figure 5.1: Two users power-domain down-link NOMA systems under the effect of I/Q imbalance.

and  $U_2$ , the received signals can be expressed as

$$y_1 = \underbrace{\sqrt{P_1}h_1s_{1i}}_{\text{desired signal}} + \underbrace{\sqrt{P_2}h_1s_{2i}}_{\text{to be removed by SIC}} + n_1, \quad (5.1)$$

$$y_2 = \underbrace{\sqrt{P_2}h_2s_{2k}}_{\text{desired signal}} + \underbrace{\sqrt{P_1}h_2s_{1k}}_{\text{treated as a noise}} + n_2, \quad (5.2)$$

where  $(i, k \in \{1, 2, \dots, M\})$ ,  $M$  is the modulation order,  $s_{1i}$  and  $s_{2k}$  are the transmitted symbols of the users, and the corresponding AWGN are  $n_1 \sim \mathcal{CN}(0, \sigma_{n_1}^2)$  and  $n_2 \sim \mathcal{CN}(0, \sigma_{n_2}^2)$ .

## 5.2.2 Imperfect SIC

SIC is achieved at the receiver by detecting the strongest signal first, and then subtracting it from the combined signal, thereby detecting the desired signal by treating the weaker signals as noise. In the presence of imperfect SIC, the channel estimation is essential to cancel the effect of the received interference signal from different users. In this regard, inaccurate calculation of the channel estimates results in residual cancellation interference

which limits the capacity of the wireless system [122]. Assuming that the SIC process at  $U_1$ 's receiver is imperfect, the cancellation error  $e$  can be modeled using Gaussian approximation (i.e.,  $e \sim \mathcal{CN}(0, \sigma_e^2)$ ) [122], and then (5.1) can be rewritten as

$$y_1 = \sqrt{P_1}h_1s_{1i} + \sqrt{P_2}e + n_1. \quad (5.3)$$

### 5.2.3 Transceiver I/Q Imbalance Model

In practical systems, the hardware imperfections that may appear at the phase-shifter, LO, and the I/Q mixer can cause phase and/or amplitude imbalance. Phase imbalance occurs when the angle between the I and Q parts is not perpendicular. Amplitude imbalance occurs when the gain of the I and Q parts are not perfectly matched. The system performance is dramatically affected due to the I/Q imbalance which corrupts the transmitted signal at the transmitter side and the received signal at the receiver side.

From Section 2.6, considering the effects of I/Q imbalance at the transmitter, the impaired transmitted signal of  $s_i$  can be given as

$$s_i^{IQI} = G_1s_i + G_2s_i^*, \quad (5.4)$$

where  $G_1 = \frac{1}{2}(1 + \xi_t e^{j\beta_t})$  and  $G_2 = \frac{1}{2}(1 - \xi_t e^{j\beta_t})$  are I/Q imbalance parameters at the transmitter. Here  $\beta_t$  and  $\xi_t$  model the phase and amplitude imbalance, respectively. Considering the total effects of I/Q imbalance and the SIC at the users, the received impaired signals are given using (5.1) and (5.2) as

$$y_1^{IQI} = \left\{ \underbrace{\sqrt{P_1}[K_1(h_1(G_1s_{1i} + G_2s_{1i}^*)) + K_2(h_1(G_1s_{1i} + G_2s_{1i}^*))^*]}_{\hat{s}_{1i}} \right\} \text{ signal part} \\ + \\ \left\{ \underbrace{K_1\sqrt{P_2}e + K_2\sqrt{P_2}e^* + K_1n_1 + K_2n_1^*}_{\psi} \right\} \text{ noise part} \quad (5.5)$$

$$\begin{aligned}
y_2^{IQI} = & \left\{ \underbrace{\sqrt{P_2}[K_1(h_2(G_1s_{2k} + G_2s_{2k}^*)) + K_2(h_2(G_1s_{2k} + G_2s_{2k}^*))^*]}_{(\tilde{s}_{2k})} \right\} \text{ signal part} \\
& + \\
& \left\{ \underbrace{\sqrt{P_1}[h_2K_1(G_1s_{1i} + G_2s_{1i}^*) + h_2^*K_2(G_1s_{1i} + G_2s_{1i}^*)^*]}_{\tilde{s}_{1i}} + \underbrace{K_1n_2 + K_2n_2^*}_{\eta} \right\} \text{ noise part}
\end{aligned} \tag{5.6}$$

where  $K_1 = \frac{1}{2} + \frac{1}{2}\xi_r \cos(\beta_r) - j\frac{1}{2}\xi_r \sin(\beta_r)$  and  $K_2 = \frac{1}{2} - \frac{1}{2}\xi_r \cos(\beta_r) + j\frac{1}{2}\xi_r \sin(\beta_r)$  are the I/Q imbalance parameters. Here,  $\xi_r$  and  $\beta_r$  represent amplitude and phase imbalance parameters, respectively.

In (5.5), we assume that  $U_1$ 's receiver is aware of the I/Q imbalance parameters. Based on this, the signal of  $U_2$  and its image are subtracted from the received signal through SIC and the cancellation error is modeled by  $e$ .  $\psi$  in (5.5) is an improper Gaussian RV where its real and imaginary parts have zero mean and its variances are given by

$$\begin{aligned}
\sigma_{\psi^I}^2 &= \frac{(\sigma_n^2 + P_2\sigma_e^2)}{2} \\
\sigma_{\psi^Q}^2 &= \frac{(K_c^2 + K_d^2)(\sigma_n^2 + P_2\sigma_e^2)}{2}.
\end{aligned} \tag{5.7}$$

where  $K_c = K_1^Q + K_2^Q$  and  $K_d = K_1^I - K_2^I$ . It can be seen that,  $\psi^I$  and  $\psi^Q$  are correlated with the correlation factor which is given by

$$\rho_\psi = \frac{K_c\sigma_n^2}{\sqrt{\sigma_{\psi^I}^2\sigma_{\psi^Q}^2}} = -\sin(\beta_r). \tag{5.8}$$

Moreover,  $\eta$  in (5.6) is an improper Gaussian RV where its real and imaginary parts have zero means and variances given by

$$\begin{aligned}
\sigma_{\eta^I}^2 &= \frac{\sigma_n^2}{2}, \\
\sigma_{\eta^Q}^2 &= \frac{(K_c^2 + K_d^2)\sigma_n^2}{2}.
\end{aligned} \tag{5.9}$$

Also,  $\eta^I$  and  $\eta^Q$  are correlated with the correlation factor which is given by

$$\rho_\eta = \frac{K_c\sigma_n^2}{\sqrt{\sigma_{\eta^I}^2\sigma_{\eta^Q}^2}} = -\sin(\beta_r). \tag{5.10}$$

## 5.3 Receiver Design and Performance Analysis

Based on the previous discussion, I/Q imbalance changes the characteristics of the received signal, thereby requiring a more sophisticated receiver design. This section proposes and analyzes a receiver design that can tackle this problem, and also compares its performance with the traditional one.

### 5.3.1 Optimal Down-link NOMA Receiver Designs

In this section, an optimal ML receiver's design is proposed for the presented two-users NOMA system, where both users have I/Q imbalance and the first user suffers from imperfect SIC. The main idea of the proposed design is to tackle the effects of I/Q imbalance on the signal and noise parts at  $U_1$  and  $U_2$ .

At  $U_1$ , the optimal receiver detects the transmitted signal from the received one in (5.5) based on the assumption  $\hat{S}_{1i} = \sqrt{P_1}[K_1(h_1(G_1s_{1i} + G_2s_{1i}^*)) + K_2(h_1(G_1s_{1i} + G_2s_{1i}^*))^*]$ , rather than  $\hat{S}_{1i} = \sqrt{P_1}h_1s_{1i}$  for the traditional receiver. In addition, this design exploits the fact that the resulted noise is improper. In like manner, the optimal receiver at  $U_2$  detects the transmitted signal from the received one in (5.6) based on the assumption  $\tilde{S}_{2k} = \sqrt{P_2}[K_1(h_2(G_1s_{2k} + G_2s_{2k}^*)) + K_2(h_2(G_1s_{2k} + G_2s_{2k}^*))^*]$ , rather than  $\tilde{S}_{2k} = \sqrt{P_2}h_2s_{2k}$  in case of the traditional receiver. In addition, this design exploits the fact that the resulted noise is improper.

#### *First User*

Considering the received signal model in (5.5), and assuming that the I/Q imbalance parameters are known at the receiver, the joint PDF of the real part  $y_1^{IQI}$ , and the imaginary part  $y_1^{IQIQ}$ , of the received signal at  $U_1$  can be written as [41]

$$f_{\mathbf{Y}}(\mathbf{y}_1|s_{1i}) = \frac{1}{(2\pi)\sqrt{|\boldsymbol{\Sigma}|}} \exp\left(-(\mathbf{y}_1 - \hat{\boldsymbol{\mu}}_i)^T \boldsymbol{\Sigma}^{-1}(\mathbf{y}_1 - \hat{\boldsymbol{\mu}}_i)\right), \quad (5.11)$$

where  $\mathbf{y}_1 = [y_1^{IQI} \ y_1^{IQIQ}]^T$ ,  $\boldsymbol{\Sigma} = \begin{bmatrix} \sigma_\psi^{I^2} & \rho_\psi \sigma_\psi^I \sigma_\psi^Q \\ \rho_\psi \sigma_\psi^I \sigma_\psi^Q & \sigma_\psi^{Q^2} \end{bmatrix}$ , and  $\hat{\boldsymbol{\mu}}_i = [\sqrt{P_1}\hat{S}_{1i}^I \ \sqrt{P_1}\hat{S}_{1i}^Q]^T$ .

The primary task of the  $U_1$  ML receiver is to choose which  $s_{1i}$  was transmitted among  $M$  hypotheses. Assuming that the transmitted symbols are equally likely, the optimal receiver is designed based on maximizing the joint PDF. Maximizing the joint PDF in (5.11) is equivalent to minimizing the following argument

$$\hat{s}_{1i} = \arg \min_{i=1, \dots, M} \left[ (\mathbf{y}_1 - \hat{\boldsymbol{\mu}}_i)^T \boldsymbol{\Sigma}^{-1} (\mathbf{y}_1 - \hat{\boldsymbol{\mu}}_i) \right]. \quad (5.12)$$

*Conditional PEP:* From (5.12), the probability of detecting  $s_{1j}$  at  $U_1$  given that the transmitted symbol was  $s_{1i}$  is given by

$$\text{PEP}_{1\text{opt}} = \Pr \left( [(\mathbf{y}_1 - \hat{\boldsymbol{\mu}}_i)^T \boldsymbol{\Sigma}^{-1} (\mathbf{y}_1 - \hat{\boldsymbol{\mu}}_i)] > [(\mathbf{y}_1 - \hat{\boldsymbol{\mu}}_j)^T \boldsymbol{\Sigma}^{-1} (\mathbf{y}_1 - \hat{\boldsymbol{\mu}}_j)] \right). \quad (5.13)$$

After some algebraic simplification, and assuming that  $\boldsymbol{\Delta} \mathbf{S}_1^T = \left[ (\hat{S}_{1i} - \hat{S}_{1j})^I \quad (\hat{S}_{1i} - \hat{S}_{1j})^Q \right]$ ,  $\text{PEP}_{1\text{opt}}$  can be given as

$$\text{PEP}_{1\text{opt}} = Q \left( \sqrt{\frac{1}{4} P_1 (\boldsymbol{\Delta} \mathbf{S}_1^T \boldsymbol{\Sigma}^{-1} \boldsymbol{\Delta} \mathbf{S}_1)} \right) = Q (\sqrt{\gamma_{1\text{opt}}}). \quad (5.14)$$

To gain more insight into the effects of I/Q imbalance on the system performance, consider the case where perfect CSI, and the in-phase and quadrature-phase components are perfectly matched. In this case,  $K_1 = 1$  and  $K_2 = 0$ . Consequently,  $\sigma_\psi^I = \sigma_\psi^Q = \frac{\sigma_n^2}{2}$ . In addition, the real and imaginary parts of  $\psi$  become uncorrelated (i.e.,  $\rho_\psi = 0$ ). As a result  $\psi$  becomes a proper Gaussian RV. Based on this,  $\boldsymbol{\Sigma}^{-1}$  in (5.14) becomes a diagonal matrix and doesn't depend on  $s_{2k}$ , and the error probability can be greatly simplified to

$$\text{PEP}_{1\text{opt}} = Q \left( \sqrt{\frac{P_1 \|\boldsymbol{\Delta} \mathbf{S}_1\|^2}{2\sigma_n^2}} \right). \quad (5.15)$$

This is a well-known formula for the user with the strongest channel conditions of the traditional NOMA system ( $U_1$  in our system model), which validates the presented analysis.

The APEP will be calculated considering the Beckmann fading channels. More details about Beckmann fading channels can be found in Section 2.4.  $h$  can be modeled as  $\mathcal{CN}(\boldsymbol{\mu}_h, \boldsymbol{\sigma}_h^2)$ . From (5.14) and denoting  $[M_i = K_1(G_1 s_{1i} + G_2 s_{1i}^*)]$ ,  $[N_i = K_2((G_1 s_{1i} +$

$G_{2s_{1i}^*})^*$ ] and  $\Delta \mathbf{S}_1^T = [x_1 \ x_2]$ , the mean and variances of  $x_1$  and  $x_2$  can be given as

$$\begin{aligned}
\mu_{x_1} &= \mu_h^I([M_i^I + N_i^I] - [\hat{M}_i^I + \hat{N}_i^I]) + \mu_h^Q([N_i^Q - M_i^Q] - [\hat{N}_i^Q - \hat{M}_i^Q]), \\
\mu_{x_2} &= \mu_h^I([N_i^Q + M_i^Q] - [\hat{N}_i^Q + \hat{M}_i^Q]) + \mu_h^Q([M_i^I - N_i^I] - (\hat{M}_i^I - \hat{N}_i^I)), \\
\sigma_{x_1}^2 &= \sigma_{h^I}^2([M_i^I + N_i^I] - [\hat{M}_i^I + \hat{N}_i^I])^2 + \sigma_{h^Q}^2([N_i^Q - M_i^Q] - [\hat{N}_i^Q - \hat{M}_i^Q])^2 + 2\rho_h \sigma_h^Q \sigma_h^I \\
&\quad \times ([M_i^I + N_i^I] - [\hat{M}_i^I + \hat{N}_i^I]) \times ([N_i^Q - M_i^Q] - [\hat{N}_i^Q - \hat{M}_i^Q]), \\
\sigma_{x_2}^2 &= \sigma_{h^I}^2([N_i^Q + M_i^Q] - [\hat{N}_i^Q + \hat{M}_i^Q])^2 + \sigma_{h^Q}^2([M_i^I - N_i^I] - [\hat{M}_i^I - \hat{N}_i^I])^2 + 2\rho_h \sigma_h^I \sigma_h^Q \\
&\quad \times ([N_i^Q + M_i^Q] - [\hat{N}_i^Q + \hat{M}_i^Q])([M_i^I - N_i^I] - [\hat{M}_i^I - \hat{N}_i^I]), \\
\mathbb{E}\{x_1 x_2\} &= \sigma_{h^I}^2([M_i^I + N_i^I] - [\hat{M}_i^I + \hat{N}_i^I])([N_i^Q + M_i^Q] - [\hat{N}_i^Q + \hat{M}_i^Q]) \\
&\quad + \sigma_{h^Q}^2([N_i^Q - M_i^Q] - [\hat{N}_i^Q - \hat{M}_i^Q])([M_i^I - N_i^I] - (\hat{M}_i^I - \hat{N}_i^I)) \\
&\quad + \rho_h \sigma_h^I \sigma_h^Q ([M_i^I + \hat{M}_i^I]^2 + [N_i^Q + \hat{N}_i^Q]^2 - [N_i^I + \hat{N}_i^I]^2 - [M_i^Q + \hat{M}_i^Q]^2), \\
\rho_x &= \text{cov}\{x_1 x_2\} / (\sigma_{x_1} \sigma_{x_2}).
\end{aligned} \tag{5.16}$$

Hence,  $\gamma_{opt_i}$  has the PDF of a quadratic form of two correlated noncentral chi-squared RVs.

From Section 2.3, the MGF of  $\gamma_{opt_1}$  can be given by

$$M_{\gamma_{opt}}(t) = \frac{\exp\left(\frac{b_1^2 \lambda_1 t}{1-2\lambda_1 t}\right)}{\sqrt{1-2\lambda_1 t}} \times \frac{\exp\left(\frac{b_2^2 \lambda_2 t}{1-2\lambda_2 t}\right)}{\sqrt{1-2\lambda_2 t}}, \tag{5.17}$$

where the eigenvalues  $\lambda_1$  and  $\lambda_2$ , and the mean values  $b_1$  and  $b_2$  are calculated as in Section 2.3. In addition, this section shows how other channel models can be considered as a special cases of Beckmann fading model.

Now, from [84], an exact closed-form expression of the average  $\text{PEP}_{1_{opt}}$  can be calculated as follows

$$\overline{\text{PEP}}_{1_{opt}} = \frac{1}{\pi} \int_0^{\frac{\pi}{2}} M_{\gamma_{1_{opt}}} \left( \frac{-P_1}{8 \sin^2 \theta} \right) d\theta. \tag{5.18}$$

The integration in (5.18) can be calculated numerically.

### **Second User**

Considering the received signal model in (5.6), the noise at  $U_2$  has the term  $\tilde{S}_{1i}$ . This term relates to  $U_1$ 's transmitted signal and is not considered when  $U_2$  detects its signal. Based

on this, the PDF of  $y_2^{IQI}$  depends only on the noise part  $\eta$ . From (5.6), the joint PDF of the real and imaginary parts of the received signal at  $U_2$  is given by

$$f_{\mathbf{Y}}(\mathbf{y}_2|s_{2k}) = \frac{1}{2\pi\sqrt{|\nabla|}} \exp\left(-(\mathbf{y}_2 - \tilde{\boldsymbol{\mu}}_k)^T \nabla^{-1}(\mathbf{y}_2 - \tilde{\boldsymbol{\mu}}_k)\right), \quad (5.19)$$

where  $\mathbf{y}_2 = \begin{bmatrix} y_2^{IQI} & y_2^{IQIQ} \end{bmatrix}^T$ ,  $\nabla = \begin{bmatrix} \sigma_\eta^2 & \rho_\eta \sigma_\eta^I \sigma_\eta^Q \\ \rho_\eta \sigma_\eta^I \sigma_\eta^Q & \sigma_\eta^{Q^2} \end{bmatrix}$ , and  $\tilde{\boldsymbol{\mu}}_k = \begin{bmatrix} \sqrt{P_2} \tilde{S}_{2k}^I & \sqrt{P_2} \tilde{S}_{2k}^Q \end{bmatrix}^T$ .

As explained,  $U_2$ 's receiver chooses which  $s_{2k}$  was transmitted among  $M$  possibilities. Assuming that the transmitted symbols are equally likely, the optimal receiver is designed based on minimizing the following argument

$$s_{2k}^{\hat{}} = \arg \min_{k=1, \dots, M} \left[ (\mathbf{y}_2 - \tilde{\boldsymbol{\mu}}_k)^T \nabla^{-1}(\mathbf{y}_2 - \tilde{\boldsymbol{\mu}}_k) \right]. \quad (5.20)$$

It can be seen from (5.20) that,  $U_1$ 's transmitted signal is not known and treated as a noise at  $U_2$ . This agrees with (5.2). i.e., power-domain NOMA's assumption that treats the signals of lower power orders as a noise.

*Conditional PEP:* From (5.20), the probability of detecting  $s_{2k}$  at  $U_2$  given that the transmitted symbol was  $s_{2q}$  is given by

$$\text{PEP}_{2\text{opt}} = \Pr \left( [(\mathbf{y}_2 - \tilde{\boldsymbol{\mu}}_k)^T \nabla^{-1}(\mathbf{y}_2 - \tilde{\boldsymbol{\mu}}_k)] > [(\mathbf{y}_2 - \tilde{\boldsymbol{\mu}}_q)^T \nabla^{-1}(\mathbf{y}_2 - \tilde{\boldsymbol{\mu}}_q)] \right) \quad (5.21)$$

Here, to find the  $\text{PEP}_{2\text{opt}}$  analytically, we need the characteristics of the accumulative noise. These characteristics depend on the term  $\tilde{S}_{1i}$ . This term is related to  $U_1$ 's transmitted signal. Based on this, the conditional error probability should be calculated. The conditional probability of detection error at  $U_2$ , i.e., detecting  $s_{2q}$  given that the transmitted symbol was  $s_{2k}$  depends on  $U_1$  transmitted symbol  $s_{1i}$  and can be given by:

$$P(s_{2q}|s_{2k}) = \sum_{i=1}^M P((s_{2q}|s_{2k}) | s_{1i}) P(s_{1i}), \quad (5.22)$$

Noting that these conditional probabilities are equally likely to occur with probability equal to  $1/M$ , (5.22) can be written as

$$\text{PEP}_{2\text{opt}} = \frac{1}{M} \sum_{i=1}^M P(\text{PEP}_{2\text{opt}} | s_{1i}). \quad (5.23)$$

Based on this, the probability of detecting  $s_{2q}$  at  $U_2$  given that the transmitted symbols at  $U_2$  and  $U_1$  were  $s_{2k}$  and  $s_{1i}$  respectively is given by

$$\text{PEP2}_{\text{opt}} = \frac{1}{M} \sum_{i=1}^M \left( \left( \Pr \left[ (\mathbf{y}_2 - \tilde{\boldsymbol{\mu}}_k)^T \boldsymbol{\nabla}^{-1} (\mathbf{y}_2 - \tilde{\boldsymbol{\mu}}_k) \right] > \left[ (\mathbf{y}_2 - \tilde{\boldsymbol{\mu}}_q)^T \boldsymbol{\nabla}^{-1} (\mathbf{y}_2 - \tilde{\boldsymbol{\mu}}_q) \right] \right) \mid s_{1i} \right). \quad (5.24)$$

After some algebraic simplification, and assuming that  $\boldsymbol{\Delta} \mathbf{S}_2^T = \left[ (S_{2k} - S_{2q})^I \quad (S_{2k} - S_{2q})^Q \right]$ , and  $\mathbf{S}_{1i}^T = \left[ (\tilde{S}_{1i})^I \quad (\tilde{S}_{1i})^Q \right]$ ,  $\text{PEP2}_{\text{opt}}$  can be given as

$$\begin{aligned} \text{PEP2}_{\text{opt}} &= \frac{1}{M} \sum_{i=1}^M Q \left( \sqrt{\frac{[P_2(\boldsymbol{\Delta} \mathbf{S}_2^T \boldsymbol{\nabla}^{-1} \boldsymbol{\Delta} \mathbf{S}_2) + 2\sqrt{P_1 P_2}(\mathbf{S}_{1i}^T \boldsymbol{\nabla}^{-1} \mathbf{S}_2)]^2}{4P_2(\boldsymbol{\Delta} \mathbf{S}_2^T \boldsymbol{\nabla}^{-1} \boldsymbol{\Delta} \mathbf{S}_2)}} \right) \\ &= \frac{1}{M} \sum_{i=1}^M Q(\sqrt{\gamma_{2\text{opt}_i}}) \end{aligned} \quad (5.25)$$

It is clear from the PDF of  $\gamma_{2\text{opt}_i}$  that it is very difficult to find a closed-form expression for the average  $\text{PEP2}_{\text{opt}}$ . Thus, the average is calculated numerically by averaging the  $\text{PEP2}_{\text{opt}}$  over a large number of channel realizations for each SNR value.

### 5.3.2 Traditional (Blind) NOMA Receivers

The traditional receiver can be defined as a one that utilizes the ML receiver to detect the received signal as if no I/Q imbalance exists at NOMA users, even in the case where it does. This receiver also ignores the fact that the noise at the receivers is IGN.

#### *First User*

The traditional receiver of the first user depends on minimizing the following statement

$$\hat{s}_{1i} = \arg \min_{i=1, \dots, M} \left\{ |y_1^{IQI} - \sqrt{P_1} h_1 s_{1i}|^2 \right\}. \quad (5.26)$$

Now, it should be noted that  $U_1$ 's receiver is unaware of the I/Q imbalance parameters. Based on this, only  $\sqrt{P_2} h_1 s_{2k}$  is subtracted from the  $y_1^{IQI}$  through SIC (rather than  $\sqrt{P_2} [h_1 K_1 (G_1 s_{2k} + G_2 s_{2k}^*) + h_1^* K_2 (G_1 s_{2k} + G_2 s_{2k}^*)^*]$ ). In this case  $y_1^{IQI}$  in (5.5) is rewritten

ten as

$$\begin{aligned}
y_1^{IQI} = & \left\{ \underbrace{\sqrt{P_1}[K_1(h_1(G_1s_{2i} + G_2s_{2i}^*)) + K_2(h_1(G_1s_{2i} + G_2s_{2i}^*))^*]}_{\hat{s}_{1i}} \right\} \text{ signal part} \\
& + \\
& \left\{ \begin{aligned} & \sqrt{P_2}[h_1K_1(G_1s_{2k} + G_2s_{2k}^*) + h_1^*K_2(G_1s_{2k} + G_2s_{2k}^*)^* - h_1s_{2k}] \\ & + \\ & \underbrace{K_1\sqrt{P_2}e + K_2\sqrt{P_2}e^* + K_1n_1 + K_2n_1}_{\psi} \end{aligned} \right\} \text{ noise part}
\end{aligned} \tag{5.27}$$

*Conditional PEP:* From (5.26), the probability of detecting  $s_{1j}$  at  $U_1$  given that the transmitted symbol was  $s_{1i}$  is given by

$$\text{PEP1}_{\text{tra}} = \Pr \left( |y_1^{IQI} - \sqrt{P_1}h_1s_{1i}|^2 > |y_1^{IQI} - \sqrt{P_1}h_1s_{1j}|^2 \right). \tag{5.28}$$

Now, to find the  $\text{PEP1}_{\text{tra}}$  analytically, we should note that it depends on  $s_{2k}$  which is unknown at  $U_1$ . Based on this, the summation of the conditional probabilities can be used. The probability of detection error at  $U_1$ , i.e., detecting  $s_{1j}$  given that the transmitted symbol was  $s_{1i}$  depends on  $U_2$  transmitted symbol  $s_{2k}$  and can be given by:

$$\text{PEP1}_{\text{tra}} = \frac{1}{M} \sum_{k=1}^M P(\text{PEP1}_{\text{tra}} | s_{2k}). \tag{5.29}$$

From (5.27) and (5.28),  $\text{PEP1}_{\text{opt}}$  is given as

$$\text{PEP1}_{\text{tra}} = \frac{1}{M} \sum_{k=1}^M \left( \Pr \left( |y_1^{IQI} - \sqrt{P_1}h_1s_{1i}|^2 > |y_1^{IQI} - \sqrt{P_1}h_1s_{1j}|^2 \right) \mid s_{2k} \right). \tag{5.30}$$

After some mathematical simplifications, the conditional error probability can be written as

$$\text{PEP1}_{\text{tra}} = \frac{1}{M} \sum_{k=1}^M Q \left( \sqrt{\frac{P_1\vartheta_k^2}{4\Lambda^T\Sigma\Lambda}} \right) = \frac{1}{M} \sum_{k=1}^M Q \left( \sqrt{\gamma_{1\text{tra}k}} \right), \tag{5.31}$$

where  $\Lambda^T = \left[ (h_1s_{1i} - h_1s_{1j})^I \quad (h_1s_{1i} - h_1s_{1j})^Q \right]$ , and  $\vartheta_k = |\hat{S}_{1i} + \sqrt{(P_2/P_1)}\bar{S}_{2k} - h_1s_{1i}|^2 - |\hat{S}_{1i} + \sqrt{(P_2/P_1)}\bar{S}_{2k} - h_1s_{1j}|^2$ , and  $[\bar{S}_{2k} = h_1K_1(G_1s_{2k} + G_2s_{2k}^*) + h_1^*K_2(G_1s_{2k} + G_2s_{2k}^*)^* - h_1s_{2k}]$ .

If it is assumed that in-phase and quadrature-phase are perfectly matched, in this case the traditional receiver must have the same performance as the optimal one. This can be proven by noting that in this case  $\bar{S}_{2k} = 0$  and  $\hat{S}_{1i} = h_1 s_{1i}$ . Also,  $\Sigma$  becomes a diagonal matrix. Based on this, the error probability in (5.31) can be greatly simplified as in (5.15), which validates the presented analysis.

### Second User

Following the same way of calculating the PEP of  $U_1$  and starting from (5.6), The traditional receiver of the second user depends on minimizing the following statement

$$s_{2k} = \arg \min_{k=1, \dots, M} \left\{ |y_2^{IQI} - \sqrt{P_1} h_1 s_{2k}|^2 \right\}. \quad (5.32)$$

*Conditional PEP:* From (5.32), the probability of detecting  $s_{2q}$  at  $U_2$  given that the transmitted symbol was  $s_{2k}$  is given by

$$\text{PEP}_{2\text{tra}} = \Pr \left( |y_2^{IQI} - \sqrt{P_1} h_1 s_{1k}|^2 > |y_2^{IQI} - \sqrt{P_1} h_1 s_{1q}|^2 \right). \quad (5.33)$$

Now, depending on the analysis in (5.22)-(5.24) and after some mathematical simplifications, the analytical  $\text{PEP}_{2\text{tra}}$  can be founded as

$$\text{PEP}_{2\text{tra}} = \frac{1}{M} \sum_{i=1}^M Q \left( \sqrt{\frac{P_2 \omega_i^2}{4 \Omega^T \nabla \Omega}} \right) = \frac{1}{M} \sum_{i=1}^M Q \left( \sqrt{\gamma_{2\text{tra}i}} \right). \quad (5.34)$$

where  $\Omega^T = \left[ (h_2 s_{2k})^I - (h_2 s_{2q})^I \quad (h_2 s_{2k})^Q - (h_2 s_{2q})^Q \right]$ , and  $\omega_i = |\tilde{S}_{2k} + (P_1/P_2)\tilde{S}_{1i} - h_2 s_{2k}|^2 - |\tilde{S}_{2k} + (P_1/P_2)\tilde{S}_{1i} - h_2 s_{2q}|^2$ .

As it appears from (5.31) and (5.34), it is complicated to find closed-form expressions either for the average  $\text{PEP}_{1\text{tra}}$  or for  $\text{PEP}_{2\text{tra}}$ . Based on that, their averages are calculated numerically by averaging over a large number of channel realizations for each SNR value.

### 5.3.3 BER Calculations

BER of optimal and traditional users' receivers can be obtained using a well-known union bound formula [42]. The BER of the aforementioned receivers can be calculated as

$$\text{BER}_B \leq \frac{1}{M} \sum_{t=1}^M \sum_{\hat{i}=t+1}^M \frac{N(\chi_i, \hat{\chi}_i) \text{PEP}_B}{\log_2(M)}, \quad (5.35)$$

where  $N(\chi_i, \hat{\chi}_i)$  is the number of error bits associated with the corresponding pairwise error event,  $M$  is the modulation order, and  $B \in \{U_{1\text{opt}}, U_{1\text{sub}}, U_{2\text{opt}}, U_{2\text{sub}}\}$ .

## 5.4 Numerical Analysis and Results

This section investigates the effects of I/Q imbalance on down-link NOMA systems with two users. Comprehensive Monte Carlo simulations were carried out to validate the analytical results and to assess the system's performance. Unless specified otherwise, a SISO system scenario with 4-QAM modulation is assumed, a power allocation factor of  $\alpha = 0.8$  and Rayleigh fading channel conditions with  $\sigma_{h_1}^2 = 4$  and  $\sigma_{h_2}^2 = 1$  is used. Both users are affected by PGN  $n \sim \mathcal{CN}(0, 1)$  and perfect SIC is assumed at the  $U_1$ . Moreover, for a fair comparison, the transmitted power of  $U_1$  is normalized by  $(|x_i G_1 + x_i^* G_2|^2)$  and the transmitted power of  $U_2$  is normalized by  $(|x_k G_1 + x_k^* G_2|^2)$ . All the comparisons are made against a system with perfect I/Q balance. Finally, the simulation results of the ABER are plotted against the SNR for all figures using (5.35).

Figs. 5.2 and 5.3 show that the simulation and analytical results when the average PEP is calculated numerically by averaging the conditional PEP over a large number of channel realizations for both the optimal and the traditional receivers of  $U_1$  and  $U_2$  at different values of power allocation coefficients. In addition, the closed form of average  $\text{PEP}_{1\text{opt}}$  is plotted in this figure. The channels of  $U_1$  and  $U_2$  are Beckmann fading channels where  $U_1$ 's channel is characterized by  $\mu_{h_1^I} = 0.1$ ,  $\mu_{h_1^Q} = 0.2$ ,  $\sigma_{h_1^I}^2 = 0.6$ ,  $\sigma_{h_1^Q}^2 = 1.4$ ,  $\rho_{h_1} = 0.3$ , and  $\sigma_e^2 = 0.002$ , and  $U_2$ 's channel is characterized by  $\mu_{h_2^I} = 0.1$ ,  $\mu_{h_2^Q} = 0.05$ ,  $\sigma_{h_2^I}^2 = 0.2$ ,  $\sigma_{h_2^Q}^2 = 0.3$ , and  $\rho_{h_2} = 0.3$ . These figures prove that the simulation results match the analytical analysis for both users, which validates the given analysis. The performance of  $U_1$ 's receivers saturates in the high SNR region because of the channel estimation error.

Figs. 5.4 and 5.5 demonstrate the effects of I/Q imbalance at the transmitter and receiver of  $U_1$ , respectively, at three different levels of I/Q imbalance. The amplitude imbalance and phase mismatch values for these levels are  $\xi_r = 0.6$  dB,  $\beta_r = 3^\circ$ ,  $\xi_r = 1.2$  dB,  $\beta_r = 5^\circ$ ,  $\xi_r = 2$  dB,  $\beta_r = 8^\circ$ . This figure shows that, as expected, the level of performance

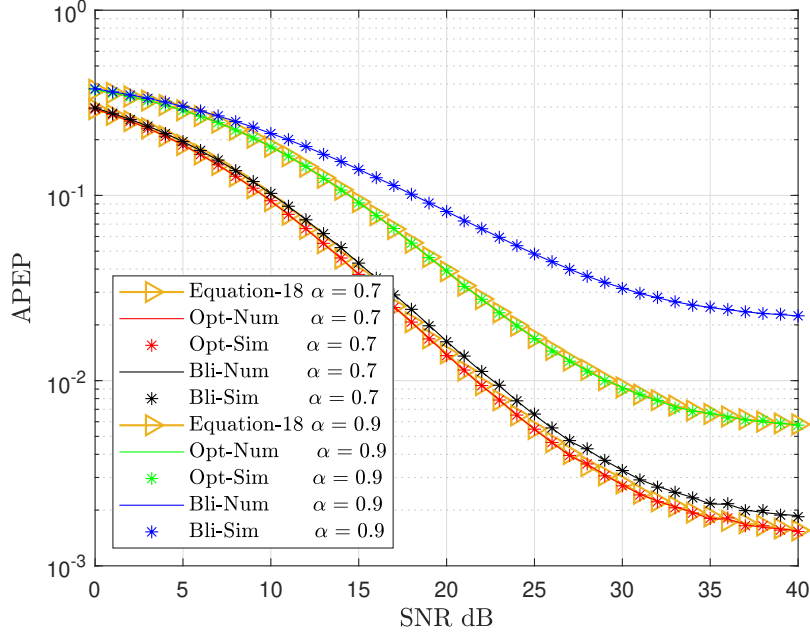


Figure 5.2: APEP of  $U_1$  at 1 dB amplitude mismatch and  $5^\circ$  phase imbalance when  $\mu_{h_1 I} = 0.1$ ,  $\mu_{h_1 Q} = 0.2$ ,  $\sigma_{h_1 I}^2 = 0.6$ ,  $\sigma_{h_1 Q}^2 = 1.4$ ,  $\rho_{h_1} = 0.3$ , and  $\sigma_e^2 = 0.002$ .

degradation increases with the level of I/Q imbalance increases. Moreover, the optimal receiver can totally mitigate the effects of I/Q imbalance at the receiver side while there is a minor degradation (less than 0.5 dB) of its performance when the transmitter has a high level of imbalance. In contrast, the traditional receiver shows poor performance in both figures. Key results in these figures can be explained by noting two points from (5.5) and (5.27). First, in the noise part of (5.5), only the imperfect SIC term is maximized when it is multiplied by  $P_2$ , which minimizes I/Q imbalance effects at  $U_1$ . This is not the case for the traditional receiver where only the term  $\sqrt{P_2}h_1s_{2k}$  is cancelled from  $y_1^{IQI}$  rather than  $\sqrt{P_2}[h_1K_1(G_1s_{2k} + G_2s_{2k}^*) + h_1^*K_2(G_1s_{2k} + G_2s_{2k}^*)]$ , which maximize I/Q imbalance effects. Second, the optimal receiver detects the transmitted signal from the received one based on different assumptions that  $\hat{S}_{1i} = \sqrt{P_1}h_1(G_1s_{1i} + G_2s_{1i}^*)$  in Fig. 5.4 and  $\hat{S}_{1i} = \sqrt{P_1}(K_1(h_1s_{1i}) + K_2(h_1s_{1i})^*)$  in Fig. 5.5 as opposed to  $\hat{S}_{1i} = \sqrt{P_1}h_1s_{1i}$  which is used in both figures for the traditional receiver.

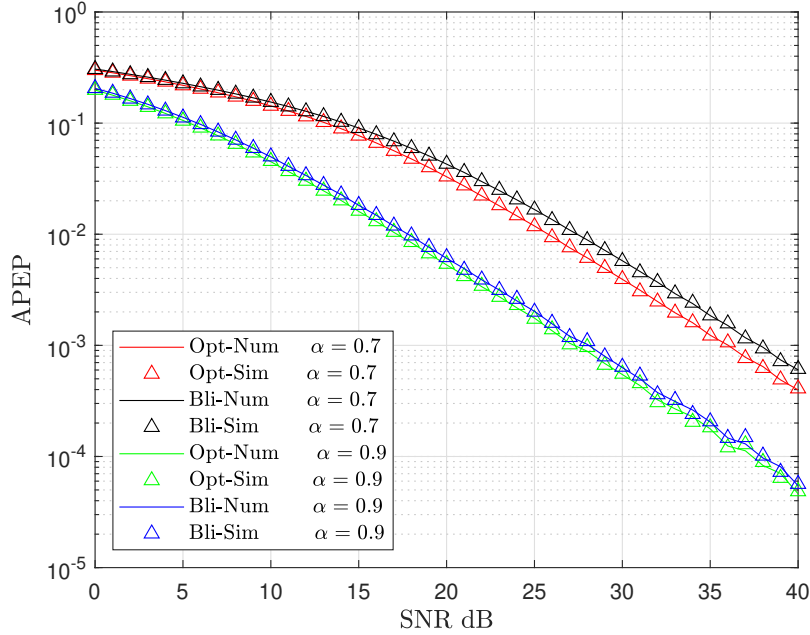


Figure 5.3: APEP of  $U_2$  at 1 dB amplitude mismatch and  $5^\circ$  phase imbalance when  $\mu_{h_2^I} = 0.1$ ,  $\mu_{h_2^Q} = 0.05$ ,  $\sigma_{h_2^I}^2 = 0.2$ ,  $\sigma_{h_2^Q}^2 = 0.3$ , and  $\rho_{h_2} = 0.3$ .

Figs. 5.6 and 5.7 illustrate the effects of I/Q imbalance at the transmitter and receiver of  $U_2$ , respectively, at the same three levels of I/Q imbalance used in the previous analysis for  $U_1$ . As with  $U_1$ , the optimal receiver of  $U_2$  outperforms the traditional one. However unlike with  $U_1$ , the noise term  $[K_1(h_2s_1) + K_2(h_2s_1)^*]$  in (5.6) is multiplied by  $P_1$ , which maximizes the effects of I/Q imbalance when the transmitted power is increased ( $P_1 = \alpha * P_t$ ). Consequently degrading the performance of both receivers. This degradation appears worse for the traditional receiver because the optimal receiver detects the transmitted signal based on different assumptions that  $\hat{S}_{2k} = \sqrt{P_2}h_1(G_1s_{2k} + G_2s_{2k}^*)$  in Fig. 5.6 and  $\hat{S}_{2k} = \sqrt{P_2}(K_1(h_2s_{2k}) + K_2(h_2s_{2k})^*)$  in Fig. 5.7 as opposed to  $\hat{S}_{2k} = \sqrt{P_2}h_1s_{2k}$  which is used for the traditional receiver.

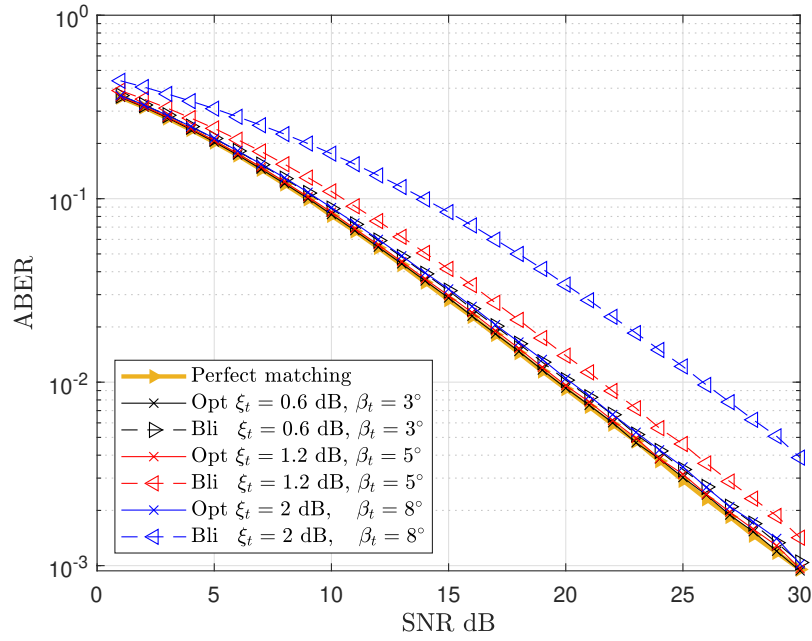


Figure 5.4: ABER performance of  $U_1$  when the transmitter under the effects of different levels of I/Q imbalances and  $\alpha = 0.8$ .

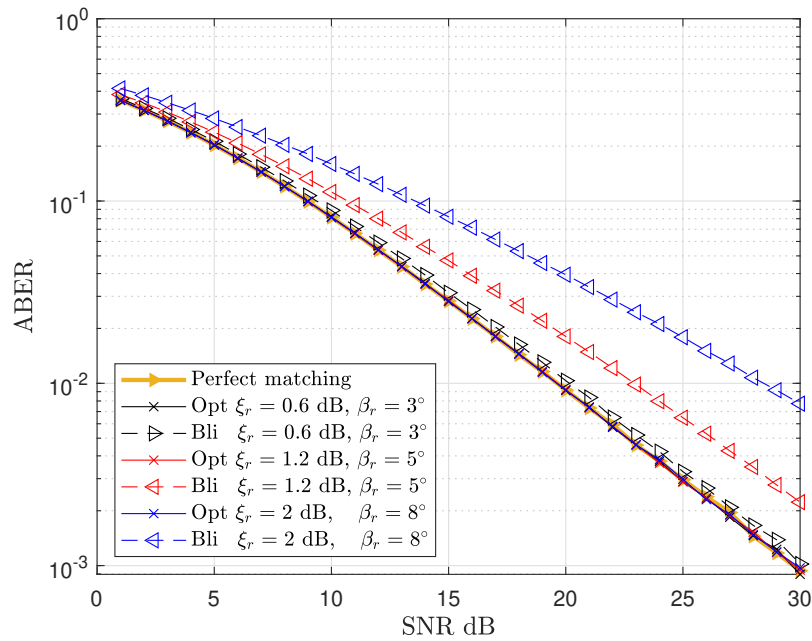


Figure 5.5: ABER performance of  $U_1$  when the receiver under the effects of different levels of I/Q imbalances and  $\alpha = 0.8$ .

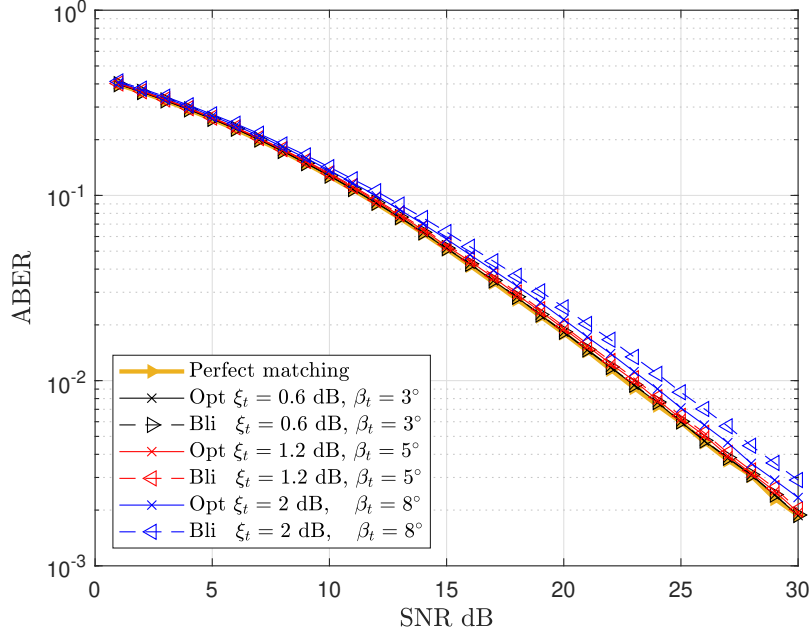


Figure 5.6: ABER performance of  $U_2$  when the transmitter under the effects of different levels of I/Q imbalances and  $\alpha = 0.8$ .

Figs. 5.8 and 5.9 display the ABER of NOMA users for different values of power allocation coefficient values. It can be seen in these figures that the ABER of NOMA users depends on the power allocation among the users. Three points can be drawn from these figures. First, the contrast in performance between the optimal and the traditional receiver for the same I/Q imbalance level depends on the users' power allocation. This contrast varies among the users' orders. Second, there is a trade off in the performance of  $U_2$ 's traditional receiver in the presence of I/Q imbalance where increasing the power factor maximizes the level of blindness (the difference between  $\tilde{S}_{2k} = \sqrt{P_2}[K_1(h_2(G_1 s_{2k} + G_2 s_{2k}^*)) + K_2(h_2(G_1 s_{2k} + G_2 s_{2k}^*))^*]$  and  $\tilde{S}_{2k} = \sqrt{P_2} h_2 s_{2k}$ ) while decreasing it increases the noise level caused by  $U_1$ . This trade-off appears at 30 dB SNR in Fig. 5.9; for lower region of SNR the noise level is smaller when  $\alpha = 0.8$  while it is larger for higher region of SNR for the same  $\alpha$ . The opposite occurs when  $\alpha = 0.7$ .

Fig. 5.10 illustrates performance of  $U_1$  under the effect of different levels of imperfect SIC when  $\xi_{t,r} = 1$  dB and  $\beta_{t,r} = 5^\circ$ . This figure shows that the imperfect SIC has big impact on both receivers, where the performance saturates in the high SNR region, leading

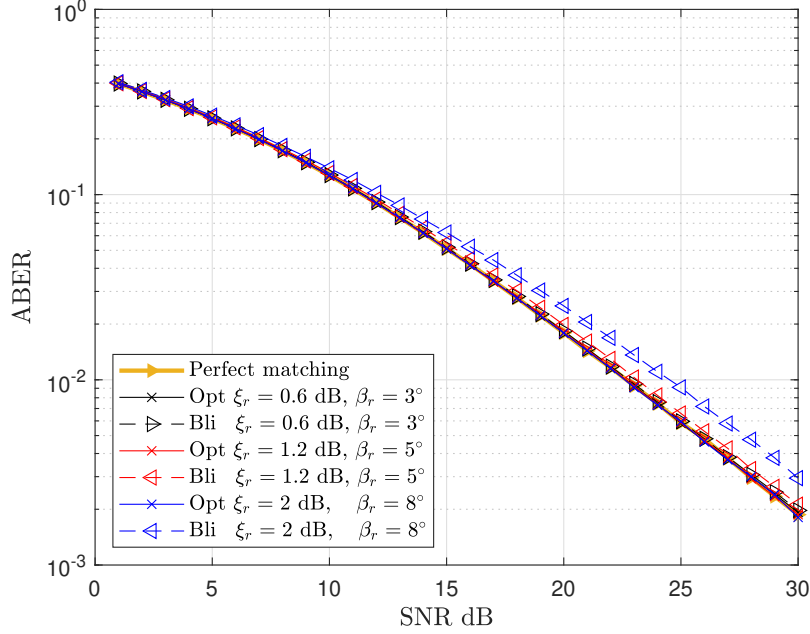


Figure 5.7: ABER performance of  $U_2$  when the receiver under the effects of different levels of I/Q imbalances and  $\alpha = 0.8$ .

to an error floor and zero power gain. The saturation happens with small values of  $\sigma_e^2$  even when using the optimal receiver. However, the effect of imperfect SIC has more impact in case of the blind receiver.

Figs. 5.11 and 5.12 study the effects of channel parameters (more details about these parameters can be found in Section 2.4). For a fair comparison,  $\Omega = 2$  for all channels in Fig. 5.11, and  $\Omega = 1$  for all channels in Fig. 5.12.  $\Omega = \mu_{h_I}^2 + \mu_{h_Q}^2 + \sigma_{h_I}^2 + \sigma_{h_Q}^2$ , and indicates the average power of the fading channel. The results in both figures agree with the one in Section. 3.6 where the Rician fading channel has the best performance, and this is because of the LoS component. In addition, the channel correlation factor reduces the power gain as can be seen between the Rician and Beckmann channel-1. The same thing can also be seen between the Rayleigh channel and the Beckmann-2. The ABER of  $U_1$  optimal receiver saturate in the high SNR region even in the presence of LoS component.

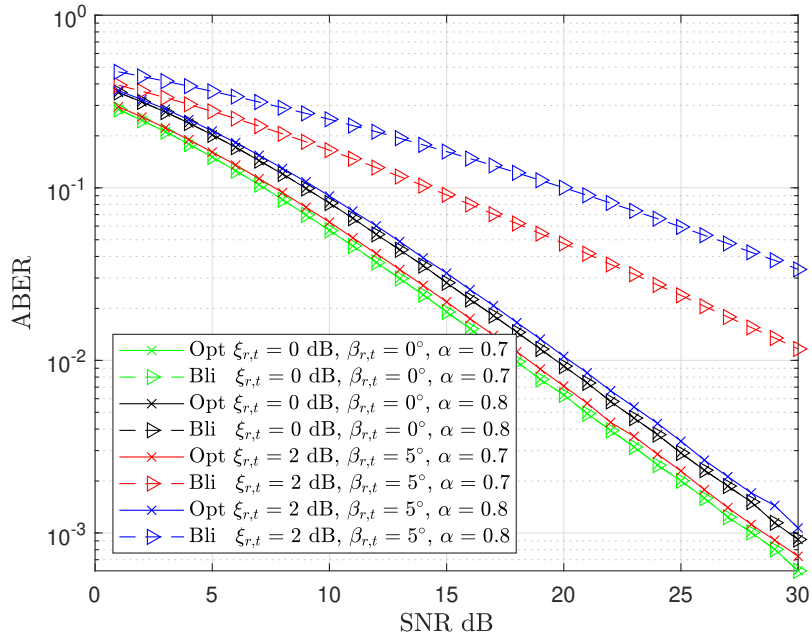


Figure 5.8: ABER performance of  $U_1$  when using different power allocation factors.

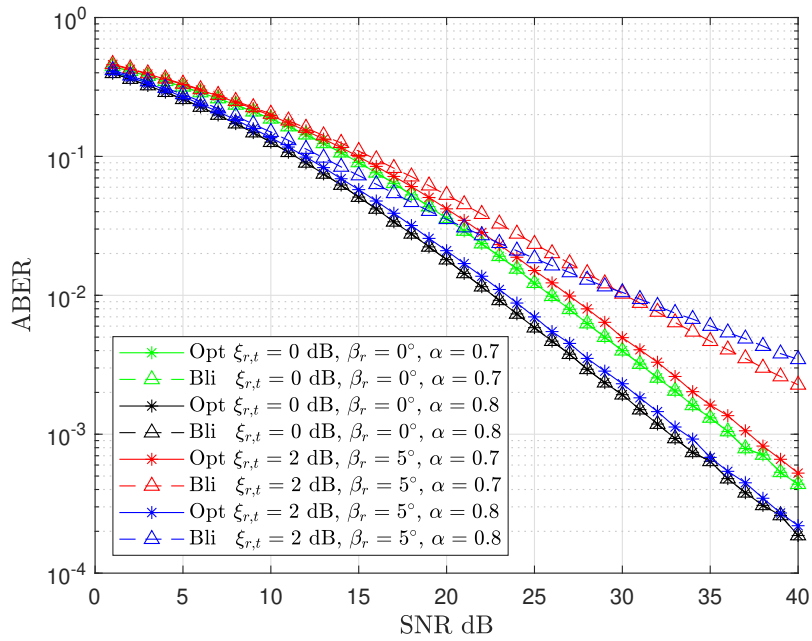


Figure 5.9: ABER performance of  $U_2$  when using different power allocation factors.

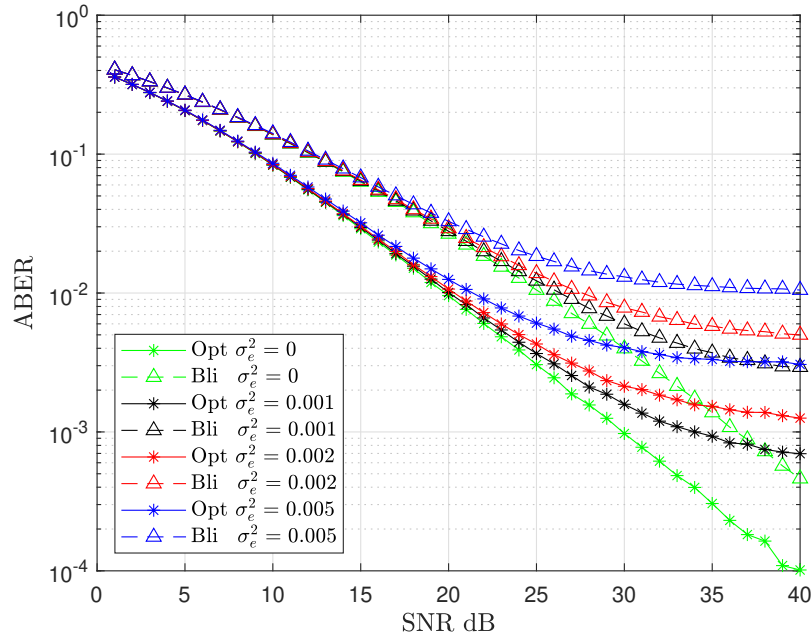


Figure 5.10: ABER performance of  $U_1$  under the effects of different imperfect SIC levels when  $\xi_{t,r} = 1$  dB and  $\beta_{t,r} = 5^\circ$ .

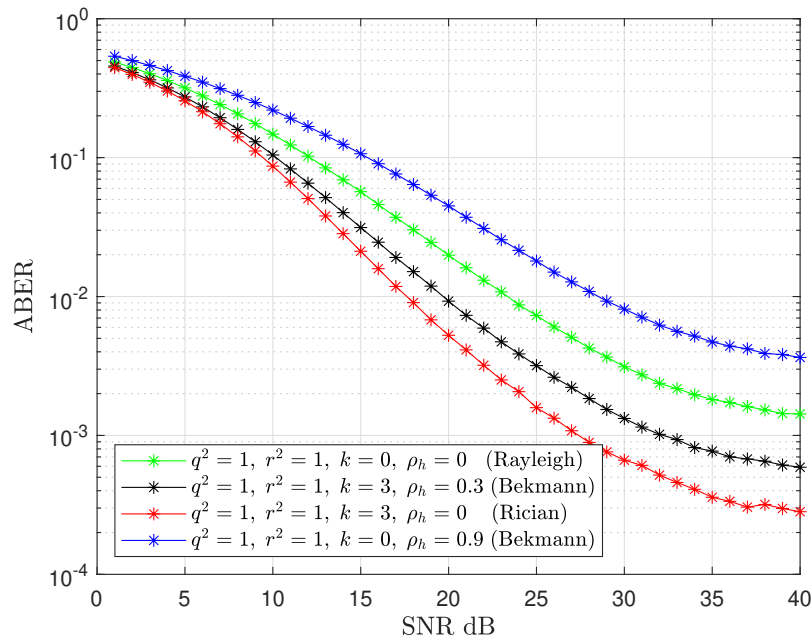


Figure 5.11:  $U_1$ 's optimal receiver performance over Beckmann fading channels with imperfect SIC ( $\sigma_e^2 = .001$ ) and I/Q impaired transmitter and receiver ( $\xi_{t,r}=1.5$  dB,  $\beta_{t,r} = 5^\circ$ ).

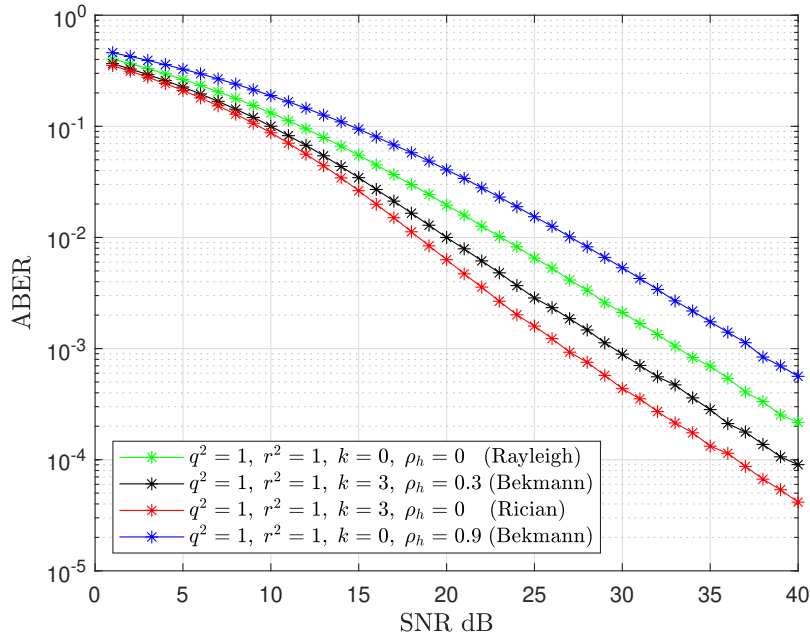


Figure 5.12:  $U_2$ 's optimal receiver performance over Beckmann fading channels with I/Q impaired transmitter and receiver ( $\xi_{t,r}=1.5$  dB,  $\beta_{t,r}=5^\circ$ ).

## 5.5 Conclusion

This chapter presented an analytical framework to study the performance of a down-link NOMA system under the effects of I/Q imbalance and imperfect SIC. It was shown that I/Q imbalance affects the system performance, and this effect can be critical to some users. An optimal receiver that can resist the I/Q imbalance and has almost the same performance regardless of the level of I/Q imbalance was designed for each user. In addition, it was shown that the contrast in performance between the optimal and the traditional receivers for the same I/Q imbalance level depends on the users' power allocation factor. The SIC has a significant impact on the users with stronger channel conditions and can lead to noise floor in the high SNR region even when using our proposed optimal receiver.

# Chapter 6

## Conclusions and Future Work

### 6.1 Conclusions

This thesis studies the effects of HWIs on some promising wireless systems. In particular, it covers the effects of I/Q imbalance and IGN on three modern communication system techniques: CR, QSM, and NOMA. It was shown that I/Q imbalance has a dramatic impact on the the system's performance and this impact increases with larger signal constellations. Traditional QSM shows very poor performance against I/Q imbalance. On the other hand, the performance of NOMA systems depends of the power allocation factor, the channel conditions, and the accuracy of the SIC. In addition, it was shown that exploiting the improperness characteristics of the AWGN can enhance the BER performance.

Receiver designs that can mitigate the effects of I/Q imbalance and exploit the improperness characteristics of the noise were proposed and analyzed. Closed forms of APEP and upper bounds for the ABER, alongside asymptotic formulas were derived for all receivers. All analytical results are verified by Monte Carlo simulations. In addition, exact FIM and CRLB matrices were also calculated, proving that if the noise at the SRx is PGN, then the CRLB elements are equal and uncorrelated even if the I/Q imbalance changes the noise behavior from proper to improper.

We calculated the APEP expressions considering the Beckmann channel model, which assumes a channel with arbitrary means and variances for its correlated real and imaginary

parts. This leads to a more general fading channel model, where most other well-known models can be considered as special cases. To obtain fair comparisons about the effects of channel models, we addressed different channel models where each channel has the same average power ( $\Omega$ ) in part of our analysis. Under this condition, different communications systems demonstrated different behaviours.

## 6.2 Future Work

There are still several issues related to the I/Q imbalance problem for the discussed communication systems, and the proposed solutions in this work constitute a favorable platform for several future extensions. The CR and NOMA systems can be extended to a MIMO model and the channel models of all the discussed communication systems can be extended to correlated channel models. Moreover, less complex receivers can be proposed for the QSM and NOMA systems, and the proposed NOMA solution can be extended to the general case of  $M$  users. Improper Gaussian signalling to optimize the system performance in the presence of the I/Q imbalance can also be addressed.

This thesis used a single carrier model, another possible direction is multi-carrier OFDMA systems. In addition, other fading models, such as frequency and time selective fading channels can be tackled when the studied system is under the effects of I/Q imbalance and IGN. Cell-free massive MIMO is a promising wireless technology. It helps to reduce the cost and energy consumption of wireless networks. Intelligent reflecting surface (IRS) has also recently been also proposed as a promising new wireless technology to realize spectral, energy, and cost efficient wireless communication. However, the impact of HWIs on cell-free massive MIMO and IRS is still an active research area that needs to be pursued.

# Bibliography

- [1] F. Boccardi, R. W. Heath, A. Lozano, T. L. Marzetta, and P. Popovski, “Five disruptive technology directions for 5G,” *IEEE Commun. Mag.*, vol. 52, no. 2, pp. 74–80, February 2014.
- [2] E. Hossain and M. Hasan, “5G cellular: key enabling technologies and research challenges,” *IEEE Instru. Measure. Mag.*, vol. 18, no. 3, pp. 11–21, June 2015.
- [3] L. Chettri and R. Bera, “A comprehensive survey on internet of things (IoT) toward 5G wireless systems,” *IEEE Internet of Things Jour.*, vol. 7, no. 1, pp. 16–32, 2020.
- [4] Erafimovski, Nikola and Sinanovic sinanovic, Sinan and Renzo, Marco Di and Haas, Harald, “Multiple access spatial modulation,” *EURASIP Journal on Wireless Commun. and Net.*, vol. 2012, no. 1, p. 299, 2012.
- [5] S. M. R. Islam, N. Avazov, O. A. Dobre, and K. Kwak, “Power-domain non-orthogonal multiple access (NOMA) in 5G systems: Potentials and challenges,” *IEEE Commun. Surv. Tut.*, vol. 19, no. 2, pp. 721–742, Secondquarter 2017.
- [6] S. Gökçeli, O. Kucur, M. Aldababsa, M. Toka, and G. K. Kurt, “A Tutorial on Nonorthogonal Multiple Access for 5G and Beyond,” *Wireless Commun. and Mobi. Comp.*, vol. 2018, pp. 1–24, 2018.
- [7] P. Yang, Y. Xiao, Y. L. Guan, Z. Liu, S. Li, and W. Xiang, “Adaptive SM-MIMO for mmWave communications with reduced RF chains,” *IEEE Journal on Selected Areas in Commun.*, vol. 35, no. 7, pp. 1472–1485, 2017.

- [8] M. Lee and W. Chung, "Transmitter design for analog beamforming aided spatial modulation in millimeter wave MIMO systems," in *2016 IEEE 27th Annual int. Symp. on Personal, Indoor, and Mobile Radio Commun. (PIMRC)*, 2016, pp. 1–6.
- [9] M. Wen, B. Zheng, K. J. Kim, M. Di Renzo, T. A. Tsiftsis, K. Chen, and N. Al-Dhahir, "A survey on spatial modulation in emerging wireless systems: Research progresses and applications," *IEEE Journal on Selected Areas in Commun.*, vol. 37, no. 9, pp. 1949–1972, 2019.
- [10] Z. Ding, P. Fan, and H. V. Poor, "Random beamforming in millimeter-wave NOMA networks," *IEEE Acc.*, vol. 5, pp. 7667–7681, 2017.
- [11] L. Zhu, Z. Xiao, X. Xia, and D. Oliver Wu, "Millimeter-wave communications with non-orthogonal multiple access for B5G/6G," *IEEE Acc.*, vol. 7, pp. 116 123–116 132, 2019.
- [12] B. Wang, L. Dai, Z. Wang, N. Ge, and S. Zhou, "Spectrum and energy-efficient beamspace MIMO-NOMA for millimeter-wave communications using lens antenna array," *IEEE Journal on Selected Areas in Commun.*, vol. 35, no. 10, pp. 2370–2382, 2017.
- [13] S. Javed, O. Amin, S. S. Ikki, and M. Alouini, "On the achievable rate of hardware-impaired transceiver systems," in *GLOBECOM 2017 - 2017 IEEE Glob. Commun. Conf.*, Dec 2017, pp. 1–6.
- [14] S. Javed, O. Amin, S. S. Ikki, and M.-S. Alouini, "Asymmetric modulation for hardware impaired systems. error probability analysis and receiver design," *IEEE Trans. on Wireless Commun.*, vol. 18, no. 3, pp. 1723–1738, 2019.
- [15] O. Semiari, B. Maham, and C. Yuen, "On the effect of I/Q imbalance on energy detection and a novel four-level hypothesis spectrum sensing," *IEEE Tran. on Vehc. Tech.*, vol. 63, no. 8, pp. 4136–4141, Oct 2014.

- [16] L. Anttila, M. Valkama, and M. Renfors, “Circularity-based I/Q imbalance compensation in wideband direct-conversion receivers,” *IEEE Tran. on Vehc. Tech.*, vol. 57, no. 4, pp. 2099–2113, July 2008.
- [17] M. Valkama, M. Renfors, and V. Koivunen, “Advanced methods for I/Q imbalance compensation in communication receivers,” *IEEE Tran.on Sig.Proc.*, vol. 49, no. 10, pp. 2335–2344, Oct 2001.
- [18] U. Oruthota *et al.*, “Performance analysis and mitigation techniques for I/Q-Corrupted OFDM systems,” *Doctoral Dissertations 219/2015, Aalto University, Finland*, 2015.
- [19] J. Zhu, D. W. K. Ng, N. Wang, R. Schober, and V. K. Bhargava, “Analysis and design of secure massive MIMO systems in the presence of hardware impairments,” *IEEE Trans. Wireless Commun.*, vol. 16, no. 3, pp. 2001–2016, Mar. 2017.
- [20] B. Selim, S. Muhaidat, P. C. Sofotasios, B. S. Sharif, T. Stouraitis, G. K. Karagiannidis, and N. Al-Dhahir, “Performance analysis of single carrier coherent and noncoherent modulation under I/Q imbalance,” in *2018 IEEE 87th Veh. Tech. Conf. (VTC Spring)*, June 2018, pp. 1–5.
- [21] CISCO, “IEEE 802.11ax: The sixth generation of Wi-Fi,” 2017. [Online]. Available: <https://www.cisco.com/c/dam/en/us/products/collateral/wireless/white-paper-c11-740788.pdf>
- [22] R. Want, B. N. Schilit, and S. Jenson, “Enabling the internet of things,” *Computer*, vol. 48, no. 1, pp. 28–35, Jan 2015.
- [23] M. Kim and S. Chang, “A consumer transceiver for long-range IoT communications in emergency environments,” *IEEE Tran. on Consumer Electro.*, vol. 62, no. 3, pp. 226–234, August 2016.
- [24] The 3rd Generation Partnership Project (3GPP), “Evolved Universal Terrestrial Radio Access (E-UTRA); User Equipment (UE) radio transmission and reception,” *3GPP*, 2017.

- [25] M. Gavell, “Advanced Analog MMICs for mm-wave Communication and Remote Sensing in 0.15  $\mu\text{m}$  mHEMT Technology,” *Chalmers University of Technology*, 2013.
- [26] S. E. Gunnarsson, C. Karnfelt, H. Zirath, R. Kozhuharov, D. Kuylenstierna, C. Fager, and A. Alping, “Single-Chip 60 GHz Transmitter and Receiver MMICs in a GaAs mHEMT Technology,” in *2006 IEEE MTT-S International Microwave Symposium Digest*, June 2006, pp. 801–804.
- [27] S. Javed, O. Amin, S. S. Ikki, and M. Alouini, “Impact of improper Gaussian signaling on hardware impaired systems,” in *2017 IEEE int. Conf. on Commun. (ICC)*, May 2017, pp. 1–6.
- [28] M. Mailand, R. Richter, and H.-J. Jentschel, “IQ-imbalance and its compensation for non-ideal analog receivers comprising frequency-selective components,” *Advances in Radio Sci.*, vol. 4, no. D. 1, pp. 189–195, 2006.
- [29] A. Kiayani, L. Anttila, Y. Zou, and M. Valkama, “Advanced receiver design for mitigating multiple RF impairments in OFDM systems: algorithms and RF measurements,” *J. Elect. Comput. Eng.*, vol. 2012, p. 3, 2012.
- [30] B. Maham, O. Tirkkonen, and A. Hjørungnes, “Impact of transceiver I/Q imbalance on transmit diversity of beamforming OFDM systems,” *IEEE Trans. Commun.*, vol. 60, no. 3, pp. 643–648, Mar. 2012.
- [31] I. Barhumi and M. Moonen, “Frequency-domain IQ-imbalance and carrier frequency offset compensation for OFDM over doubly selective channels,” in *2006 14th European Signal Processing Conference*, Sep. 2006, pp. 1–5.
- [32] A. E. Canbilen, M. M. Alsmadi, E. Basar, S. S. Ikki, S. S. Gultekin, and I. Develi, “Spatial modulation in the presence of I/Q imbalance: Optimal detector amp; performance analysis,” *IEEE Commun. Lett.*, vol. 22, no. 8, pp. 1572–1575, Aug 2018.
- [33] S. Javed, O. Amin, S. S. Ikki, and M. Alouini, “On the optimal detection and error performance analysis of the hardware impaired systems,” in *GLOBECOM 2017 - 2017 IEEE Glob. Commun. Conf.*, Dec 2017, pp. 1–7.

- [34] P. J. Schreier and L. L. Scharf, *Statistical signal processing of complex-valued data: the theory of improper and noncircular signals*. Cambridge university press, 2010.
- [35] E. Ollila, “On the circularity of a complex random variable,” *IEEE Sig. proc. Lett.*, vol. 15, pp. 841–844, 2008.
- [36] E. Ollila, J. Eriksson, and V. Koivunen, “Complex elliptically symmetric random variables—generation, characterization, and circularity tests,” *IEEE Tran. on Sig. Proc.*, vol. 59, no. 1, pp. 58–69, Jan 2011.
- [37] J. M. Romero-Jerez and F. J. Lopez-Martinez, “On the distribution of the squared norm of non-circular complex Gaussian random variables with applications,” in *2015 IEEE int. Symp. on Info. Theory (ISIT)*, June 2015, pp. 341–345.
- [38] A. A. Mohsenipour, “On the distribution of quadratic expressions in various types of random vectors,” *Electronic Thesis and Dissertation Repository, The University of Western Ontario*, vol. 955, no. December, pp. 1–164, 2012.
- [39] B. Baldessari, “The distribution of a quadratic form of normal random variables,” *The Annals of Mathematical Statistics*, vol. 38, no. 6, pp. 1700–1704, 1967. [Online]. Available: <http://www.jstor.org/stable/2238649>
- [40] E. Ollila, J. Eriksson, and V. Koivunen, “Complex elliptically symmetric random variables generation, characterization, and circularity tests,” *IEEE Trans. Sign. proc.*, vol. 59, no. 1, pp. 58–69, Jan. 2011.
- [41] N. Balakrishnan, N. Johnson, and S. Kotz, “Continuous multivariate distributions. models and applications,” 1985.
- [42] J. G. Proakis, “Digital communications through fading multipath channels,” *Digital Commun.*, pp. 824–825, 2001.
- [43] P. Beckmann, “Statistical distribution of the amplitude and phase of a multiply scattered field,” *Journal of Research of the National Bureau of Standards, 66D*, vol. 3, pp. 231–240, 1962.

- [44] —, “Rayleigh distribution and its generalizations,” *Radio Science Journal of Research NBS/USNC-URSI*, vol. 68, no. 9, pp. 927–932, 1964.
- [45] M. Rangaswamy, D. D. Weiner, and A. Ozturk, “Non-Gaussian random vector identification using spherically invariant random processes,” *IEEE Tran. Aerospace and Electro. Sys.*, vol. 29, no. 1, pp. 111–124, Jan 1993.
- [46] V. A. Aalo, G. P. Efthymoglou, and C. Chayawan, “On the envelope and phase distributions for correlated Gaussian quadratures,” *IEEE Commun. Lett.*, vol. 11, no. 12, pp. 985–987, December 2007.
- [47] S. S. Ikki and R. Mesleh, “A general framework for performance analysis of space shift keying (SSK) modulation in the presence of Gaussian imperfect estimations,” *IEEE Commun. Letters*, vol. 16, no. 2, pp. 228–230, Feb. 2012.
- [48] A. Afana, I. A. Mahady, and S. Ikki, “Quadrature spatial modulation in MIMO cognitive radio systems with imperfect channel estimation and limited feedback,” *IEEE Tran. on Commun.*, vol. 65, no. 3, pp. 981–991, March 2017.
- [49] R. Mesleh and S. S. Ikki, “On the effect of Gaussian imperfect channel estimations on the performance of space modulation techniques,” in *2012 IEEE 75th Veh. Tech. Conf. (VTC Spring)*, May 2012, pp. 1–5.
- [50] A. Afana, T. M. N. Ngatched, and O. A. Dobre, “Spatial modulation in MIMO limited-feedback spectrum-sharing sys. with mutual interference and channel estimation errors,” *IEEE Commun. Lett.*, vol. 19, no. 10, pp. 1754–1757, Oct 2015.
- [51] A. Afana, T. M. N. Ngatched, O. A. Dobre, and S. Ikki, “Spatial modulation in MIMO spectrum-sharing systems with imperfect channel estimation and multiple primary users,” in *2015 IEEE Glob. Commun. Conf. (GLOBECOM)*, Dec 2015, pp. 1–5.
- [52] E. Basar, U. Aygolu, E. Panayirci, and H. V. Poor, “Performance of spatial modulation in the presence of channel estimation errors,” *IEEE Commun. Lett.*, vol. 16, no. 2, pp. 176–179, February 2012.

- [53] R. Mesleh and O. S. Badarneh, "Quadrature spatial modulation in correlated  $\eta - \mu$  fading channels with imperfect channel state information," in *2017 int. Conf. on Wireless Commun., Sig. Proc. and Net. (WiSPNET)*, March 2017, pp. 887–892.
- [54] M. M. Alsmadi, A. E. Canbilen, S. S. Ikki, E. Basar, S. S. Gultekin, and I. Develi, "Imperfect CSI and improper Gaussian noise effects on SSK: Optimal detection and error analysis," in *2018 IEEE Glob. Commun. Conf. (GLOBECOM)*, Dec 2018, pp. 1–6.
- [55] M. M. Alsmadi, A. E. Canbilen, N. Abu Ali, S. S. Ikki, and E. Basar, "Cognitive networks in the presence of I/Q imbalance and imperfect CSI: Receiver design and performance analysis," *IEEE Acc.*, vol. 7, pp. 49 765–49 777, 2019.
- [56] A. K. Jagannatham, *Principles of modern wireless communication systems*. McGraw-Hill Education, 2015.
- [57] A. Gokceoglu, S. Dikmese, M. Valkama, and M. Renfors, "Energy detection under IQ imbalance with single- and multi-channel direct-conversion receiver: Analysis and mitigation," *IEEE Journal on Selected Areas in Commun.*, vol. 32, no. 3, pp. 411–424, March 2014.
- [58] A. A. Boulogeorgos, H. A. B. Salameh, and G. K. Karagiannidis, "Spectrum sensing in full-duplex cognitive radio networks under hardware imperfections," *IEEE Tran. on Vehc. Tech.*, vol. 66, no. 3, pp. 2072–2084, March 2017.
- [59] P. K. Sharma and P. K. Upadhyay, "Cognitive relaying with transceiver hardware impairments under interference constraints," *IEEE Commun. Lett.*, vol. 20, no. 4, pp. 820–823, April 2016.
- [60] D. K. Nguyen and H. Ochi, "On the impact of transceiver impairments to cognitive df relay networks," in *2014 IEEE Asia Pacific Conf. on Cir.and Sys. (APCCAS)*, Nov 2014, pp. 125–128.

- [61] —, “Transceiver impairments in df/af dual-hop cognitive relay networks: Outage performance and throughput analysis,” in *2015 IEEE 81st Veh. Tech. Conf. (VTC Spring)*, May 2015, pp. 1–5.
- [62] D. K. Nguyen, D. N. K. Jayakody, and H. Ochi, “Soft information relaying with transceiver hardware impairments in cognitive networks,” in *2015 10th int. Conf. on Info. Commun. and Sig. Proc. (ICICS)*, Dec 2015, pp. 1–5.
- [63] A. Afana, N. Abu-Ali, and S. Ikki, “On the joint impact of hardware and channel imperfections on cognitive spatial modulation MIMO systems: Cramer amp;x2013;rao bound approach,” *IEEE Sys. Journal*, pp. 1–12, 2018.
- [64] S. Solanki, P. K. Upadhyay, D. B. da Costa, P. S. Bithas, A. G. Kanatas, and U. S. Dias, “Joint impact of RF hardware impairments and channel estimation errors in spectrum sharing multiple-relay networks,” *IEEE Tran. on Commun.*, vol. 66, no. 9, pp. 3809–3824, Sep. 2018.
- [65] G. M. Matalkah, J. M. Sabatier, and M. M. Matalgah, “A generalized likelihood ratio test for detecting targets in multiple-band spectral images with improper complex Gaussian noise,” in *2008 15th IEEE int. Conf. on Image Proc.*, Oct 2008, pp. 1856–1859.
- [66] A. S. Aghaei, K. N. Plataniotis, and S. Pasupathy, “Maximum likelihood binary detection in improper complex Gaussian noise,” in *2008 IEEE int. Conf. on Acoustics, Speech and Sig. Proc.*, March 2008, pp. 3209–3212.
- [67] Y. C. Yoon and H. Leib, “Maximizing snr in improper complex noise and applications to cdma,” *IEEE Communications Letters*, vol. 1, no. 1, pp. 5–8, 1997.
- [68] M. Alam and Q. Zhang, “A survey: Non-orthogonal multiple access with compressed sensing multiuser detection for mmhc,” *arXiv preprint arXiv:1810.05422*, 2018.
- [69] H. Haas, E. Costa, and E. Schulz, “Increasing spectral efficiency by data multiplexing using antenna arrays,” in *The 13th IEEE Intern.Symp. on Personal, Indoor and Mobile Radio Commun.*, vol. 2, 2002, pp. 610–613 vol.2.

- [70] R. Mesleh, H. Haas, C. W. Ahn, and S. Yun, "Spatial modulation - a new low complexity spectral efficiency enhancing technique," in *2006 First Intern. Conf. on Commun.s and Net.in China*, 2006, pp. 1–5.
- [71] R. Y. Mesleh, H. Haas, S. Sinanovic, C. W. Ahn, and S. Yun, "Spatial modulation," *IEEE Tran. on Veh. Tech.*, vol. 57, no. 4, pp. 2228–2241, 2008.
- [72] J. Jeganathan, A. Ghrayeb, L. Szczecinski, and A. Ceron, "Space shift keying modulation for MIMO channels," *IEEE Tran. on Wireless Commun.*, vol. 8, no. 7, pp. 3692–3703, July 2009.
- [73] A. Younis, N. Serafimovski, R. Mesleh, and H. Haas, "Generalised spatial modulation," in *2010 Conf.Record of the Forty Fourth Asilomar Conf.e on Sig., Sys. and Comp.*, 2010, pp. 1498–1502.
- [74] J. Jeganathan, A. Ghrayeb, and L. Szczecinski, "Generalized space shift keying modulation for MIMO channels," in *2008 IEEE 19th Intern. Symp. on Personal, Indoor and Mobile Radio Commun.*, 2008, pp. 1–5.
- [75] R. Mesleh, S. S. Ikki, and H. M. Aggoune, "Quadrature spatial modulation," *IEEE Tran. on Vehc. Tech.*, vol. 64, no. 6, pp. 2738–2742, June 2015.
- [76] FCC, "Spectrum policy task force," *ET Docket*, vol. 02-135, no. 5, Nov. 2002.
- [77] J. Mitola and G. Q. Maguire, "Cognitive radio: making software radios more personal," *IEEE Person. Commun.*, vol. 6, no. 4, pp. 13–18, Aug. 1999.
- [78] A. Goldsmith, S. A. Jafar, I. Maric, and S. Srinivasa, "Breaking spectrum gridlock with cognitive radios: An information theoretic perspective," *Proc. of the IEEE*, vol. 97, no. 5, pp. 894–914, May 2009.
- [79] S. K. Sharma, T. E. Bogale, S. Chatzinotas, B. Ottersten, L. B. Le, and X. Wang, "Cognitive radio techniques under practical imperfections: A survey," *IEEE Commun. Surv. Tut.*, vol. 17, no. 4, pp. 1858–1884, Fourthquarter 2015.

- [80] L. Anttila, M. Valkama, and M. Renfors, “Circularity-based I/Q imbalance compensation in wideband direct-conversion receivers,” *IEEE Tran. on Vehc. Tech.*, vol. 57, no. 4, pp. 2099–2113, 2008.
- [81] M. Valkama, M. Renfors, and V. Koivunen, “Advanced methods for I/Q imbalance compensation in communication receivers,” *IEEE Tran. Sig. Proc.*, vol. 49, no. 10, pp. 2335–2344, Oct. 2001.
- [82] S. Lim, H. Wang, H. Kim, and D. Hong, “Mean value-based power allocation without instantaneous CSI feedback in spectrum sharing systems,” *IEEE Trans. Wireless Commun.*, vol. 11, no. 3, pp. 874–879, Mar. 2012.
- [83] K. Tourki, F. A. Khan, K. A. Qaraqe, H. C. Yang, and M. S. Alouini, “Exact performance analysis of MIMO cognitive radio systems using transmit antenna selection,” *IEEE J. Sel. Areas Commun.*, vol. 32, no. 3, pp. 425–438, Mar. 2014.
- [84] M. K. Simon and M. Alouini, “Digital communications over fading channels [book review],” *IEEE Tran. on Info. Theory*, vol. 54, no. 7, pp. 3369–3370, July 2008.
- [85] E. Björnson, J. Hoydis, and L. Sanguinetti, “Massive MIMO networks: Spectral, energy, and hardware efficiency,” *Foundations and Trends in Signal Process.*, vol. 11, no. 3-4, pp. 154–655, 2017.
- [86] A. Younis, S. Sinanovic, M. Di Renzo, R. Mesleh, and H. Haas, “Generalised sphere decoding for spatial modulation,” *IEEE Tran.on Commun.*, vol. 61, no. 7, pp. 2805–2815, 2013.
- [87] I. Al-Nahhal, O. A. Dobre, E. Basar, and S. Ikki, “Low-cost uplink sparse code multiple access for spatial modulation,” *IEEE Tran. on Veh. Tech.*, vol. 68, no. 9, pp. 9313–9317, 2019.
- [88] E. Dahlman, G. Mildh, S. Parkvall, J. Peisa, J. Sachs, and Y. Selén, “5G radio access,” *Ericsson review*, vol. 6, pp. 2–7, 2014.

- [89] E. Basar, M. Wen, R. Mesleh, M. D. Renzo, Y. Xiao, and H. Haas, "Index modulation techniques for next-generation wireless networks," *IEEE Acc.*, vol. 5, pp. 16 693–16 746, 2017.
- [90] Q. Li, G. Li, W. Lee, M. Lee, D. Mazzarese, B. Clerckx, and Z. Li, "MIMO techniques in wimax and lte: a feature overview," *IEEE Commun. Mag.*, vol. 48, no. 5, pp. 86–92, May 2010.
- [91] R. Mesleh, S. Althunibat, and A. Younis, "Differential quadrature spatial modulation," *IEEE Tran. on Commun.*, vol. 65, no. 9, pp. 3810–3817, Sep. 2017.
- [92] R. Mesleh, H. Haas, C. W. Ahn, and S. Yun, "Spatial modulation - a new low complexity spectral efficiency enhancing technique," in *2006 First International Conf. Commun. and Net. in China*, Oct 2006, pp. 1–5.
- [93] P. Yang, M. D. Renzo, Y. Xiao, S. Li, and L. Hanzo, "Design guidelines for spatial modulation," *IEEE Communications Surv. Tut.*, vol. 17, no. 1, pp. 6–26, Firstquarter 2015.
- [94] F. S. Al-Qahtani, S. Ikki, M. D. Renzo, and H. Alnuweiri, "Performance analysis of space shift keying modulation with imperfect estimation in the presence of Co-Channel interference," *IEEE Commun. Lett.*, vol. 18, no. 9, pp. 1587–1590, Sep. 2014.
- [95] A. Afana and S. Ikki, "Analytical framework for space shift keying MIMO systems with hardware impairments and Co-Channel interference," *IEEE Commun. Lett.*, vol. 21, no. 3, pp. 488–491, March 2017.
- [96] S. Sallem, J. Delmas, and P. Chevalier, "Optimal simo mlse receivers for the detection of linear modulation corrupted by noncircular interference," in *2012 IEEE Statistical Signal Processing Workshop (SSP)*, Aug 2012, pp. 840–843.
- [97] N. Kolomvakis, M. Matthaiou, and M. Coldrey, "IQ imbalance in multiuser systems: Channel estimation and compensation," *IEEE Tran. on Commun.*, vol. 64, no. 7, pp. 3039–3051, July 2016.

- [98] R. Mesleh, S. S. Ikki, and F. S. Almeahmadi, "Impact of IQ imbalance on the performance of QSM multiple-input–multiple-output system," *IET Communications*, vol. 10, no. 17, pp. 2391–2395, 2016.
- [99] A. Younis, R. Mesleh, and H. Haas, "Quadrature spatial modulation performance over nakagami-  $m$  fading channels," *IEEE Tran. on Vehc. Tech.*, vol. 65, no. 12, pp. 10 227–10 231, Dec 2016.
- [100] O. S. Badarneh and R. Mesleh, "A comprehensive framework for quadrature spatial modulation in generalized fading scenarios," *IEEE Tran. on Commun.*, vol. 64, no. 7, pp. 2961–2970, July 2016.
- [101] R. Mesleh, S. S. Ikki, and O. S. Badarneh, "Impact of cochannel interference on the performance of quadrature spatial modulation MIMO systems," *IEEE Commun. Lett.*, vol. 20, no. 10, pp. 1927–1930, Oct 2016.
- [102] R. Mesleh and S. S. Ikki, "On the impact of imperfect channel knowledge on the performance of quadrature spatial modulation," in *2015 IEEE Wireless Commun. and Net. Conf. (WCNC)*, March 2015, pp. 534–538.
- [103] A. Afana, I. Atawi, S. Ikki, and R. Mesleh, "Energy efficient quadrature spatial modulation MIMO cognitive radio systems with imperfect channel estimation," in *2015 IEEE int. Conf. on Ubiquitous Wireless Broadband (ICUWB)*, Oct 2015, pp. 1–5.
- [104] A. Afana, R. Mesleh, S. Ikki, and I. E. Atawi, "Performance of quadrature spatial modulation in amplify-and-forward cooperative relaying," *IEEE Commun. Lett.*, vol. 20, no. 2, pp. 240–243, Feb 2016.
- [105] Z. Yigit and E. Basar, "Low-complexity detection of quadrature spatial modulation," *Electronics Letters*, vol. 52, no. 20, pp. 1729–1731, 2016.
- [106] R. Mesleh and A. Younis, "LOS millimeter-wave communication with quadrature spatial modulation," in *2016 IEEE int. Symp. on Sign. Proc. and Info. Tech. (ISSPIT)*, Dec 2016, pp. 109–113.

- [107] A. Younis, N. Abuzgaia, R. Mesleh, and H. Haas, “Quadrature spatial modulation for 5G outdoor millimeter-wave communications: Capacity analysis,” *IEEE Tran. on Wireless Commun.*, vol. 16, no. 5, pp. 2882–2890, May 2017.
- [108] L. Xiao, P. Yang, S. Fan, S. Li, L. Song, and Y. Xiao, “Low-complexity signal detection for large-scale quadrature spatial modulation systems,” *IEEE Commun. Lett.*, vol. 20, no. 11, pp. 2173–2176, Nov 2016.
- [109] M. M. Alsmadi, N. A. Ali, and S. S. Ikki, “SSK in the presence of improper Gaussian noise: Optimal receiver design and error analysis,” in *2018 IEEE Wireless Commun. and Net. Conf. (WCNC)*, Apr. 2018, pp. 1–6.
- [110] Wikipedia contributors, “Gamma function — Wikipedia, the free encyclopedia,” 2019, [Online; accessed 14-February-2019]. [Online]. Available: [https://en.wikipedia.org/w/index.php?title=Gamma\\_function&oldid=881055749](https://en.wikipedia.org/w/index.php?title=Gamma_function&oldid=881055749)
- [111] A. E. Mostafa, Y. Zhou, and V. W. S. Wong, “Connectivity maximization for narrowband iot systems with NOMA,” in *2017 IEEE Int. Conf. on Commun. (ICC)*, May 2017, pp. 1–6.
- [112] L. Dai, B. Wang, Y. Yuan, S. Han, I. Chih-Lin, and Z. Wang, “Non-orthogonal multiple access for 5G: solutions, challenges, opportunities, and future research trends,” *IEEE Commun. Magaz.*, vol. 53, no. 9, pp. 74–81, 2015.
- [113] Chi-Bao Le, Dinh-Thuan Do, and Miroslav Voznak, “Exploiting impact of hardware impairments in NOMA: Adaptive transmission mode in FD/HD and application in internet-of-things,” *Sensors (Basel)*, vol. PMID: 30875822, no. 2, pp. 1586–1599, Mar 2019.
- [114] C. Deng, M. Liu, X. Li, and Y. Liu, “Hardware impairments aware full-duplex NOMA networks over rician fading channels,” *IEEE Systems Journal*, 2020.
- [115] X. Li, J. Li, and L. Li, “Performance analysis of impaired SWIPT NOMA relaying networks over imperfect Weibull channels,” *IEEE Systems Journal*, vol. 14, no. 1, pp. 669–672, 2020.

- [116] B. Selim, S. Muhaidat, P. C. Sofotasios, B. S. Sharif, T. Stouraitis, G. K. Karagiannidis, and N. Al-Dhahir, “Outage probability of multi-carrier NOMA systems under joint I/Q imbalance,” in *2018 Int. Conf. on Advan. Commun. Tech. and Net. (CommNet)*. IEEE, 2018, pp. 1–7.
- [117] B. Selim, S. Muhaidat, P. C. Sofotasios, B. S. Sharif, T. Stouraitis, G. K. Karagiannidis, and N. Al-Dhahir, “Performance analysis of non-orthogonal multiple access under I/Q imbalance,” *IEEE Acc.*, vol. 6, pp. 18 453–18 468, 2018.
- [118] B. Selim, S. Muhaidat, P. C. Sofotasios, A. Al-Dweik, B. S. Sharif, and T. Stouraitis, “Radio-frequency front-end impairments: Performance degradation in nonorthogonal multiple access communication systems,” *IEEE Veh. Tech. Maga.*, vol. 14, no. 1, pp. 89–97, March 2019.
- [119] L. Bariah, B. Selim, L. Mohjazi, S. Muhaidat, P. C. Sofotasios, and W. Hamouda, “Pairwise error probability of non-orthogonal multiple access with I/Q imbalance,” in *2019 UK/China Emerging Tech. (UCET)*, Aug 2019, pp. 1–4.
- [120] X. Li, M. Liu, C. Deng, P. T. Mathiopoulos, Z. Ding, and Y. Liu, “Full-duplex cooperative NOMA relaying systems with I/Q imbalance and imperfect SIC,” *IEEE Wireless Commun. Lett.*, pp. 1–1, 2019.
- [121] M. M. Alsmadi, N. Abu Ali, M. Hayajneh, and S. S. Ikki, “Down-link NOMA networks in the presence of IQI and imperfect SIC: Receiver design and performance analysis,” *IEEE Tran. on Vehc. Tech.*, pp. 1–1, 2020.
- [122] A. Hasan and J. G. Andrews, “Cancellation error statistics in a CDMA system using successive interference cancellation,” in *Proceedings of The Annual Allerton Conf. on Commun. Control. and Comp.*, vol. 41, no. 3. The University; 1998, 2003, pp. 1797–1806.

# Appendix A

## Proofs of CRN Chapter

### A.1 Proof of the result in 3.30

From (4.13), and after simple algebraic operations, the received signal  $y$  can be written as

$$\begin{aligned} y = & (\sqrt{E}K_1hG_1 + \sqrt{E}K_2h^*G_2^*)x_i + (\sqrt{E}K_1hG_2 + \sqrt{E}K_2h^*G_1^*)x_i^* \\ & + (\sqrt{E}K_1G_1x_i + \sqrt{E}K_1G_2x_i^*)e + (\sqrt{E}K_2G_2^*x_i + \sqrt{E}K_2G_1^*x_i^*)e^* + K_1n + K_2n^*. \end{aligned} \quad (\text{A.1})$$

As mentioned, the proposed filter multiplies the received signal  $y$  and its conjugate  $y^*$  by the scaling factors  $w_1$  and  $w_2$  respectively. The result of this scaling can be given as

$$\begin{aligned} Y = & w_1 \times y + w_2 \times y^* \\ = & \{w_1(K_1hG_1 + K_2h^*G_2^*) + w_2(K_1^*h^*G_2^* + K_2^*hG_1)\}\sqrt{E}x_i \\ & + \{w_1(K_1hG_2 + K_2h^*G_1^*) + w_2(K_1^*h^*G_1^* + K_2^*hG_2)\}\sqrt{E}x_i^* \\ & + \{w_1(K_1G_1x_i + K_1G_2x_i^*) + w_2(K_2^*G_2x_i^* + K_2^*G_1x_i)\}\sqrt{E}e \\ & + \{w_1(K_2G_2^*x_i + K_2G_1^*x_i^*) + w_2(K_1^*G_1^*x_i^* + K_1^*G_2^*x_i)\}\sqrt{E}e^* \\ & + w_1K_1n + w_1K_2n^* + w_2K_1^*n^* + w_2K_2^*n. \end{aligned} \quad (\text{A.2})$$

In order to cancel the I/Q imbalance and get the transmitted symbol  $\sqrt{E}x_i$ , the proposed filter matches the resulting signal  $Y$  with the transmitted signal  $\sqrt{E}x_i$ . Consequently, the values of  $w_1$  and  $w_2$  should validate the following:

$$w_1(K_1hG_1 + K_2h^*G_2^*) + w_2(K_1^*h^*G_2^* + K_2^*hG_1) = 1. \quad (\text{A.3})$$

$$w_1(K_1hG_2 + K_2h^*G_1^*) + w_2(K_1^*h^*G_1^* + K_2^*hG_2) = 0. \quad (\text{A.4})$$

Solving (A.3) and (A.4) to find the values of  $w_1$  and  $w_2$  ends up with

$$w_1 = \frac{\alpha^*}{(\alpha\alpha^* - \beta\beta^*)}, \quad w_2 = \frac{-\beta}{(\alpha\alpha^* - \beta\beta^*)}, \quad (\text{A.5})$$

where  $\alpha = K_1hG_1 + K_2h^*G_2^*$ , and  $\beta = K_1hG_2 + K_2h^*G_1^*$ . Substituting  $w_1$  and  $w_2$  values in (A.2) ends up with

$$Y = \sqrt{E}x_i + \underbrace{\Omega_1n + \Omega_2n^* + \sqrt{E}\Omega_3e + \sqrt{E}\Omega_4e^*}_Z. \quad (\text{A.6})$$

where,  $\Omega_1 = w_1K_1 + w_2K_2^*$ ,  $\Omega_2 = w_1K_2 + w_2K_1^*$ ,  $\Omega_3 = w_1(K_1G_1x_i + K_1G_2x_i^*) + w_2(K_2^*G_1x_i + K_2^*G_2x_i^*)$ , and  $\Omega_4 = w_2(K_1^*G_2^*x_i + K_1^*G_1^*x_i^*) + w_1(K_2G_2^*x_i + K_2G_1^*x_i^*)$ . Let us rewrite (A.6) as

$$Y = \sqrt{E}x_i + Z_i^I + jZ_i^Q. \quad (\text{A.7})$$

Considering that,  $\Omega_1 = \Omega_1^I + j\Omega_1^Q$ ,  $\Omega_2 = \Omega_2^I + j\Omega_2^Q$ ,  $\Omega_3 = \sqrt{E}(\Omega_3^I + j\Omega_3^Q)$ , and  $\Omega_4 = \sqrt{E}(\Omega_4^I + j\Omega_4^Q)$ .  $Z_i^I$  and  $Z_i^Q$  can be written after some mathematical manipulations as

$$\begin{aligned} Z_i^I &= (\Omega_1^I + \Omega_2^I)n^I + (\Omega_2^Q - \Omega_1^Q)n^Q + (\Omega_3^I + \Omega_4^I)\sqrt{E}e^I + (\Omega_4^Q - \Omega_3^Q)\sqrt{E}e^Q. \\ Z_i^Q &= (\Omega_1^Q + \Omega_2^Q)n^I + (\Omega_1^I - \Omega_2^I)n^Q + (\Omega_3^Q + \Omega_4^Q)\sqrt{E}e^I + (\Omega_3^I - \Omega_4^I)\sqrt{E}e^Q. \end{aligned} \quad (\text{A.8})$$

The variances of  $Z_i^I$  and  $Z_i^Q$  are  $\sigma_{Z_i^I}^2$  and  $\sigma_{Z_i^Q}^2$  respectively which can be calculated as

$$\begin{aligned} \sigma_{Z_i^I}^2 &= (\Omega_1^I + \Omega_2^I)^2\sigma_{n^I}^2 + (\Omega_2^Q - \Omega_1^Q)^2\sigma_{n^Q}^2 + 2\rho_n(\Omega_1^I + \Omega_2^I)(\Omega_2^Q - \Omega_1^Q)\sigma_n^I\sigma_n^Q \\ &\quad + (\Omega_3^I + \Omega_4^I)^2E\sigma_{e^I}^2 + (\Omega_4^Q - \Omega_3^Q)^2E\sigma_{e^Q}^2 + 2\rho_e(\Omega_3^I + \Omega_4^I)(\Omega_4^Q - \Omega_3^Q)E\sigma_e^I\sigma_e^Q. \\ \sigma_{Z_i^Q}^2 &= (\Omega_1^Q + \Omega_2^Q)^2\sigma_{n^I}^2 + (\Omega_1^I - \Omega_2^I)^2\sigma_{n^Q}^2 + 2\rho_n(\Omega_1^Q + \Omega_2^Q)(\Omega_1^I - \Omega_2^I)\sigma_n^I\sigma_n^Q \\ &\quad + (\Omega_3^Q + \Omega_4^Q)^2E\sigma_{e^I}^2 + (\Omega_3^I - \Omega_4^I)^2E\sigma_{e^Q}^2 + 2\rho_e(\Omega_3^Q + \Omega_4^Q)(\Omega_3^I - \Omega_4^I)E\sigma_e^I\sigma_e^Q. \end{aligned} \quad (\text{A.9})$$

It can be seen that,  $Z_i^I$  and  $Z_i^Q$  are correlated where the correlation factor is given by

$$\rho_{Z_i} = \frac{\mathbb{E}\{Z_i^I Z_i^Q\}}{\sqrt{\sigma_{Z_i^I}^2 \sigma_{Z_i^Q}^2}}, \quad (\text{A.10})$$

where  $\mathbb{E}\{Z_i^I Z_i^Q\}$  is given by

$$\begin{aligned}
\mathbb{E}\{Z_i^I Z_i^Q\} &= (\Omega_1^I + \Omega_2^I)(\Omega_1^Q + \Omega_2^Q)\sigma_{n^I}^2 + (\Omega_2^Q - \Omega_1^Q)(\Omega_1^I - \Omega_2^I)\sigma_{n^Q}^2 \\
&\quad + \rho_n\{(\Omega_1^I + \Omega_2^I)(\Omega_1^I - \Omega_2^I) + (\Omega_2^Q + \Omega_1^Q)(\Omega_2^Q - \Omega_1^Q)\}\sigma_n^I\sigma_n^Q \\
&\quad + E(\Omega_3^I + \Omega_4^I)(\Omega_3^Q + \Omega_4^Q)\sigma_{e^I}^2 + E(\Omega_4^Q - \Omega_3^Q)(\Omega_3^I - \Omega_4^I)\sigma_{e^Q}^2 \\
&\quad + E\rho_e\{(\Omega_3^I + \Omega_4^I)(\Omega_3^I - \Omega_4^I) + (\Omega_4^Q + \Omega_3^Q)(\Omega_4^Q - \Omega_3^Q)\}\sigma_e^I\sigma_e^Q.
\end{aligned} \tag{A.11}$$

Finally, the received signal  $Y$  can be written as

$$Y = \sqrt{E}x_i + Z_i, \tag{A.12}$$

Now, what will be the accumulated noise  $Z_i$  if the AWGN is PGN. In this case,  $\sigma_{e^I}^2 = \sigma_{e^Q}^2 = \frac{\sigma_e^2}{2}$ ,  $\rho_e = 0$ ,  $\sigma_{n^I}^2 = \sigma_{n^Q}^2 = \frac{\sigma_n^2}{2}$ , and  $\rho_n = 0$ . Consequently, the variances of  $Z_i^I$  and  $Z_i^Q$  are given by

$$\begin{aligned}
\sigma_{Z_i^I}^2 &= \{(\Omega_1^I + \Omega_2^I)^2 + (\Omega_2^Q - \Omega_1^Q)^2\} \frac{\sigma_n^2}{2} + E\{(\Omega_3^I + \Omega_4^I)^2 + (\Omega_4^Q - \Omega_3^Q)^2\} \frac{\sigma_e^2}{2}. \\
\sigma_{Z_i^Q}^2 &= \{(\Omega_1^Q + \Omega_2^Q)^2 + (\Omega_1^I - \Omega_2^I)^2\} \frac{\sigma_n^2}{2} + E\{(\Omega_3^Q + \Omega_4^Q)^2 + (\Omega_3^I - \Omega_4^I)^2\} \frac{\sigma_e^2}{2}.
\end{aligned} \tag{A.13}$$

It can be seen that,  $Z_i^I$  and  $Z_i^Q$  are correlated where the correlation factor is given by

$$\rho_{Z_i} = \frac{\mathbb{E}\{Z_i^I Z_i^Q\}}{\sqrt{\sigma_{Z_i^I}^2 \sigma_{Z_i^Q}^2}}, \tag{A.14}$$

where  $\mathbb{E}\{Z_i^I Z_i^Q\}$  is given by

$$\begin{aligned}
\mathbb{E}\{Z_i^I Z_i^Q\} &= \{(\Omega_1^I + \Omega_2^I)(\Omega_1^Q + \Omega_2^Q) + (\Omega_2^Q - \Omega_1^Q)(\Omega_1^I - \Omega_2^I)\} \frac{\sigma_n^2}{2} \\
&\quad + E\{(\Omega_3^I + \Omega_4^I)(\Omega_3^Q + \Omega_4^Q) + (\Omega_4^Q - \Omega_3^Q)(\Omega_3^I - \Omega_4^I)\} \frac{\sigma_e^2}{2}.
\end{aligned} \tag{A.15}$$

Finally, the received signal  $Y$  can be written as

$$Y = \sqrt{E}x_i + Z_i, \tag{A.16}$$

Te results in (A.12) and (A.12) which conclude the proof.

## A.2 Proof of the result in 3.42

To find the CRLB, the received signal in (3.6) can be written as

$$y = \sqrt{E}h \underbrace{(K_1(G_1x_i + G_2x_i^*))}_{Q_1} + \sqrt{E}h^* \underbrace{(x_iK_2(G_1x_i + G_2x_i^*))^*}_{Q_2} + \underbrace{K_1n + K_2n^*}_u. \quad (\text{A.17})$$

To simplify the derivation, let us rewrite  $y$  as

$$y = \sqrt{E}Ah^I + \sqrt{E}Bh^Q + j(\sqrt{E}Ch^I + \sqrt{E}Dh^Q) + u^I + ju^Q, \quad (\text{A.18})$$

where,  $A = Q_1^I + Q_2^I$ ,  $B = Q_2^Q - Q_1^Q$ ,  $C = Q_2^Q + Q_1^Q$ , and  $D = Q_1^I - Q_2^I$ . Noting that  $u$  is an improper Gaussian noise with  $u^I \sim \mathcal{N}(0, \sigma_{n^I}^2)$ , and  $u^Q \sim \mathcal{N}(0, K_c^2\sigma_{n^I}^2 + K_d^2\sigma_{n^Q}^2 + 2\rho_n K_c K_d \sigma_n^I \sigma_n^Q)$  with correlation factor  $\Psi = K_c \sigma_{n^I}^2 + 2\rho_n K_d \sigma_n^I \sigma_n^Q$ .

From the previous equation, the joint likelihood function can be written as

$$P_{\bar{y}}(\bar{y}; \theta) = \left( \frac{1}{2\pi\sigma_u^I\sigma_u^Q\sqrt{1-\Psi^2}} \right)^{N_P} \exp \left( - \frac{1}{2(1-\Psi^2)} \sum_{N=0}^{N_P-1} \left[ \frac{(y^I - \sqrt{E}Ah^I + \sqrt{E}Bh^Q)^2}{\sigma_{u^I}^2} + \frac{(y^Q - \sqrt{E}Ch^I - \sqrt{E}Dh^Q)^2}{\sigma_{u^Q}^2} - \frac{2\Psi(y^I - \sqrt{E}Ah^I + \sqrt{E}Bh^Q)(y^Q - \sqrt{E}Ch^I - \sqrt{E}Dh^Q)}{\sigma_u^I\sigma_u^Q} \right] \right), \quad (\text{A.19})$$

where  $N_P$  is the number of samples, and  $\theta = [h^I \ h^Q]^T$ . Based on that, the log likelihood function can be written as

$$\ln(P_{\bar{y}}(\bar{y}; \theta)) = -N_P \ln(2\pi\sigma_u^I\sigma_u^Q\sqrt{1-\Psi^2}) - \frac{1}{2(1-\Psi^2)} \sum_{N=0}^{N_P-1} \left[ \frac{(y^I - \sqrt{E}Ah^I - \sqrt{E}Bh^Q)^2}{\sigma_{u^I}^2} + \frac{(y^Q - \sqrt{E}Ch^I - \sqrt{E}Dh^Q)^2}{\sigma_{u^Q}^2} - \frac{2\Psi(y^I - \sqrt{E}Ah^I - \sqrt{E}Bh^Q)(y^Q - \sqrt{E}Ch^I - \sqrt{E}Dh^Q)}{\sigma_u^I\sigma_u^Q} \right]. \quad (\text{A.20})$$

In order to find CRLB, first, we need to obtain the FIM as follows

$$I_{(\theta)}(\theta) = \begin{bmatrix} I_{(h^I)} = -\mathbb{E} \left\{ \frac{\partial^2 \ln(P_{\bar{y}}(\bar{y}; \theta))}{\partial (h^I)^2} \right\} & I_{(h^I, h^Q)} = -\mathbb{E} \left\{ \frac{\partial^2 \ln(P_{\bar{y}}(\bar{y}; \theta))}{\partial (h^I) \partial (h^Q)} \right\} \\ I_{(h^I, h^Q)} = -\mathbb{E} \left\{ \frac{\partial^2 \ln(P_{\bar{y}}(\bar{y}; \theta))}{\partial (h^I) \partial (h^Q)} \right\} & I_{(h^Q)} = -\mathbb{E} \left\{ \frac{\partial^2 \ln(P_{\bar{y}}(\bar{y}; \theta))}{\partial (h^Q)^2} \right\} \end{bmatrix}. \quad (\text{A.21})$$

To find FIM, we find the first, and then the second derivatives as follows

$$\frac{\partial \ln(\mathbb{P}_{\bar{y}}(\bar{y}; \theta))}{\partial(h^I)} = \sum_{N=0}^{N_p-1} \frac{\sqrt{E}}{(1-\Psi^2)} \times \left[ \frac{A(y^I - \sqrt{E}Ah^I - \sqrt{E}Bh^Q)}{\sigma_{u^I}^2} + \frac{C(y^Q - \sqrt{E}Ch^I - \sqrt{E}Dh^Q)}{\sigma_{u^Q}^2} - \frac{\Psi A(y^Q - \sqrt{E}Ch^I - \sqrt{E}Dh^Q)}{\sigma_{u^I}\sigma_{u^Q}^Q} - \frac{\Psi C(y^I - \sqrt{E}Ah^I - \sqrt{E}Bh^Q)}{\sigma_{u^I}\sigma_{u^Q}^Q} \right]. \quad (\text{A.22})$$

$$\frac{\partial^2 \ln(\mathbb{P}_{\bar{y}}(\bar{y}; \theta))}{\partial(h^I)^2} = \sum_{N=0}^{N_p-1} \frac{E}{(1-\Psi^2)} \left[ -\frac{C^2}{\sigma_{u^Q}^2} - \frac{A^2}{\sigma_{u^I}^2} + \frac{2\Psi AC}{\sigma_{u^I}\sigma_{u^Q}^Q} \right]. \quad (\text{A.23})$$

From (A.21) and (A.23),  $I_{(h^I)}$  can be calculated as

$$I_{(h^I)} = \frac{N_p E}{(1-\Psi^2)} \left[ \frac{A^2}{\sigma_{u^I}^2} + \frac{C^2}{\sigma_{u^Q}^2} - \frac{2\Psi AC}{\sigma_{u^I}\sigma_{u^Q}^Q} \right]. \quad (\text{A.24})$$

Similar to the derivation of  $I_{(h^I)}$ ,  $I_{(h^Q)}$  can be derived as

$$I_{(h^Q)} = \frac{N_p E}{(1-\Psi^2)} \left[ \frac{B^2}{\sigma_{u^I}^2} + \frac{D^2}{\sigma_{u^Q}^2} - \frac{2\Psi BD}{\sigma_{u^I}\sigma_{u^Q}^Q} \right]. \quad (\text{A.25})$$

In the same way,  $I_{(h^I, h^Q)} = I_{(h^Q, h^I)}$  can be obtained by

$$I_{(h^I, h^Q)} = \frac{N_p E}{(1-\Psi^2)} \left[ \frac{AB}{\sigma_{u^I}^2} + \frac{CD}{\sigma_{u^Q}^2} - \frac{\Psi AD}{\sigma_{u^I}\sigma_{u^Q}^Q} - \frac{\Psi BC}{\sigma_{u^I}\sigma_{u^Q}^Q} \right]. \quad (\text{A.26})$$

which concludes the proof.

### A.3 Proof of the result in 3.46

To complete this poof, the values of  $A$ ,  $B$ ,  $C$ , and  $D$  need to be simplified. From Section 2.6,  $G_1$ ,  $G_2$ ,  $K_1$ , and  $K_2$  are given by

$$G_1 = \frac{1}{2}(1 + \xi_t e^{j\beta t}), \quad G_2 = \frac{1}{2}(1 - \xi_t e^{j\beta t}), \quad K_1 = \frac{1}{2}(1 + \xi_r e^{-j\beta r}), \quad K_2 = \frac{1}{2}(1 - \xi_r e^{j\beta r}) \quad (\text{A.27})$$

Based on (A.27),  $K_1^I + K_2^I = 1$ ,  $K_1^Q - K_2^Q = 0$ ,  $G_1^I + G_2^I = 1$ ,  $G_1^Q + G_2^Q = 0$ . Consequently,  $A$ ,  $B$ ,  $C$ , and  $D$  are given by:

$$\begin{aligned}
A &= x_i^I - x_i^Q \xi_t \sin \beta_t, \\
B &= -x_i^Q \xi_t \cos \beta_t, \\
C &= x_i^Q \xi_r \xi_t \cos \beta_r \cos \beta_t + x_i^Q \xi_r \xi_t \sin \beta_r \sin \beta_t - x_i^I \xi_r \sin \beta_r, \\
D &= x_i^I \xi_r \cos \beta_r + x_i^Q \xi_r \xi_t \sin \beta_r \cos \beta_t - x_i^Q \xi_r \xi_t \cos \beta_r \sin \beta_t,
\end{aligned} \tag{A.28}$$

Noting that  $\sigma_{u^I}^2 = \frac{\sigma_n^2}{2}$ ,  $\sigma_{u^Q}^2 = \xi_r^2 \frac{\sigma_n^2}{2}$  and  $1 - \Psi^2 = \cos(\beta_r)^2$ , and after some mathematical simplifications, it can be proven that

$$\begin{aligned}
I_{(h^I)} &= I_{(h^Q)} = \frac{2N_p E(x_i^{I^2} + x_i^{Q^2} \xi_t^2 - 2x_i^I x_i^Q \xi_t \sin(\beta_t))}{\sigma_n^2} \\
I_{(h^I, h^Q)} &= 0
\end{aligned} \tag{A.29}$$

which concludes the proof.

# Appendix B

## Proofs of QSM Chapter

### B.1 Proof of the result in 4.5

Now, denoting that  $K_c = K_1^Q + K_2^Q$  and  $K_d = K_1^I - K_2^I$ , and noting that  $K_1^I + K_2^I = 1$  and  $K_1^Q - K_2^Q = 0$ , (4.4) can be rewritten after some mathematical operations by using (4.1) as

$$y_l = K_1 \left[ \sqrt{E}((h_{l,i} + e_{l,i})\tilde{x}_k^I + j(h_{l,q} + e_{l,q})\tilde{x}_k^Q) + n_l \right] + K_2 \left[ \sqrt{E}((h_{l,i} + e_{l,i})\tilde{x}_k^I + j(h_{l,q} + e_{l,q})\tilde{x}_k^Q) + n_l \right]^*, \quad (\text{B.1})$$

$$y_l = \sqrt{E}\tilde{x}_i^I (K_1 h_{l,i} + K_2 h_{l,i}^*) + \sqrt{E}\tilde{x}_i^I (K_1 e_{l,i} + K_2 e_{l,i}^*) + j \left[ \sqrt{E}\tilde{x}_i^Q (K_1 h_{l,q} - K_2 h_{l,q}^*) + \sqrt{E}\tilde{x}_i^Q (K_1 e_{l,q} - K_2 e_{l,q}^*) \right] + K_1 n_l + K_2 n_l^*; \quad (\text{B.2})$$

$$\begin{aligned} y_l = & \sqrt{E}\tilde{x}_i^I \left( K_1^I h_{l,i}^I - K_1^Q h_{l,i}^Q \right) + \sqrt{E}\tilde{x}_i^I \left( K_2^I h_{l,i}^I + K_2^Q h_{l,i}^Q \right) \\ & + j\sqrt{E}\tilde{x}_i^I \left( K_1^I h_{l,i}^Q + K_1^Q h_{l,i}^I \right) + j\sqrt{E}\tilde{x}_i^I \left( K_2^Q h_{l,i}^I - K_2^I h_{l,i}^Q \right) \\ & - \sqrt{E}\tilde{x}_i^Q \left( K_1^I h_{l,q}^Q + K_1^Q h_{l,q}^I \right) + \sqrt{E}\tilde{x}_i^Q \left( K_2^Q h_{l,q}^I - K_2^I h_{l,q}^Q \right) \\ & + j\sqrt{E}\tilde{x}_i^Q \left( K_1^I h_{l,q}^I - K_1^Q h_{l,q}^Q \right) - \sqrt{E}\tilde{x}_i^Q \left( K_2^I h_{l,q}^I + K_2^Q h_{l,q}^Q \right) \\ & + \sqrt{E}\tilde{x}_i^I \left( K_1^I e_{l,i}^I - K_1^Q e_{l,i}^Q \right) - \sqrt{E}\tilde{x}_i^I \left( K_2^I e_{l,i}^I + K_2^Q e_{l,i}^Q \right) \end{aligned}$$

$$\begin{aligned}
& + j\sqrt{E}\tilde{x}_i^I \left( K_1^I e_{l,i}^Q + K_1^Q e_{l,i}^I \right) - j\sqrt{E}\tilde{x}_i^I \left( K_2^Q e_{l,i}^I - K_2^I e_{l,i}^Q \right) \\
& - \sqrt{E}\tilde{x}_i^Q \left( K_1^I e_{l,q}^Q + K_1^Q e_{l,q}^I \right) - \sqrt{E}\tilde{x}_i^Q \left( K_2^Q e_{l,q}^I - K_2^I e_{l,q}^Q \right) \\
& + j\sqrt{E}\tilde{x}_i^Q \left( K_1^I e_{l,q}^I - K_1^Q e_{l,q}^Q \right) + j\sqrt{E}\tilde{x}_i^Q \left( K_2^I e_{l,q}^I + K_2^Q e_{l,q}^Q \right) \\
& + K_1^I n_l^I - K_1^Q n_l^Q + j[K_1^I n_l^Q + K_1^Q n_l^I] + K_2^I n_l^I + K_2^Q n_l^Q + j[K_2^Q n_l^I - K_2^I n_l^Q] \tag{B.3}
\end{aligned}$$

$$\begin{aligned}
y_l = & \sqrt{E}(\tilde{h}_{l,i}^I \tilde{x}_k^I - \tilde{h}_{l,q}^Q \tilde{x}_k^Q) + j(\tilde{h}_{l,i}^I \tilde{x}_k^I K_c + \tilde{h}_{l,i}^Q \tilde{x}_k^I K_d - \tilde{h}_{l,q}^Q \tilde{x}_k^Q K_c + \tilde{h}_{l,q}^I \tilde{x}_k^Q K_d) + n_l^I \\
& + \sqrt{E}(e_{l,i}^I \tilde{x}_k^I - e_{l,q}^Q \tilde{x}_k^Q) + j\sqrt{E}(e_{l,i}^I \tilde{x}_k^I K_c + e_{l,i}^Q \tilde{x}_k^I K_d - e_{l,q}^Q \tilde{x}_k^Q K_c + e_{l,q}^I \tilde{x}_k^Q K_d) \\
& + j(n_l^I K_c + n_l^Q K_d). \tag{B.4}
\end{aligned}$$

$$\begin{aligned}
y_l = & \sqrt{E}\{\tilde{h}_{l,i}^I(x_k^I - x_k^Q G_c) - \tilde{h}_{l,q}^Q x_k^Q G_d\} \\
& + j\{\tilde{h}_{l,i}^I(x_k^I - x_k^Q G_c)K_c + \tilde{h}_{l,i}^Q(x_k^I - x_k^Q G_c)K_d - \tilde{h}_{l,q}^Q x_k^Q G_d K_c + \tilde{h}_{l,q}^I x_k^Q G_d K_d\} + n_l^I \\
& + \sqrt{E}\{e_{l,i}^I(x_k^I - x_k^Q G_c) - e_{l,q}^Q x_k^Q G_d\} \\
& + j\sqrt{E}\{e_{l,i}^I(x_k^I - x_k^Q G_c)K_c + e_{l,i}^Q(x_k^I - x_k^Q G_c)K_d - e_{l,q}^Q x_k^Q G_d K_c + e_{l,q}^I x_k^Q G_d K_d\} \\
& + j\{n_l^I K_c + n_l^Q K_d\}. \tag{B.5}
\end{aligned}$$

## B.2 Proof of the result in 4.50

The exact FIM) at each SSK reciver can be given as

$$I_{(\theta)}(\theta) = \begin{bmatrix} I_{(h^I)} & I_{(h^I, h^Q)} \\ I_{(h^I, h^Q)} & I_{(h^Q)} \end{bmatrix}. \tag{B.6}$$

CRLB matrix can be obtained by finding  $(I_{(\theta)}(\theta))^{-1}$ . From (4.41), the joint likelihood function at each SSK receiver can be given as

$$\begin{aligned}
P_{\bar{y}}(\bar{y}; \theta) = & \left( \frac{1}{2\pi\sigma_I\sigma_Q\sqrt{1-\rho^2}} \right)^{N_P} \exp \left( -\frac{1}{2(1-\rho^2)} \sum_{N=0}^{N_P-1} \left[ \frac{(y^I - \sqrt{E}h^I)^2}{\sigma_I^2} \right. \right. \\
& \left. \left. + \frac{(y^Q - \sqrt{E}h^Q)^2}{\sigma_Q^2} - \frac{2\rho(y^I - \sqrt{E}h^I)(y^Q - \sqrt{E}h^Q)}{\sigma_I\sigma_Q} \right] \right), \tag{B.7}
\end{aligned}$$

where  $N_P$  is the number of training pilots. Consequently, the log-likelihood can be written as

$$\begin{aligned} \ln(P_{\bar{y}}(\bar{y}; \theta)) = & -N_P \ln \left( 2\pi\sigma_I\sigma_Q\sqrt{1-\rho^2} \right) - \frac{1}{2(1-\rho^2)} \sum_{N=0}^{N_P-1} \left[ \frac{(y^I - \sqrt{E}h^I)^2}{\sigma_I^2} \right. \\ & \left. + \frac{(y^Q - \sqrt{E}h^Q)^2}{\sigma_Q^2} - \frac{2\rho(y^I - \sqrt{E}h^I)(y^Q - \sqrt{E}h^Q)}{\sigma_I\sigma_Q} \right]. \end{aligned} \quad (\text{B.8})$$

The elements of the matrix (B.6) can be found as

$$I_{(h^I)} = -\mathbb{E} \left\{ \frac{\partial^2 \ln(P_{\bar{y}}(\bar{y}; \theta))}{\partial h^{I^2}} \right\}. \quad (\text{B.9})$$

The first derivative of  $\ln(P_{\bar{y}}(\bar{y}; \theta))$  is given by

$$\frac{\partial \ln(P_{\bar{y}}(\bar{y}; \theta))}{\partial h^I} = \frac{\sqrt{E}}{(1-\rho^2)} \times \sum_{N=0}^{N_P-1} \left[ \frac{(y^I - \sqrt{E}h^I)}{\sigma_I^2} - \frac{\rho(y^Q - \sqrt{E}h^Q)}{\sigma_I\sigma_Q} \right]. \quad (\text{B.10})$$

The second derivative of  $\ln(P_{\bar{y}}(\bar{y}; \theta))$  is given by

$$\frac{\partial^2 \ln(P_{\bar{y}}(\bar{y}; \theta))}{\partial h^{I^2}} = -\frac{N_P E}{(1-\rho^2)\sigma_I^2}. \quad (\text{B.11})$$

From (B.9),  $I_{(h^I)}$  can be given by

$$I_{(h^I)} = \frac{N_P E}{(1-\rho^2)\sigma_I^2}. \quad (\text{B.12})$$

Similar to the derivation of  $I_{(h^I)}$ ,  $I_{(h^Q)}$  can be derived as

$$I_{(h^Q)} = \frac{N_P E}{(1-\rho^2)\sigma_Q^2}. \quad (\text{B.13})$$

In the same way,  $I_{(h^I, h^Q)} = I_{(h^Q, h^I)}$  is obtained from

$$I_{(h^I, h^Q)} = -\mathbb{E} \left\{ \frac{\partial^2 \ln(P_{\bar{y}}(\bar{y}; \theta))}{\partial h^I \partial h^Q} \right\} = -\frac{N_P \rho E}{(1-\rho^2)\sigma_I\sigma_Q}. \quad (\text{B.14})$$

Combining (B.12), (B.13), and (B.14), the FIM can be given as

$$I_{(\theta)}(\theta) = \begin{bmatrix} \frac{N_P E}{(1-\rho^2)\sigma_I^2} & -\frac{N_P \rho E}{(1-\rho^2)\sigma_I\sigma_Q} \\ -\frac{N_P \rho E}{(1-\rho^2)\sigma_I\sigma_Q} & \frac{N_P E}{(1-\rho^2)\sigma_Q^2} \end{bmatrix}. \quad (\text{B.15})$$

Consequently, CRLB matrix can be obtained by finding  $(I_{(\theta)}(\theta))^{-1}$  as

$$\text{CRLB} = \begin{bmatrix} \frac{\sigma_I^2}{N_P E} & \frac{\sigma_I\sigma_Q\rho}{N_P E} \\ \frac{\sigma_I\sigma_Q\rho}{N_P E} & \frac{\sigma_Q^2}{N_P E} \end{bmatrix}. \quad (\text{B.16})$$